ABSTRACT

Title of Document:	SELF-ORGANIZING DIRECTIONAL WIRELESS BACKBONE NETWORKS
	Jaime Llorca, Doctor of Philosophy, 2008
Directed By:	Professor Christopher C. Davis, Department of Electrical and Computer Engineering

Directional wireless communications is emerging as a viable, cost-effective technology for rapidly deployable broadband wireless communication infrastructures. This technology provides extremely high data rates through the use of narrow-beam free space optical (FSO) and/or radio-frequency (RF) point-to-point links. The use of directional wireless communications to form flexible backbone networks, which provide broadband connectivity to capacity-limited wireless networks or hosts, promises to circumvent the scalability limitations of traditional wireless networks.

The main challenge in the design of directional wireless backbone (DWB) networks is to assure robustness and survivability in a dynamic wireless environment. DWB networks must assure highly available broadband connectivity and be able to regain connectivity in the face of loss or degradation. This dissertation considers the use of topology control to provide assured connectivity in dynamic environments. Topology control is defined as the autonomous network capability to dynamically reconfigure its physical topology. In the case of DWB networks, the physical

topology can be reconfigured through 1) redirection of point-to-point links and/or 2) reposition of backbone nodes. Coverage and connectivity are presented as the two most important issues in DWB-based networks. The aim of this dissertation is to provide initial designs for scalable self-organized DWB networks, which could autonomously adapt their physical topology to maximize coverage to terminals or hosts while maintaining robust backbone connectivity.

This dissertation provides a novel approach to the topology control problem by modeling communication networks as physical systems where network robustness is characterized in terms of the system's potential energy. In our model, communication links define physical interactions between network nodes. Topology control mechanisms are designed to mimic physical systems' natural reaction to external excitations which drive the network topology to energy minimizing configurations based on local forces exerted on network nodes. The potential energy of a communications network is defined as the total communications energy usage for a given target performance. Accurate link physics models that take into account the variation of the wireless channel due to atmospheric attenuation, turbulence-induced fading, node mobility, and different antenna patterns have been developed in order to characterize the behavior of the potential energy stored at each wireless link in the network. The net force at each backbone node is computed as the negative gradient of the potential energy function at the node's location. Mobility control algorithms are designed to reposition backbone nodes in the direction of the net force. The algorithms developed are completely distributed, show constant time complexity and

produce optimal solutions from local interactions, thus proving the system's self-organizing capability.

This dissertation provides: 1) An improved understanding of the physical nature of next generation wireless networks; 2) Applicability and feasibility studies of topology control for performance improvement in dynamic wireless networks; and 3) Initial designs for self-organizing DWB networks through topology control.

SELF-ORGANIZING DIRECTIONAL WIRELESS BACKBONE NETWORKS

By

Jaime Llorca

Dissertation submitted to the Faculty of the Graduate School of the
University of Maryland, College Park, in partial fulfillment
of the requirements for the degree of
Doctor of Philosophy
2008

Advisory Committee:
Professor Christopher C. Davis, Chair
Professor Mark Shayman
Professor Gregory B. Baecher
Associate Professor Tomas E. Murphy
Faculty Research Professor Stuart D. Milner
Faculty Research Professor Mehdi Kalantari Kandani

Dedication

To my family

for their unconditional love and support

Acknowledgements

I gratefully thank my advisor and co-advisor, Professor Christopher C. Davis and Dr Stuart D. Milner, for their continuous guidance, friendship, and support throughout my graduate studies at the University of Maryland. I also want to thank the members of the dissertation committee for their time and service.

I want to thank Professor Uzi Vishkin, Professor Steven Gabriel and Dr Mehdi Kalantari for our helpful technical discussions and fruitful collaborations.

I am thankful to all of my colleagues in the Maryland Optics Group and the Center for Infrastructure Sensors at the University of Maryland for the valuable discussions we have held and assistance we have exchanged throughout my years of graduate study at the University of Maryland. I am particularly thankful to Aniket Desai, Shawn Ho, Sugianto Trisno, Eswaran Baskaran, Yohan Shim, Ruud Egging, Heba Yuksel and Clint Edwards for the technical and non-technical discussions we continuously held.

Finally, I want to thank my family and friends. I can not thank enough my parents, Federico Llorca and Clemencia Sanz, my sister, Raquel Llorca, and my brother Mario Llorca, for their continuous love, patience, and support throughout my entire educational path. I truly appreciate my parents' devotion in helping me to always enjoy, progress and succeed, and providing all of the necessary support, even when being so far apart during most of my graduate studies. I would also like to thank my unconditional friends Antonio Trias and Jesus Bengoechea, who have become my

family away from home, being with me throughout my entire stay at the University of Maryland. I really appreciate the unforgettable time we have spent together, their friendship, love and support. I could not have done it without them.

Table of Contents

List of Tables

List of Figures

Chapter 1: Introduction

1.1 Motivation

1.1.1 Ubiquitous broadband connectivity

Directional wireless communications is emerging as a viable, cost-effective technology for rapidly deployable broadband wireless communication infrastructures [1-3]. This technology provides extremely high data rates, as compared to traditional wireless networks, through the use of narrow-beam free-space optical (FSO) and/or radio-frequency (RF) links, which can transmit large amounts of information point-to-point without causing interference [1-3]. In this dissertation, directional wireless communications is presented as a promising technology for the flexible deployment of broadband wireless backbone networks.

The internet2 and other optical fiber backbone networks provide very high capacity through the guided transmission of laser beams. The physical topology underlying the fiber infrastructure constitutes a fixed and robust mesh, but its deployment is costly and time-consuming. Hosts within reach of the fiber backbone can have broadband connectivity that allows access to next generation multimedia services. The main problem is that a lot of actual and potential users are not likely to be within reach of the fiber backbone. Indeed, it has been estimated that over 90% of U.S. businesses fall less than a mile short of a fiber backbone [2]. Also, broadband

connectivity might be required in remote areas or difficult-to-reach locations. Yet the extension of fiber connectivity to everywhere seems unlikely in the near future. Moreover, as a fixed wired infrastructure, dynamic changes in traffic demands, host mobility, etc, are very hard to handle. The physical topology cannot be dynamically reconfigured and only routing can try to solve problems such as traffic congestion. Thus, ubiquitous broadband connectivity needs flexible extensions to the fiber backbone.

Wireless communication technologies, on the other hand, provide connectivity to mobile hosts and/or hosts away from the fiber backbone. Ad-hoc wireless networks are infrastructure-less. Nodes are both hosts and routers and connect to each other in an ad-hoc manner. The physical topology is flexible allowing for node mobility and reconfiguration, but the interference caused by omnidirectional RF transmissions makes these networks not scalable. Gupta and Kumar showed that the throughput capacity of homogeneous wireless networks decreases with the square root of the number of nodes [4]. In cellular telephony or other base-station oriented wireless networks, hosts are organized in limited size clusters and each cluster is assigned a base-station or access point [4]. In this type of architecture, the very devices that provide wireless service to hosts/clients need lots of wiring themselves to connect to private networks and the Internet. This wiring is expensive to install and change, and deployment must be carefully planned and timed to minimize disruption to normal business operations.

There is a need for flexible broadband infrastructures that could bridge the gap between capacity-limited wireless networks and fixed high capacity backbone

networks. Directional wireless communications combines the high capacity features of point-to-point interference-free communication systems (such as optical fiber networks) with the flexibility of wireless networks.

1.1.2 Directional wireless backbone (DWB) networks

In this dissertation, a novel backbone-based wireless network architecture is presented [5]. The concept is similar to the one adopted in base-station oriented networks, but the advantages of directional wireless communications are used to link together the base-station nodes and form a flexible high capacity network at the backbone layer. Fig. 1.1 illustrates this two-tiered architecture. The lower tier consists of clusters of flat ad-hoc networks based on standard diffused RF technology. The higher tier constitutes a mesh backbone network consisting of a set of base station nodes connected using directional wireless technologies. The advantages of directional wireless communications can be very well exploited at the backbone layer, where line of sight constraints are less restrictive, high data rate is a requirement and interference-free point-to-point communications is extremely attractive to provide a scalable broadband wireless mesh backbone. The interface between both layers is achieved by allowing the backbone nodes the capability of an omnidirectional RF antenna. This way, backbone nodes can give coverage to terminal nodes at the host layer through omnidirectional RF (as is the case of cellular base stations) and make use of directional wireless communications to route aggregated traffic from covered users, over the backbone, with very high data rates and without causing interference. Just like having fiber in the sky!

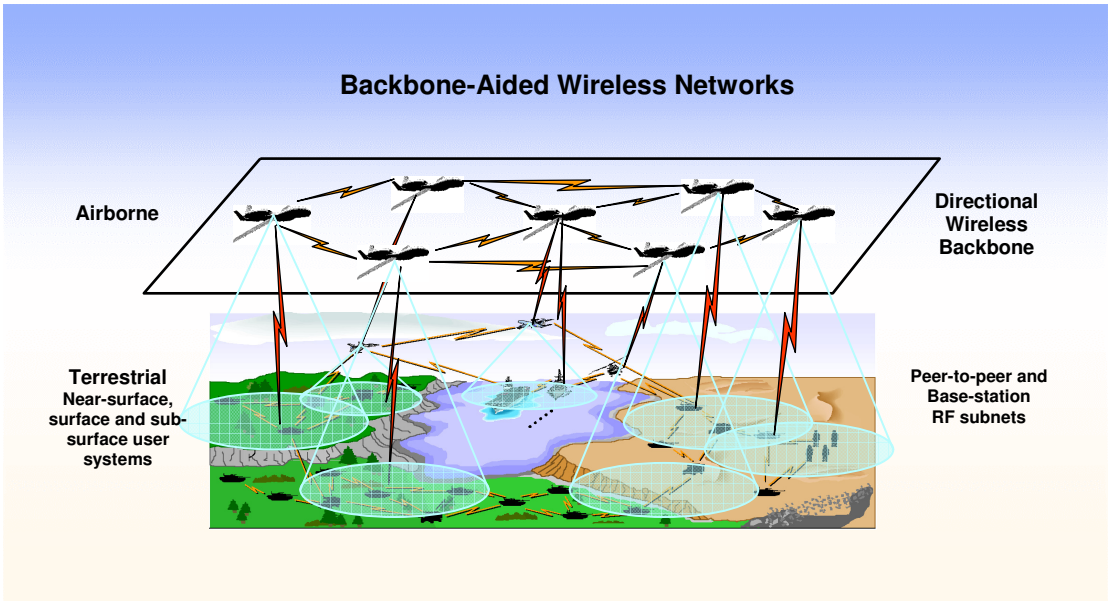

Figure 1.1: Backbone-based wireless network architecture.

The ability to rapidly deploy a broadband backbone to support limited capability hosts or networks will enable what we refer to as “broadband connectivity on demand”. A set of directional wireless base-stations can be rapidly deployed in “demand areas” (demand for broadband connectivity) forming a flexible backbone that will rapidly provide broadband connectivity. Moreover, the fact of being a flexible infrastructure, where base stations can move and links reconfigure, allows for the possibility to adapt to dynamic changes such as host mobility, traffic demands and link state changes. All these issues make directional wireless backbone networks a very promising technology for providing instant broadband communications capabilities in a wide range of situations and scenarios such as: disaster recovery, event response, temporary missions in remote areas, developing or infrastructure-less areas, high-quality real-time video surveillance, monitoring critical infrastructures,

internetworking, last mile solutions, etc. Fig. 1.2 illustrates some of these applications.

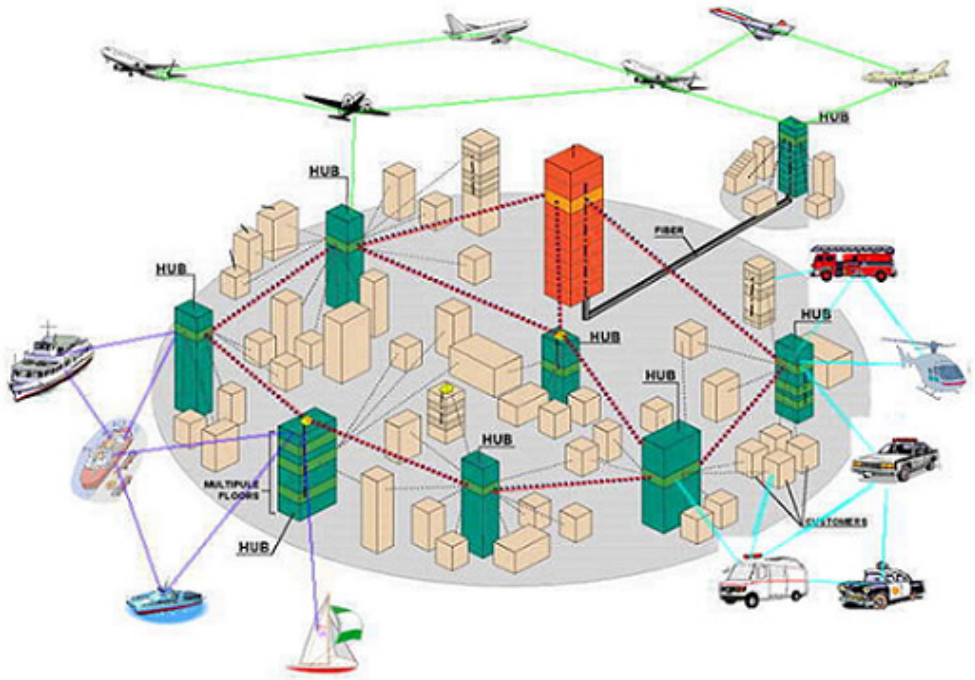

Figure 1.2: Rapidly deployable, flexible broadband communications using directional wireless technologies.

The main challenge in the design of directional wireless backbone (DWB) networks is to provide assured connectivity in dynamic environments. A backbone network must provide highly available broadband connectivity. In this context, two key metrics are defined: robustness and survivability. Robustness refers to the strength of connectivity and its availability. Survivability refers to the ability of the network to regain connectivity in the face of loss or degradation. Optical fiber or other wireline backbones are inherently robust. They are fixed infrastructures with strong, highly available connections, but lack the flexibility to react to dynamic

changes and reach every host in every environment. Ubiquitous broadband connectivity needs broadband wireless backbones. DWB networks put together the high capacity of fiber backbones with the flexibility of wireless networks. The wireless medium, though, has dynamic behavior due to mobility, fading and obscuration. Thus, assuring robustness and survivability in a dynamic wireless environment is a challenging problem. The objective of this dissertation is to: 1) provide a good understanding of the physical nature and dynamics of DWB networks and 2) develop algorithms and protocols for the design of self-organizing DWB networks that could provide assured broadband connectivity in such a dynamic environment.

1.1.3 Self-organization

Topology control is presented as the means to provide self-organization in DWB networks. We define self-organization as the network capability to autonomously reorganize its physical topology.

Controlling the topology of a directional wireless network is fundamentally different from the case of wireless networks based on omnidirectional transmissions. In ad-hoc and sensor wireless networks, power control is used to create topologies that maintain network connectivity while reducing energy consumption and improving network capacity [31]. In directional wireless networks, power control does not change the physical topology and has a negligible effect on the network capacity. The physical nature of directional wireless networks, where links are formed by physically pointing two directional transceivers at each other, and

information is transmitted point-to-point, drives the need to consider new mechanisms for providing self-organization in DWB networks.

In this dissertation, topology control is defined in the context of directional wireless networks, where the physical topology can be reorganized through: 1) topology reconfiguration (TR), which refers to the process by which point-to-point links are broken and set-up for creating a new topology; and 2) mobility control (MC), which refers to the process by which backbone nodes are repositioned to adjust actual and potential link states. The potential of these two mechanisms for creating robust backbone topologies will be studied.

Coverage and connectivity are perhaps two of the most important issues in DWB-based networks. In our backbone-based architecture, the lower tier determines the service demand. From the backbone perspective, there is no control over the lower tier. Clusters at the host layer move according to their respective missions or tasks. Traffic generated at this layer varies accordingly, etc. The objective of the DWB is to dynamically adjust to the lower layer needs and assure overall connectivity. Two main objectives are considered in this dissertation: terminal coverage and backbone connectivity. That is, the DWB must provide coverage to as many terminal nodes as possible and maintain connectivity or bi-connectivity. These are typically competing objectives. That is, maximizing terminal coverage involves backbone configurations where nodes are spread in regions where clusters are deployed, whereas assuring robust backbone connectivity typically involves bringing backbone nodes together to increase connectivity and/or strength of connectivity.

This dissertation presents the design of algorithms and protocols to jointly optimize these two objectives in dynamic environments.

Optimal backbone configurations will strongly depend on the cost model of communications. Thus, a good understanding of the physical nature of the wireless channel is needed. DWB-based networks are heterogeneous in terms of their communication capabilities. Wireless communications technologies DWB networks include RF and infrared transmissions with different antenna patterns (directional versus omnidirectional transmissions). Standard wireless channel models are based on homogeneous RF transmissions and do not take into account effects such as atmospheric attenuation and turbulence-induced fading which are shown to be significant in directional wireless communications. Line of sight (LOS) constraints, atmospheric obscuration, turbulence-induced fading and node mobility are the main contributors to the time variation of the directional wireless channel. In this dissertation, we present atmospheric propagation models for both FSO and directional RF communications. These include attenuation models based on scattering of electromagnetic radiation by suspended water particles in the atmosphere and turbulence-induce fading models. These models are used to characterize communication cost (and as a result, strength of connectivity) in DWB networks. Realistic simulation scenarios including moving cloud layers at different altitudes and turbulence effects have been developed for performance analysis of topology control techniques in dynamic DWB-based networks.

Our overall topology control scheme is aimed to be self-organized. The inspiration for the system's self-organizing capability presented in this dissertation

comes from the theory of potential fields. We propose to model the network as a system of particles in a potential field. A potential energy function, which is related to the energy used for communications in the network system, is used to characterize the cost of a given backbone configuration. Forces between nodes are defined based on network connectivity. The effects of the host layer (cluster mobility) and of the environment (atmospheric turbulence and obscuration) are modeled as external forces changing the potential energy of the network system. Analogies from physical systems such as spring systems are used to model the reaction of the DWB network, which autonomously adjusts its physical topology based on resulting forces to achieve energy minimizing configurations. Mechanisms to mimic this self-organizing behavior are presented in the context of topology reconfiguration and mobility control. The aim is to design a powerful and self-organizing primitive that can achieve diverse configuration goals and that can be gracefully tuned to ensure desirable network properties such as connectivity, coverage, and power efficiency.

1.2 Dissertation Contributions

This dissertation provides a new framework for the modeling, characterization and control of next generation wireless networks. Heterogeneous and dynamic networks are modeled as physical systems where network robustness is characterized by the system's potential energy. A self-organized topology control capability has been developed that mimics the behavior of analogous physical systems whose topologies are adaptive and robust as a result of internal physical interactions among

the nodes forming the network. The algorithms developed are completely distributed, show constant time complexity, achieve optimal solutions from local interactions and ensure desirable network properties such as coverage, connectivity and power efficiency.

The contributions of this work can thus be summarized as follows:

- *Communication networks as physical systems*:

Heterogeneous and dynamic networks are modeled as physical systems whose topologies are adaptive and robust as a result of internal physical interactions among the nodes forming the network. Network robustness is characterized by the system's potential energy. The potential energy of a communications network is defined as the communications energy needed to maintain its physical topology at the required target performance. The network dynamics, in the form of node mobility and channel variations, are modeled as external excitations that change the energy of the network system. Topology control strategies have been developed in order to mimic the natural and self-organized reaction of physical systems to external excitations to minimize the energy of the system by reacting to internal forces exerted on network nodes.

- *Improved link physics models for heterogeneous and dynamic wireless networks*:

Link physics models that account for the variation of the wireless channel due to atmospheric attenuation, turbulence-induced fading, node mobility, and different antenna patterns, have been developed. The developed link physics models are used

to characterize the dynamic behavior of the potential energy stored at the heterogeneous set of wireless links forming the network.

- *Joint coverage-connectivity optimization*:

The topology control problem is formulated as a convex energy minimization problem whose solution is shown to jointly optimize coverage and connectivity in highly dynamic scenarios.

- *Force-driven mobility control*:

The convex optimization method developed results in force-driven mobility control algorithms which make nodes adjust their position in the direction of the net force acting at the node's location. The net force is defined as the negative gradient of the potential energy function at the node's location. Force-driven mobility control algorithms which minimize the energy of the network system are shown to be distributed, scalable, and to ensure desirable global network properties such as coverage, connectivity and power efficiency, from local interactions, thus proving the systems self-organizing capability.

1.3 Organization

The remainder of this dissertation is organized as follows: Chapter 2 introduces the concept of topology control. Previous work on topology control in homogeneous networks is presented and the key differences with respect to topology control in heterogeneous networks are described. Chapter 3 presents our novel physics-based approach to topology control in heterogeneous dynamic networks. In

Chapter 4, link physics models for characterizing the behavior of the heterogeneous set of wireless links forming the network are described. Chapter 5 presents topology reconfiguration algorithms for degree constraint directional wireless backbone networks. Chapter 6 is the main chapter of this dissertation. In chapter 6, a convex optimization method for joint coverage-connectivity optimization is presented as an energy minimization problem. As a result, force-driven mobility control algorithms that are able to react to the network dynamics by autonomously adjusting its physical topology are described. Simulation results show the effectiveness of the algorithms developed. Chapter 7 states the conclusion, summarizes the main contributions of this dissertation and introduces future work.

Chapter 2: Topology Control

2.1 Introduction and background

We define topology control as the autonomous network capability to change its physical configuration (arrangement or layout of the nodes in the network and its communication links). The network topology is represented by a communication graph $G = (V, E)$ where the vertex set V represents the network nodes and the edge set E, the links between them.

Topology control in ad-hoc wireless and sensor networks has been extensively studied in terms of power control. Energy efficiency [31] and network capacity are perhaps two of the most important issues in wireless ad hoc networks and sensor networks. Topology control algorithms have been proposed to maintain network connectivity while reducing energy consumption and improving network capacity. The key idea to power control is that, instead of transmitting using the maximal power, nodes in a wireless multi-hop network collaboratively determine their transmission power and define the network topology by forming the proper neighbor relation under certain criteria. By enabling wireless nodes to use adequate transmission power (which is usually much smaller than the maximal transmission power), topology control can not only save energy and prolong network lifetime, but

also improve spatial reuse (and hence the network capacity) and mitigate MAC-level medium contention [32].

A key feature of the omnidirectional wireless channel is that it is a shared medium. Thus, choosing an excessively high power level causes excessive interference as seen in Fig. 2.1a. This reduces the traffic carrying capacity of the network in addition to reducing battery life. On the other hand, in Fig. 2.1b, having a very small power level results in fewer links and hence network partitioning. When the power level is just right, the network is still connected and there is no excessive interference as shown in Fig. 2.2c. Several topology control algorithms [31-36] have been proposed to create power-efficient network topology in wireless multi-hop networks with limited mobility.

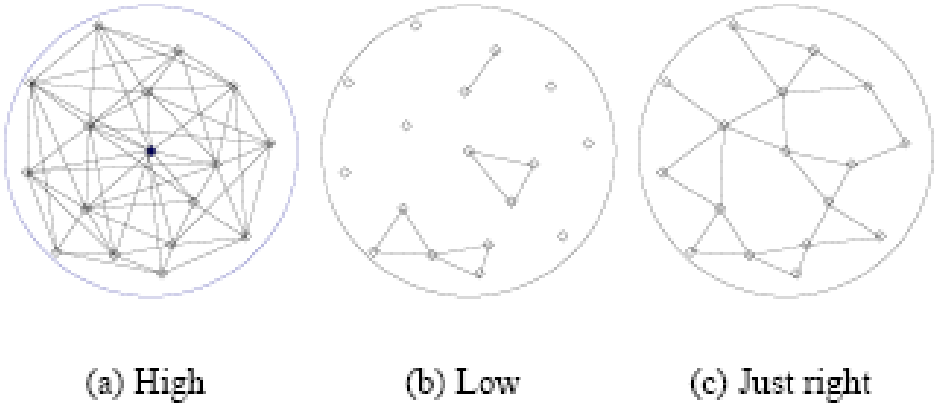

Figure 2.1: Power control in ad-hoc wireless networks.

Despite all this work, Gupta and Kumar showed that wireless networks based on omnidirectional transmissions are inherently not scalable. Their capacity is constrained by the mutual interference of concurrent transmissions between nodes.

The main result shows that as the number of nodes per unit area increases, the throughput per source-to-destination (S-D) pair decreases approximately like $1/\sqrt{n}$, where n is the number of nodes in the network. This is the best performance achievable even allowing for optimal scheduling, routing, and relaying of packets in the network and is a somewhat pessimistic result on the scalability of such networks, as the traffic rate per S–D pair actually goes to zero [4].

In [38], Grossglauser and Tse introduced mobility into the model and considered the situation in which users move independently around the network. Their main result shows that the average long-term throughput per S–D pair can be kept constant even as the number of nodes per unit area increases. This is in sharp contrast to the fixed network scenario and the dramatic performance improvement is obtained through the exploitation of the time variation of the users' channels due to mobility. The result implies that, at least in terms of growth rate as a function of n, there is no significant loss in throughput per S–D pair when there are many nodes in the network as compared to having just a single S–D pair. A caveat of this result is that the attained long-term throughput is averaged over the time-scale of node mobility and, hence, delays of that order will be incurred. In the fixed ad hoc network model, the fundamental performance limitation comes from the fact that long-range direct communication between many user pairs is infeasible due to the excessive interference caused. As a result, most communication has to occur between nearest neighbors, at distances of order $1/\sqrt{n}$ [4], with each packet going through many other nodes (serving as relays) before reaching the destination. The number of hops in a typical route is of order $\sqrt{n}$. Because much of the traffic carried by the nodes is

relayed traffic, the actual useful throughput per user pair has to be small. With mobility, a seemingly natural strategy to overcome this performance limitation is to transmit only when the source and destination nodes are close together, at distances of order $1/\sqrt{n}$. However, this strategy turns out to be too naive. The problem is that the fraction of time two nodes are nearest neighbors is too small, of the order of $1/n$. Instead, the strategy in [38] is for each source node to split its packet stream to as many different nodes as possible. These nodes then serve as mobile relays and whenever they get close to the final destination, they hand the packets off to the final destination. The basic idea is that since there are many different relay nodes, the probability that at least one is close to the destination is significant. On the other hand, each packet goes through at most one relay node and, hence, the throughput can be kept high. Although the basic communication problem is point-to-point, this strategy effectively creates multi-user diversity by distributing packets to many different intermediate nodes that have independent time-varying channels to the final destination.

In the model used in [38], mobility is a random uncontrolled parameter, but the fact that the node mobility changes the network topology is used to improve communication performance. Thus, controlling the mobility of some nodes in the network could be very promising to further improve network performance. However, using controlled node mobility to improve communication performance is a capability that the mobile networking community has not yet paid much attention. In [39], Goldenberg et al. studied mobility as a network control primitive. They presented a completely distributed mobility control scheme where relay nodes align themselves to

provide power-efficient routes for one flow, multiple flows, and many-to-one concast flows. They provided evaluations of the feasibility of mobility control and showed that there are many scenarios where controlled mobility can provide substantial performance improvement.

2.2 Topology control in DWB networks

Next generation wireless networks, and in particular DWB-based networks, are becoming increasingly complex systems due to their heterogeneous architecture and their dynamic behavior. Diverse communication technologies are used at different layers of the architecture in order to provide end-to-end broadband connectivity. The use of directional wireless communication technologies at the backbone layer and its unique behavior compared to traditional omnidirectional RF transmissions needs to be studied in the context of topology control.

In directional wireless communications energy is transmitted point-to-point. Changing transmitted power or moving a node does not necessarily change the actual connections between nodes. Power and mobility control can be used to change potential connectivity and actual energy usage, but in order to establish a new connection a reconfiguration process must occur, where two directional transceivers (one from each node) are pointed to each other so that communication can occur. This makes topology control in directional wireless networks a fundamentally new problem.

In the context of DWB networks:

- *Power control* is used to determine communication cost. The higher the transmitted power needed to maintain a given link BER, the higher the communication cost.
- *Mobility control* is used to change the communication cost of actual and potential links in the network.
- *Topology reconfiguration* is used to break and set up point-to-point links to create a new backbone topology.

Topology control strategies need to address two fundamental questions: 1) what defines a "good" topology (or communication graph), and 2) how to configure such "good" topologies.

With respect to the first question, in DWB networks we seek the formation of robust backbone topologies. That is, topologies that provide the network with the continued ability to perform its function in the face of loss or degradation. A main advantage of directional wireless communications is that the channel is not shared. Directional wireless links are dedicated point-to-point links. Therefore, dense communication graphs do not translate into excessive interference with the resulting reduction in network capacity, as is the case in omnidirectional wireless networks. In DWB networks, on the other hand, dense mesh topologies lead to high network robustness. Constraints come from the limitation on the number of directional transceivers per node and power usage. The cost of a mesh network in terms of number of transceivers and power usage is higher the denser the topology. In this work, TR algorithms to find degree-limited minimum cost topologies in polynomial time are presented. Algorithms have been developed for ring and 3-degree networks

[42]. Also, for a given topology structure, communication cost can be different based on the location of the nodes forming that topology. MC algorithms have been developed to provide power-efficient topologies without breaking or creating new point-to-point links [55, 56].

With respect to the second question above, the process by which a new DWB topology is formed requires 1) the physical redirection of directional transceivers and/or 2) the physical reposition of backbone nodes.

The hardware process that achieves the formation of a new directional wireless link is referred to as pointing acquisition and tracking or PAT [29]. A lot of work has been done in this area and it still remains a very challenging problem, especially when nodes are mobile [29]. This process requires the joint coordination of two nodes for:

- Agreeing in making a connection.
- Identifying each other (location, distance, potential connectivity, etc).
- Coordinating their hardware executions.

Moreover, when several links are changed during the reconfiguration process the network goes into a state of degraded connectivity (which may involve network partitions). Thus, the reconfiguration process has a cost associated with it that needs to be taken into account before making a decision for reconfiguration. On the other hand, moving a backbone node does not incur any loss of data as long as there is enough power to guarantee a minimum BER-defined link performance.

In this dissertation, MC and TR mechanisms have been studied and developed as part of a self-organizing network capability that allows optimizing network performance in dynamic scenarios.

It is important to note that what makes the topology control problem in DWB-based networks a unique problem is the heterogeneous and dynamic nature of such networks. DWB networks form a wireless backbone infrastructure that interconnects a dynamic set of users with lower communication capabilities. Backbone nodes use different communication technologies to communicate with end users and neighbor backbone nodes, whose dynamic behavior and its effect on network performance need to be taken into account.

2.3 Coverage and connectivity

We address the topology control problem for DWB-based networks as a joint coverage-connectivity optimization problem.

Not known approaches till date have considered the joint coverage-connectivity optimization problem in dynamic networks. Work has been done for separately optimizing network coverage and backbone connectivity in relatively fixed scenarios. Optimal base station placement for network coverage optimization is typically addressed as a design problem in the context of clustering or facility location problems (FLP), which are known to be NP-Complete [40]. Centralized approximation algorithms have been developed that achieve close-to-optimal solutions in a relatively fixed scenario. But the need for global network information

makes them not suitable for coping with the heterogeneous and dynamic nature of next generation wireless networks. Also, backbone connectivity is usually assumed to be guaranteed by a fixed backbone infrastructure, a very limiting assumption in a dynamic scenario.

Recent work has addressed the backbone connectivity optimization problem in directional wireless networks [42-50]. In this context, approaches have either considered the topology reconfiguration process in which the location of the backbone nodes is given and the optimization is done over the assignment of links between them; or the relay node placement problem which considers the addition of backbone nodes to provide connectivity between already placed, typically fixed, base stations. In both cases, global network information is required to compute the new topologies. Also, in order to implement them, new point-to-point links need to be set-up, which involve the physical redirection of directional beams with its associated loss of data.

New mathematical models and optimization methods that can address the increasing heterogeneity and dynamic behavior of next generation complex network systems are required. Specifically, new methodologies need to provide:

- Accurate link physics models in order to precisely characterize the behavior of the heterogeneous set of communication links in the network
- Distributed low complexity algorithms for dynamically optimizing network performance by providing the network with the required self-organizing capability.
- Joint coverage-connectivity optimization

Chapter 3: A Physics-based approach to topology control in dynamic wireless networks

3.1 Introduction

Next generation communication networks are becoming increasingly complex systems due to their heterogeneous architecture and dynamic behavior. The need for ubiquitous broadband connectivity is driving communication networks to adopt hierarchical architectures with diverse communication technologies and node capabilities at different layers that provide end-to-end broadband connectivity in a wide range of scenarios.

Modeling such complex systems is a very challenging and cumbersome mathematical problem. New network scientific approaches to modeling such dynamic networks are needed, while at the same time retaining physical reality within the modeling parameters. This dissertation provides new analytical tools to understand the nature of communications in complex wireless networks and its effect on network performance, and control strategies to dynamically optimize network performance in uncertain environments.

3.2 Network robustness and potential energy

We seek methodologies for providing robustness through self-organization in dynamic networks. Very complex systems in a variety of fields can be modeled as networks; that is, a set of nodes that represent the physical entities in the system, and a set of links representing the physical interactions between the system's entities. In nature, physical systems have developed robust self-organizing capabilities in order to adapt to the changing environment. We present topology control mechanisms for complex dynamic wireless networks that mimic the natural and self-organizing behavior of analogous physical systems whose topologies are adaptive and robust as a result of internal physical interactions among the nodes forming the network.

Robustness in physical systems is related to the system's potential energy. Robust network configurations arise when the system's potential energy is minimized. We plan to define potential energy functions to characterize the communications cost of heterogeneous network configurations and develop topology control strategies that try to optimize desirable network properties such as coverage, connectivity and power efficiency, by minimizing the system's potential energy.

The potential energy of a physical system is defined as the energy stored within the system due to its position (physical configuration) in space. A communications network is, in essence, electromagnetic energy being propagated among the nodes forming the network. Therefore, we define the potential energy of a communications network as the total energy stored in the communication links forming the network or the energy used for communications for a given target performance. The potential energy of a communications network is thus determined

by its physical configuration in space or network topology, as defined by the location of the network nodes and the choice of communication links between them.

In dynamic DWB-based networks, changes in the cost of the network topology are due to:

1) Uncontrolled parameters:
    a. End users mobility
    b. Atmospheric obscuration
    c. Node failures.
2) Controlled parameters:
    a. Location of backbone nodes
    b. Connections between backbone nodes

Uncontrolled parameters such as the mobility of terminal nodes (whose motion is determined by their respective missions, tasks, and applications), the presence of atmospheric obscuration, and node failures, change the energy of the network system. For example, two neighbor nodes moving away from each other will increase the energy of the system as more power needs to be transmitted to maintain link performance, while the opposite will occur when the nodes move closer to each other.

In physics, any change in the energy of a system results from the presence of a net force acting on the system. In our model, we characterize uncontrolled parameters changing the energy of the network system as external forces. An external force can increase or decrease the energy of the system. Thus, we can model the network dynamics as external forces changing the energy of the network system. The presence

of atmospheric obscuration and the mobility of nodes changing link distances, act as forces perturbing the equilibrium condition of the network system. We say the network is in equilibrium when the total net force acting on the system is zero, and thus the energy is not changing.

Physical systems naturally react to minimize their potential energy and thereby increase their robustness. Internal forces are responsible for bringing the network to an equilibrium condition where the total energy is minimized. Our approach models network control strategies as internal forces minimizing the energy of the network system.

For example, mobility control schemes should adjust the location of controlled backbone nodes in the direction of the decreasing energy function. We aim to develop algorithms and protocols for mobility control by computing internal forces at each backbone node as negative energy gradients and to show how the network can autonomously achieve energy minimizing configuration driven by local forces exerted on network nodes.

The beauty of this physical energy model is that very complex systems can be characterized with continuous and convex energy functions which take into account the heterogeneity of the network system. Moreover, the network dynamics is naturally characterized as external forces perturbing the energy of the system and control strategies as internal forces reacting to external excitations in order to achieve energy minimizing configurations.

This dissertation also shows how the use of control strategies that minimize the energy of the network system, ensure desirable network properties such as coverage, connectivity and power efficiency.

3.3 Problem statement

In our network architecture, a host *s* communicates with another host *d* in the following way: host *s* transmits its information to the closest backbone node; then the traffic traverses through the backbone network until it reaches the backbone node that is closest to the destination. Finally, the backbone node that is closest to the destination transports the traffic to the host *d*. As it can be observed, this scheme is based on two properties: first, the end hosts need to be well covered by the backbone nodes, and second, the backbone nodes must have good connectivity among themselves.

We formulate the topology control problem in DWB-based networks as an energy minimization problem. We define a potential energy function for the network system as the total communications energy stored in the wireless links forming the network topology, as follows:

$$U = \underbrace{\sum_{i=1}^{N}\sum_{j=1}^{N} b_{ij}u(\mathrm{R_i},\mathrm{R_j})}_{F} + \underbrace{\sum_{k=1}^{M} u(\mathrm{R_{h(k)}},\mathrm{r_k})}_{G}, \tag{3.1}$$

where $\mathrm{R_i}$ is the location of backbone node *i*, $\mathrm{r_k}$ the location of terminal node *k*, *N* the number of backbone nodes, *M* the number of terminal nodes, *h(k)* the index of the

backbone node covering terminal node k, and b_{ij} the integer variables that determine the backbone topology:

$$b_{ij} = \begin{cases} 1 & \text{if } (i,j) \in T \\ 0 & \text{o.w.} \end{cases}, \tag{3.2}$$

where T refers to the backbone topology. The link cost function $u(\mathrm{R_i}, \mathrm{R_j})$ represents the potential energy of link (i,j) and will be precisely defined in the following chapter as the communications energy per unit time needed to send information from node i to node j at the specified BER.

Note that the first term in of the cost function, denoted by F, represents the total energy stored in the directional wireless links forming the backbone network, and the second term G represents the total energy stored in the wireless links covering the end users. Thus, F is a measure of cost for the backbone connectivity, i.e. a higher value of F indicates a backbone topology where higher communications energy needs to be provided in order to maintain backbone nodes connected. On the other hand, a higher value of G indicates a higher demand for communications energy in order to maintain end users covered at the specified QoS (BER).

Thus, we formulate the joint coverage-connectivity optimization problem as a weighted multi-objective optimization problem of the following form:

$$\begin{aligned} \min U(b_{ij}, \mathrm{R}_1, ..., \mathrm{R}_\mathrm{N}) &= \eta \cdot F + G \\ &= \eta \cdot \left(\sum_{i=1}^{N} \sum_{j=1}^{N} b_{ij} u(\mathrm{R_i}, \mathrm{R_j}) \right) + \left(\sum_{k=1}^{M} u(\mathrm{R_{h(k)}}, \mathrm{r}_k) \right). \end{aligned} \tag{3.3}$$

$$\text{s.t. } b_{ij} = \begin{cases} 1 & \text{if } (i,j) \in T \\ 0 & \text{o.w.} \end{cases}$$

Note that in the above formulation the optimization is performed over 1) the assignment of directional wireless links between backbone nodes b_{ij} and 2) the location of the N backbone nodes $(\mathrm{R}_1,...,\mathrm{R}_\mathrm{N})$. These are the controllable parameters from the topology control perspective. TR mechanisms determine the link assignments b_{ij} and MC mechanisms determine the locations $(\mathrm{R}_1,...,\mathrm{R}_\mathrm{N})$.

A stated earlier, the term F in the above cost function is a metric of connectivity of the backbone nodes, and minimizing it results in a strong DWB topology. The term G, on the other hand, is a metric of coverage and minimizing it results in high network coverage. The parameter η $(\eta \geq 0)$ acts as a balancing factor between the two optimization terms. Minimizing the above cost function J for different values of η will produce Pareto-optimal solutions.

The cost function U represents the potential energy of the communications network, i.e. the communications energy needed to create/maintain/guarantee the communications functionality in the network system. It can also be thought as the communications energy stored in the network system, i.e. the potential energy of an analogous physical system where communications links define forces of interaction between network nodes.

Of key importance in the optimization problem stated in Eq. 3.3 is therefore to define the link cost functions u_{ij} that will determine the form of the overall cost function U. In the following section, we present link cost models that take into account the energy usage for the different wireless technologies used in DWB networks.

Chapter 4: Physical layer characterization

4.1 Introduction and background

Modeling the propagation channel has always been one of the most difficult parts of the design of wireless communication systems. Typically, the channel variations are characterized statistically and are grouped into two broad categories: large-scale and small-scale variations. Large-scale propagation models are used to predict the mean signal power for any transmitter-receiver (TX-RX) separation. Small-scale signal models characterize the rapid fluctuations of the received signal strength over very short travel distances [6]. The most common channel model used in wireless communication systems has the following components.

- *Path loss*: the received signal power averaged over large scale variations has been found to have a distance dependence which is well modeled by $1/d^n$, where d denotes the TX-RX distance and the exponent n is determined from field measurements for the particular system at hand [6].
- *Large-scale variations*: these are modeled by the lognormal shadowing model. In this model, the received signal power averaged over small-scale variations is statistically described by a lognormal distribution with the distance-dependent mean obtained from the path loss calculation [6].

- *Small-scale variations*: these are modeled by a Rayleigh distribution. In the Rayleigh model, the received signal is a wide-sense stationary stochastic process whose amplitude at each point in time is a Rayleigh random variable [6].

Small-scale variations are typically due to multipath. That is, the received signal is the superposition of two or more streams of the same data that have traveled through different paths. This effect is especially common in terrestrial wireless communication systems where information is sent isotropically and different rays can reach the same receiver having traveled different paths, due to reflections in buildings or other obstacles. Typically, a wireless communication receiver is designed with diversity reception to combat small scale variations, which means that the receiver can collect streams of the same data that have traveled through independent paths. A widely used diversity technique is the Rake receiver in spread-spectrum communication systems, which collects multipath components at intervals of the chip period [6-8]. A technique called maximum ration combining (MRC) is used to optimally combine these independent streams. In a full Rake receiver, all multipath components are collected and combined optimally. Directional wireless networks, on the other hand, involve line of sight (LOS) point-to-point transmissions and thus there are no multipath effects [1].

Large scale variations are typically due to shadow fading effects caused by the presence of large obstructions in the path between the transmitter and the receiver [6]. In wireless communication systems a tolerable bit-error-rate (BER) is specified for

large scale variations. Based on the tolerable BER, a minimum received signal power is required to account for the signal fades and guarantee the specified BER.

In directional wireless communications, large scale signal variations are quite important and are mainly due to atmospheric turbulence. This effect is especially strong in FSO links. Optical turbulence is caused almost exclusively by temperature variations in the atmosphere, resulting in the random variations of refractive index. An optical field propagates through the atmospheric turbulence will experience random amplitude and phase fluctuations, which will generate a number of effects: break up of the beam into distinct patches of fluctuating illumination, wander of the centroid of the beam, and increase in the beam width over the expected diffraction limit [13-17]. In terms of communications performance, the intensity fluctuations produced by atmospheric turbulence translate into reduced signal-to-noise ratio (SNR) and increased link bit-error-rate (BER). In direct-detection FSO systems using on-off keyed (OOK) modulation, the BER is found to be:

$$BER = \frac{1}{2}\operatorname{erfc}\left(\frac{1}{2\sqrt{2}}\sqrt{SNR_0}\right), \tag{4.1}$$

where SNR_0 is the signal to noise ratio in the absence of atmospheric turbulence, defined as:

$$SNR_0 = \frac{\langle i_S \rangle^2}{\sigma_N^2} = \frac{\left(\Re\langle P_S \rangle\right)^2}{2eB\Re P_S + \frac{4kTB}{R}}, \tag{4.2}$$

where i_s is the output signal current from the detector, σ_N is the noise variance (zero-mean white Gaussian noise is assumed), P_s is the received signal power, $\Re$ is the receiver responsivity, B is the bandwidth, k is the Boltzmann constant, T is the

effective noise temperature, and *R* is the effective resistance of the receiver circuitry [9]. In Eq. 4.1 the threshold level is set at half the average signal level $i_{TH} = i_S/2$.

In the presence of optical turbulence, the signal current is a random variable $i = i_S + i_N$ with mean $\langle i_S \rangle$ and variance $\sigma_i^2 = \sigma_S^2 + \sigma_N^2$. The averaged SNR is given by:

$$\langle SNR \rangle = \frac{\langle i_S \rangle^2}{\sigma_i^2} = \frac{SNR_0}{\left[1 + 1.33\sigma_I^2 \left(\frac{2L}{kw_L^2}\right)^{5/6}\right]^2 + SNR_0 \sigma_I^2}, \tag{4.3}$$

where σ_I is the variance of the intensity fluctuations, *L* the link length and w_L the spot size [15]. Note from Eq. 4.3 that in the presence of atmospheric turbulence the average SNR is always lower than SNR_0. The resulting BER is obtained averaging Eq. 4.1 over the intensity fluctuation spectrum. This leads to the expression:

$$BER = \frac{1}{2}\int_0^\infty p_I(i_S)\,\mathrm{erfc}\left(\frac{i_s}{2\sqrt{2}\langle i_s \rangle}\sqrt{\langle SNR \rangle}\right) di_S\,, \tag{4.4}$$

where $p_I(i)$ is the probability density function (PDF) of the intensity fluctuations. A lognormal distribution is generally used to model $p_I(i)$ [15]. Fig. 4.1 shows the calculations of BER for an FSO system as a function of SNR_0, for intensity variance ranges from 0.001 to 0.5 [15].

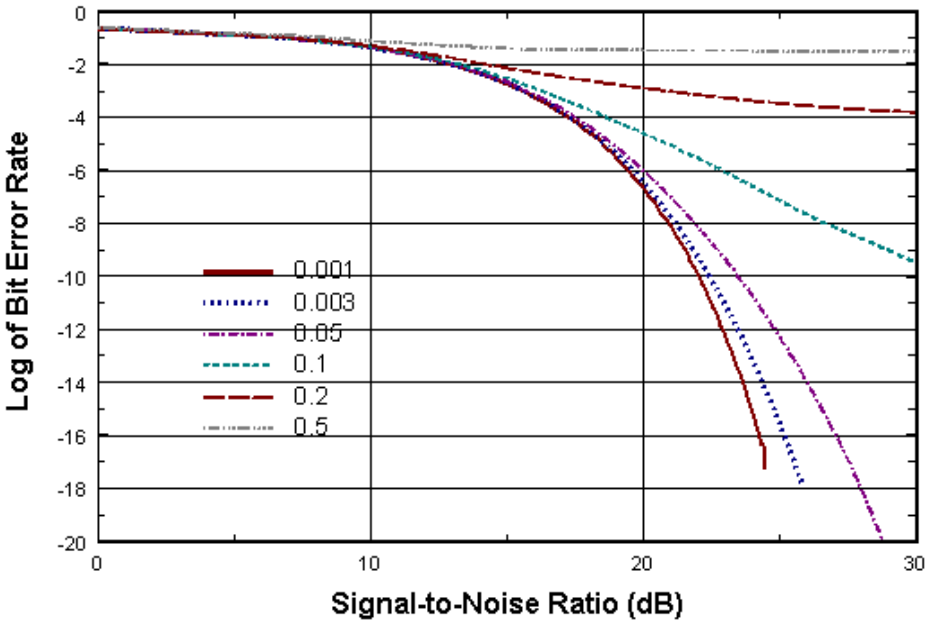

Figure 4.1: BER of an FSO system at different intensity variance values.

A lot of work has been done to design techniques for mitigating the effects of optical turbulence. These techniques involve transmitter and/or receiver designs such as aperture averaging and delay diversity techniques [18-20].

In this dissertation, turbulence-induced fading models for both RF and FSO technologies are used for link margin calculations. The minimum received power needed to guarantee a specified link BER is computed based on these models.

In the context of topology control, the most important channel factor to consider is the path loss. Given the receiver sensitivity and the link margin for turbulence-induced fading, the transmitted power needed to guarantee that the received power is above the link margin will depend on the path loss.

In general, path loss is a function of the link distance and the link directivity. In directional wireless communications, moreover, absorption of the beam by the

atmosphere can be important, especially in adverse weather conditions of fog, clouds, rain, snow, or in conditions of battlefield obscuration [21]. The combined effects of direct absorption and scattering of electromagnetic radiation can be described by a single path-dependent attenuation coefficient $\alpha(z)$. The power reaching a RX from a TX can easily be calculated for links without significant turbulence effects. The received power P_R for a RX with receiver area A, coming from a transmitter at range L and beam divergence angle θ, varies as:

$$P_R = P_T e^{-\alpha L} \frac{2A}{\pi \theta^2 L^2}, \tag{4.5}$$

where P_T is the transmitted power, and α in this case is assumed constant along the propagation path L. This result assumes a directional beam whose beam width at the receiver is significantly greater than the receiver diameter. Tightly collimated systems have been proposed [23] for which $P_R = P_T e^{-\alpha L}$.

In this dissertation, atmospheric propagation models for both FSO and RF communication will be presented. These include attenuation models based on scattering of electromagnetic radiation by suspended water particles in the form of fog and clouds, turbulence-induced fading models and directivity-driven free space path loss. These models are used to extend current wireless channel models in order to provide a more comprehensive characterization of the wireless channel in increasingly heterogeneous and dynamic wireless networks. Communication cost in DWB-based networks will be defined based on the developed models.

4.2 Communication cost model

In DWB-based networks backbone nodes use a hybrid communication mode in order to communicate with both end users and neighbor backbone nodes. Omnidirectional RF transmissions are used to cover end users at tier 1 of the architecture while directional wireless communications are used to aggregate traffic from end users and transport it through the backbone at tier 2 (see Fig. 1.1). Moreover, directional wireless communications use both RF and FSO technologies to send information point-to-point without causing interference. Thus, we need to define a general link cost function for a wireless link *(i,j)* that takes into account the behavior of the diverse wireless technologies used in next generation wireless networks (omnidirectional RF, directional RF and directional FSO).

In this work, we focus on the communications energy used at the wireless links forming the network and define the general link cost function for a given link *(i,j)* as the transmitted power needed at transmitter *i* in order to guarantee a specified BER at receiver *j*:

$$u_{ij} = P_{R0}^{j} \cdot \tau_{ij}, \tag{4.6}$$

where P_{R0}^{j} is the minimum received power at node *j* in order to guarantee the specified BER and τ_{ij} is the path loss or path attenuation for link *(i,j)*. We refer to P_{R0}^{j} as the link margin and will be described based on the large scale variations of the wireless channel in section 4.3. The path loss τ_{ij} for a link *(i,j)* with distance *L* defined as $L = \left\| \mathrm{R_i} - \mathrm{R_j} \right\|$, where $\mathrm{R_i}$ and $\mathrm{R_j}$ are the locations of nodes *i* and *j* respectively, is described in terms of two main components:

$$\tau_{ij} = \underbrace{e^{\alpha_{ij}\left\|\mathrm{R_i}-\mathrm{R_j}\right\|}}_{\tau_{obs}} \underbrace{\frac{4\pi}{D_T^i A_{eR}^j}\left\|\mathrm{R_i}-\mathrm{R_j}\right\|^n}_{\tau_{fs}}, \tag{4.7}$$

where τ_{obs} refers to the atmospheric obscuration (or attenuation) and τ_{fs} to the free space path loss. The atmospheric obscuration component is an exponential function of the link distance *L* with atmospheric attenuation coefficient α, and will be described in section 4.4.2. The free space path loss component is a polynomial function of the link distance (typically quadratic in non urban areas) and inversely proportional to de product $D_T A_R$. The product $D_T A_R$ determines the link directivity and will be described in section 4.4.1.

Using Eq. 4.7, the general link cost model becomes:

$$u_{ij} = \underbrace{\underbrace{\left(P_{R0}^j\right)}_{\text{link margin}} \underbrace{\left(e^{\alpha_{ij}\left\|\mathrm{R_i}-\mathrm{R_j}\right\|}\right)}_{\tau_{obs}} \underbrace{\left(\frac{4\pi}{D_T^i A_{eR}^j}\left\|\mathrm{R_i}-\mathrm{R_j}\right\|^n\right)}_{\tau_{fs}}}_{\tau}, \tag{4.8}$$

where again u_{ij} represents the cost of link (*i*,*j*) in terms of the communications energy per unit time needed to assure a specified BER when sending information from node *i* to node *j*, as illustrated in Fig. 4.2.

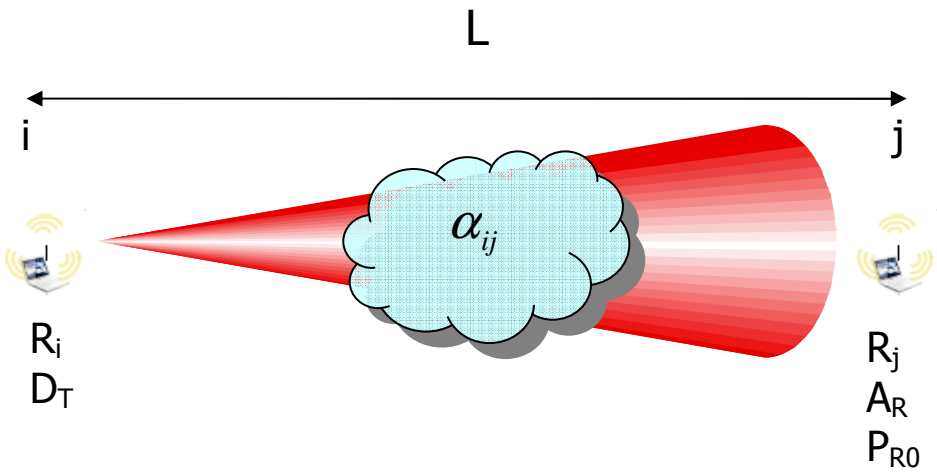

Figure 4.2: Wireless link model parameters.

The link cost function in Eq. 4.8 will be used to characterize the potential energy of the network system, as stated in Eq. 3.1. Recall that the idea is to abstract the communications network as a physical system where communication links define physical interactions between network nodes, which are determined based on the variation of the potential energy. In the following sections we precisely define the three main components of the link cost function u_{ij}: 1) link margin, 2) atmospheric attenuation, and 3) free space path loss.

4.3 Turbulence induced fading

Large scale time variations of the received signal intensity in directional wireless communications are mainly due to atmospheric turbulence. A lot of work has been done to characterize atmospheric turbulence [13-17], and several techniques have been developed to mitigate its effects on FSO communication links [18-20]. In

this dissertation we present models that characterize turbulence-induced fading for both FSO and RF links. These models are used to define the probability density function (PDF) of the intensity fluctuations $p_I(i)$ at the receiver.

In FSO communications a lognormal distribution is generally used to model $p_I(i)$ [15]. One way to measure the strength of atmospheric turbulence is by examining the variance of the log intensity fluctuations (Rytov variance [19]) described as:

$$\sigma_R^2 = 1.23 C_n^2 k^{7/6} L^{11/6}, \tag{4.9}$$

where C_n^2 is the atmosphere refractive index structure parameter, $k = 2\pi/\lambda$ is the wave number, and L is the propagation length [15]. In terms of this parameter, the turbulence is called "weak" if $\sigma_R^2 < 0.3$, and "strong" turbulence if $\sigma_R^2 > 1$, although true strong turbulence may need $\sigma_R^2 > 25$ [15].

Fig. 4.3 compares the variances calculated using Fante's weak and strong turbulence theories with the Rytov value [19]. It also shows the path of a composite curve that is predicted to be valid over all turbulence strengths.

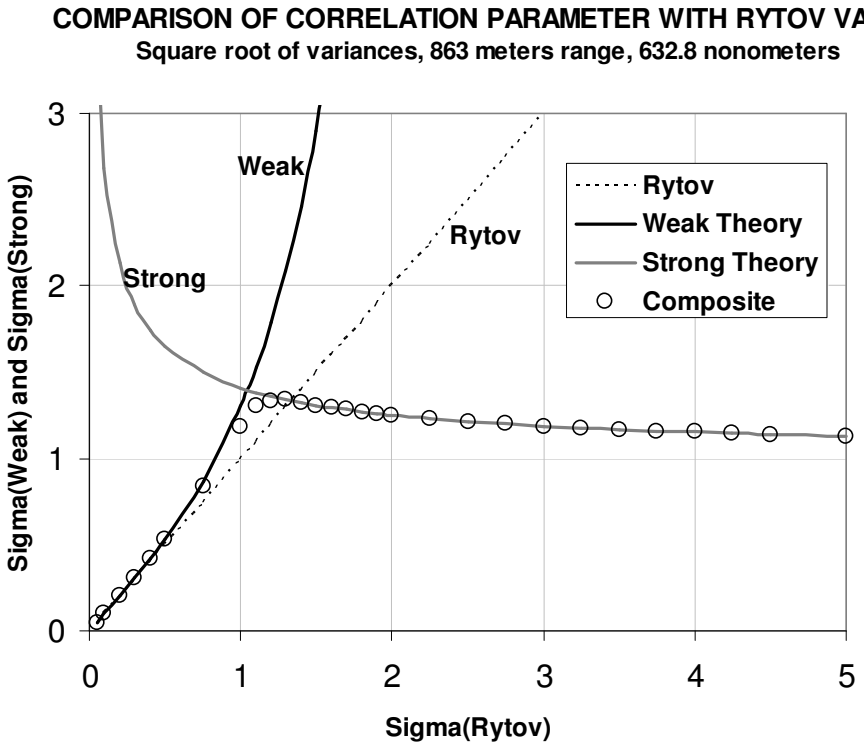

Figure 4.3: Weak and Strong Variances compared with the Rytov value [20]. Circles shown represent the path of a composite curve that is predicted to be valid over all turbulence strengths.

Note that the "Weak" curve follows the linear variation predicted by the Rytov variance well up to $\sigma_R^2 = 0.3$. The "Strong" curve is not valid for small values of σ_R^2, but should represent expected variances well for $\sigma_R^2 > 1$. The circles in Fig. 4.3 represent a path for a "composite curve" that follows σ_{weak} for small σ_R^2 and then merges with σ_{strong} for larger σ_R^2. Such a composite curve demonstrates the increase in intensity variance that occurs as turbulence increases followed by its saturation at high levels of turbulence.

Under weak turbulence conditions, where the Rytov approximation holds, the parameter that determines the turbulence strength is the C_n^2 value (from Eq. 4.9). Fig. 4.4 shows examples of the Rytov variance in the operating range below 1km for various turbulence strengths with C_n^2 values range from 10^{-13} to 10^{-17}, and an optical wavelength of 1310nm.

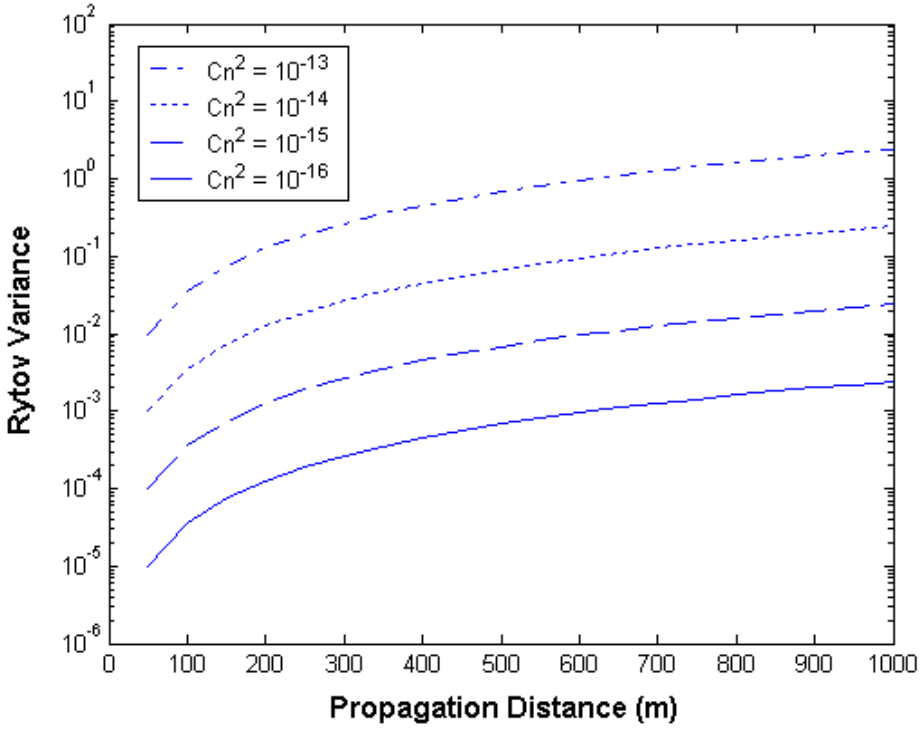

Figure 4.4: Rytov variance versus propagating distance (1310nm beam) for different Cn^2 values.

In the case of RF links, which use electromagnetic waves in the millimeter and microwave region, Clifford and Strohbehn [13] derived a general result for the amplitude and phase fluctuations, which for the most practical propagation paths of interest reduce to the formulas presented earlier for optical wavelengths. Thus the

Rytov variance as described in Eq. 4.9 will be used to determine the amplitude of intensity fluctuations for RF links as well. Note that due to the $k^{7/6}$ dependence, RF links, which use larger wavelengths than optical links, will experience less intensity fluctuations and therefore will be more resistant to turbulence effects.

The BER is used as a measure of link performance at the physical layer. A link is considered feasible for communications if its BER is below a given threshold (typically 10^{-9}-10^{-6}). The link BER can be derived from the signal-to-noise ratio (SNR) and the probability density function of the intensity fluctuations $p_I(i)$ using Eq. 4.4:

$$BER = \frac{1}{2}\int_0^\infty p_I(i_S)\,\mathrm{erfc}\left(\frac{i_s}{2\sqrt{2}\langle i_s\rangle}\sqrt{\langle SNR\rangle}\right)di_S\ .$$

From the above equation, the average signal-to-noise ratio $\langle SNR\rangle$ required to guarantee a specified BER can be computed. The required SNR_0 can then be found using Eq. 4.3:

$$\langle SNR\rangle = \frac{SNR_0}{\left[1+1.33\sigma_I^2\left(\frac{2L}{kw_L^2}\right)^{5/6}\right]^2 + SNR_0\sigma_I^2}$$

Finally, the required average received power P_{R0} is obtained using Eq. 4.2 as:

$$P_{R0} = \sqrt{SNR_0}\,\frac{\sigma_N}{\Re}, \tag{4.10}$$

where $\Re$ is the receiver responsivity and σ_N the noise standard deviation.

Based on these models, the minimum received power P_{R0} for every potential link in the network can be determined.

4.4 Path loss

Directional wireless backbone networks are typically deployed at high altitudes, where line of sight can be exploited. DWB nodes can be deployed on top of buildings or other infrastructures, or can be airborne, for example involving UAVs (Unmanned Aerial Vehicles) at very high altitudes. Thus, the propagation medium where directional wireless links are going to be deployed typically involves the low layers of the atmosphere.

Path loss is defined as the attenuation undergone by an electromagnetic wave in transit between a transmitter and a receiver. The path loss τ for a wireless link can be derived as the ratio between the transmitted power and the received power:

$$\tau = \frac{P_T}{P_R} = \underbrace{e^{\alpha L}}_{\tau_{obs}} \underbrace{\frac{4\pi}{D_T A_{eR}} L^n}_{\tau_{fs}}, \tag{4.11}$$

where τ_{obs} refers to the path loss due to atmospheric obscuration and τ_{fs} to the free-space path loss. In the following sections we will describe in detail these two main path loss components.

4.4.1 Free space path loss

The free space path loss measures the attenuation of an electromagnetic signal that would result from a line of sight path through free space, with no atmospheric obscuration effects, and it is defined as:

$$\tau_{FS} = \frac{4\pi}{D_T A_{eR}} L^n, \tag{4.12}$$

which is a polynomial function of the link distance. The $\frac{4\pi}{D_T A_{eR}}$ constant is independent of the nodes' locations and will be determined by the directivity of the transmitter antenna D_T and the effective receiver area A_{eR} [6].

In this work we are especially interested in studying the effects of different link directionalities on the free space path loss. The directivity D_T of a transmitter is defined as the ratio of the maximum power density to the power density of a completely isotropic transmission, as described by:

$$D_T = \frac{\mathrm{P}(\theta,\phi)_{\max}}{\frac{P_T}{4\pi L^n}} \tag{4.13}$$

The directivity measures the confinement of electromagnetic energy in the direction of maximum radiation and can be computed as a function of the solid angle of the electromagnetic beam as:

$$D_T = \frac{4\pi}{\Omega}. \tag{4.14}$$

The solid angle Ω can be computed in spherical coordinates as:

$$\Omega = \int_0^{2\pi}\int_0^{\theta} \sin\theta \, d\theta d\phi = 2\pi(1-\cos\theta), \tag{4.15}$$

where θ is the half angle beam divergence [6] as illustrated in Fig. 4.5:

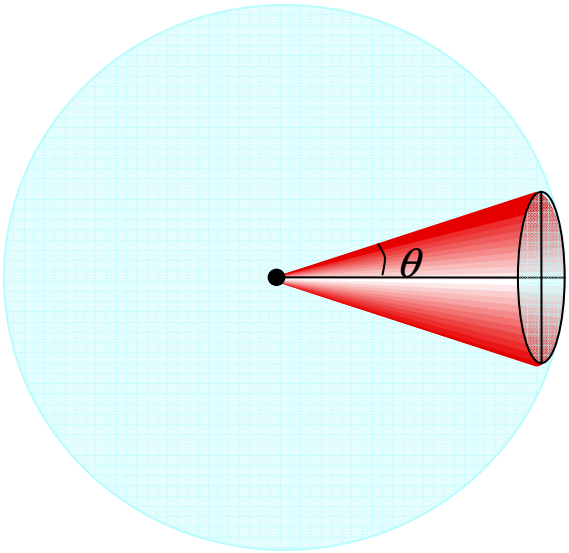

Figure 4.5: Directional wireless beam illustration.

Note that for a completely isotropic transmission, described by a half angle beam divergence of π radians, the solid angle is equal to 4π, giving a directivity of 1. As soon as the electromagnetic energy is concentrated in smaller beams, the directivity increases reducing the free space path loss. When the half angle beam divergence is small enough $\theta << 1$, we can use the Taylor expansion approximation $\cos\theta \approx 1 - \frac{\theta^2}{2}$, which leads to the following expression for the solid angle:

$$\Omega \approx \pi\theta^2 . \tag{4.16}$$

Using this approximation the free space path loss for highly directional wireless links can be computed as:

$$\tau_{fs} \approx \frac{\pi\theta^2}{A_{eR}} L^n . \tag{4.17}$$

In general, the term $\frac{4\pi}{D_T A_{eR}}$ will be computed based on the specific directivity of the wireless link in consideration, but it will always be a constant independent of the nodes' locations. Thus, the free space path loss is modeled as a polynomial function of the form $f = a \cdot x^n$, where the constant *a* is determined by the link directionality and the polynomial order *n* by the path loss exponent, which typically takes the value of 2 unless significant obstacles are present such as in urban areas, where it can take values up to 6 [6].

Thus, assuming a path loss exponent *n=2* and clear atmosphere conditions (α = 0), the general link cost function u_{ij} in Eq. 4.8 becomes:

$$u_{ij} = \left(P_{R0}^{j} \frac{4\pi}{D_T^i A_{eR}^j} \right) \left\| \mathrm{R_i} - \mathrm{R_j} \right\|^2, \tag{4.18}$$

which is a quadratic function of the link distance. As explained in the previous section, the minimum received power P_{R0} is determined by the channel fading and the receiver sensitivity, and will not change with the location of the backbone nodes (under the assumption that the deployment area of the backbone nodes share the same turbulence conditions). The $\frac{4\pi}{D_T A_{eR}}$ constant will also be independent of the backbone nodes' locations and will be determined by the directivity of the transmitter antenna D_T and the effective receiver area A_R. Thus, the link cost u_{ij} as defined in Eq. 4.18 is a function of the form $f = k \cdot x^2$, which is analogous to the potential energy of a spring, with spring constant $k = P_{R0} \frac{4\pi}{D_T A_{eR}}$ and displacement *x*, the link distance [53].

Using the link cost model form Eq. 4.18, we can model wireless links as springs which exert attraction forces between network nodes for energy minimization.

The beauty of this model is that given the required received power P_{R0}, and the effective receiver area A_{eR}, the spring constant is inversely proportional to the transmitter directivity D_T. Thus, directional wireless links which have high directivities translate into springs with low spring constants, which allow for higher link distances. On the other hand, omnidirectional wireless links use low directivity antennas associated with high spring constants that require much more energy to elongate. This result is very much in accordance with our network architecture, where directional wireless links are used to connect backbone nodes over large distances, whereas omnidirectional wireless links are used to connect each terminal node to its assigned base station (see Fig. 1.1).

As an example, Fig. 4.6 shows three wireless links with different directivity values and their associated spring models with their respective spring constant values. In these examples P_{R0} is assumed to be 1 *Watt* and A_{eR} 1 m^2.

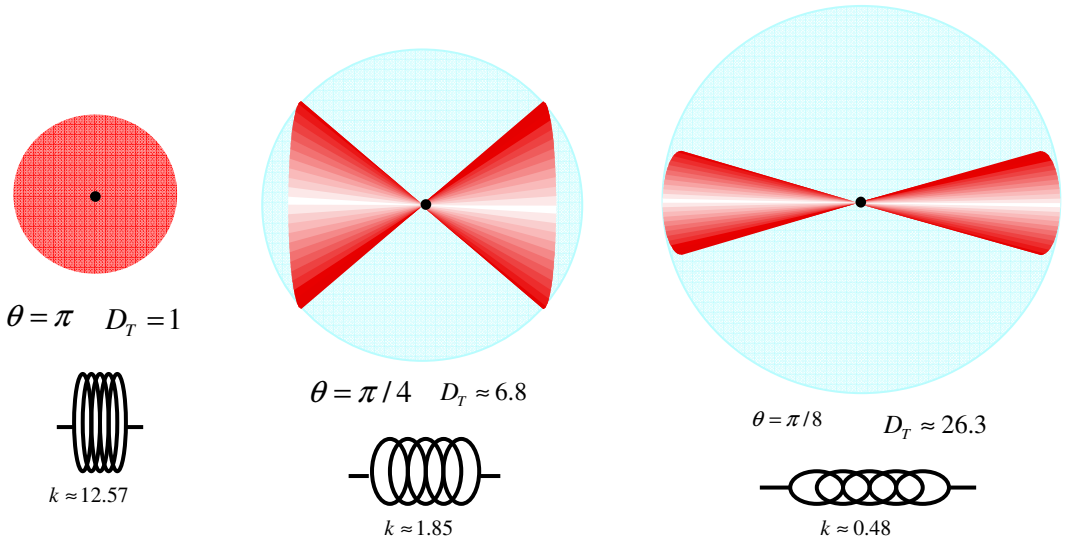

Figure 4.6: Spring model for wireless links.

4.4.2 Atmospheric attenuation

The atmospheric attenuation measures the attenuation of the electromagnetic signal due to the combined effects of absorption and scattering of the beam by the atmosphere. Atmospheric attenuation is especially important in directional wireless links deployed at high altitudes and in adverse weather conditions of fog, clouds, rain, snow, or in conditions of battlefield obscuration [21]. The combined effects of direct absorption and scattering of electromagnetic radiation are described by an exponential function of the link distance as:

$$\tau_{obs} = e^{\alpha L}, \tag{4.19}$$

where the single path-dependent attenuation coefficient $\alpha(z)$ defines the attenuation of the signal power as it travels through the atmosphere, caused by the presence of obscurants such as clouds, rain and snow. Atmospheric attenuation is mainly due to

scattering of electromagnetic radiation by the suspended water particles forming such obscurants.

The cloud attenuation (in dB per unit length) at infrared frequencies (FSO links) can be described as

$$\tau_{FSO} = 10\log(e)\cdot\alpha_{SCAT}, \tag{4.20}$$

where α_{SCAT} is the scattering coefficient and L the link length. The scattering coefficient is defined as

$$\alpha_{SCAT} = nQ\pi r^2, \tag{4.21}$$

where r is the effective radius of the water particles, n is the number of particles per unit volume, and Q is the scattering efficiency, which is approximated by a value of 2 for infrared wavelengths and typical cloud water particle sizes [23]. As seen in Eq. 4.21, the scattering coefficient is a function of the size and density of cloud water particles.

In the case of RF links, the cloud attenuation (in dB per unit length) is related to the cloud water content using the Rayleigh approximation for small water droplets [24]:

$$\tau_{RF} = 0.4343\left(\frac{3\pi v}{32\lambda\rho}\right)\mathrm{Im}\left(\frac{1-\varepsilon}{2+\varepsilon}\right), \tag{4.22}$$

where v is the cloud liquid content (for cirrus clouds, the ice water content I is used instead), ρ is the density of water, λ is the wavelength, and ε is the complex dielectric constant of water.

Table 4.1 shows typical attenuation values for both technologies and for several cloud types at different altitudes. Typical values for r, n, v and I, for different

cloud types, were obtained from the Bulletin of the American Meteorological Society [25-26]. The attenuation value is given in dB when going through 1 km of cloud obscuration. Table 4.1 values show that cloud attenuation is much more significant at infrared frequencies (FSO links), where scattering of the optical beam by water particles is dominant.

	Layer Height (km)	**Cloud Type**	**Average τ_{RF} (dB/km)**	**Average τ_{FSO} (dB/km)**
Layer 1	0-1	Fog, Stratus	0.43, 1.4	136, 274
Layer 2	1-2	Stratus, Cumulus	1.4, 2.8	274, 543
Layer 3	2-6	Altostratus, Altocumulus	0.98	191
Layer 4	6-8	Cirrus	0.17	122

Table 4.1: Typical cloud attenuation values at different atmospheric layers.

These models are used to compute the path loss for every potential link in the network. It is important to note that atmospheric attenuation is path dependent. In the path from a node A to a node B, electromagnetic radiation can encounter different atmospheric agents giving raise to different attenuation values. Thus, the total path loss due to atmospheric attenuation for a given link AB needs to be computed by integrating the path dependent attenuation parameter $\tau(z)$ along the link path, as:

$$\tau_{AB} = \int_{Z_A}^{Z_B} \tau(z) dz \,, \tag{4.23}$$

where Z_A and Z_B are the link path components of the location of nodes A and B respectively, and the integration is over the direction of propagation z. If the

obscuration factor remains constant along the path from A to B, Eq. 4.23 becomes a function of L and the total path loss can be computed as:

$$\tau = \tau_{obs} L + 10\log\left(\frac{4\pi}{D_T A_{eR}} L^n\right), \tag{4.24}$$

where the link distance L is defined as $L = \|\mathrm{R_A} - \mathrm{R_B}\|$, and $\mathrm{R_A}$ and $\mathrm{R_B}$ are two or three-dimensional vectors depending on the topology of the area on which nodes are distributed.

In our simulations, a finite grid is used in which each cell is assigned a cloud attenuation value. Free space cells are assigned a value of zero. For that case, the path loss can be approximated using the following equation:

$$\tau = \sum_i \tau_i L_i + 10\log\left(\frac{4\pi}{D_T A_{eR}} L^n\right), \tag{4.25}$$

where L is the distance between A and B, τ_i is the atmospheric attenuation per unit length for section i of the path AB, L_i the section length, and the summation is over the path AB as shown in Fig. 4.7.

In section 4.5 we describe a methodology to generate dynamic 3D scenarios including moving cloud layers at different altitudes. The objective is to develop a simulation tool that would allow 1) the generation of network dynamics in the form of node mobility, atmospheric obscuration and channel fading, and 2) the characterization of such scenario in the form of a network cost matrix using the presented link cost models.

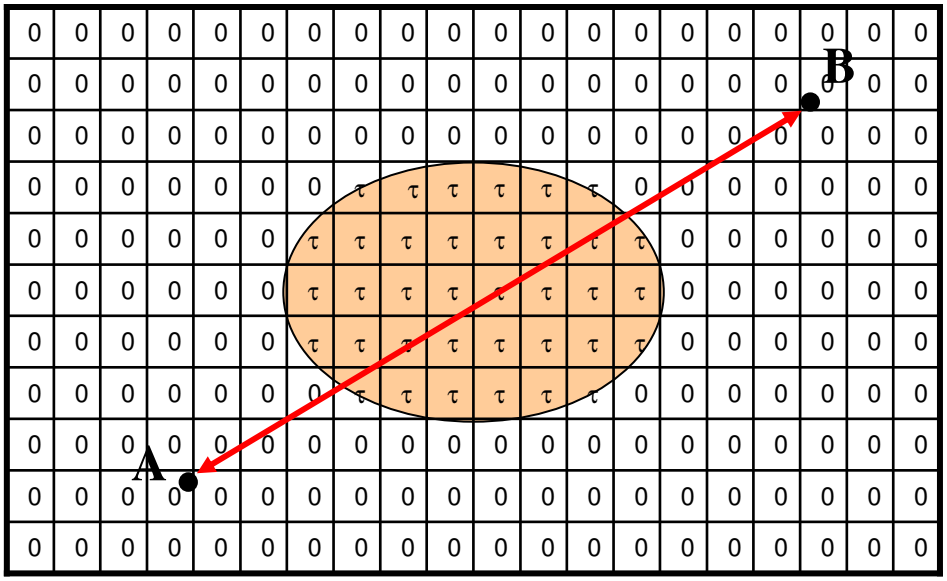

Figure 4.7: Illustration of the path loss model for a directional wireless link going through atmospheric obscuration.

4.5 Dynamic network model

In this section, we present a methodology for the generation and characterization of dynamic three-dimensional (3D) network scenarios which use the communication cost models presented earlier to describe the dynamics of DWB-based network systems.

In order to generate realistic atmospheric obscuration agents in the form of fog and clouds, digital data sets from the National Climate Data Center (NCDC) at the National Oceanic and Atmospheric Administration (NOAA) are used to obtain world wide gridded cloud analysis, including cloud layer data (base, top, type, and amount) and cloud cover values [27]. Based on this data, cloud layers are generated as the

superposition of 3D ellipsoidal shapes simulating the presence of atmospheric agents in the 3D space. Typical wind speed values at different atmospheric layers are used to move the cloud layers in the 3D space.

Matlab is used to generate these dynamic 3D scenarios. Each snapshot of a dynamic scenario generated is characterized by an obscuration matrix. The obscuration matrix is a three-dimensional matrix in which each entry contains the atmospheric attenuation for a given point in the 3D space. An example of a 2D obscuration matrix is shown in Fig. 4.7, where all entries with free space are set to zero and entries containing cloud water particles are set to the specific cloud attenuation value τ_{obs}. The set of obscuration matrices for every snapshot of the dynamic scenario defines the evolution of atmospheric obscuration over time.

Given the obscuration matrix, the location of the network nodes and the link directivities, the path loss for every potential link in the network is computed using Eq. 4.25. Thus, a set of *NxN* path loss matrices L (one for every snapshot of the dynamic 3D scenario) is generated in order to define the evolution of the path loss for every link in the network.

Fig. 4.8 shows an example of a 3D simulation scenario generated in Matlab. This scenario represents a 16x16x8km 3D space containing 4 cloud layers with different cloud types at different altitudes and a 10 node directional wireless network using FSO and directional RF communication technologies. Values for the path loss (FSO/RF) in dB are shown on every link.

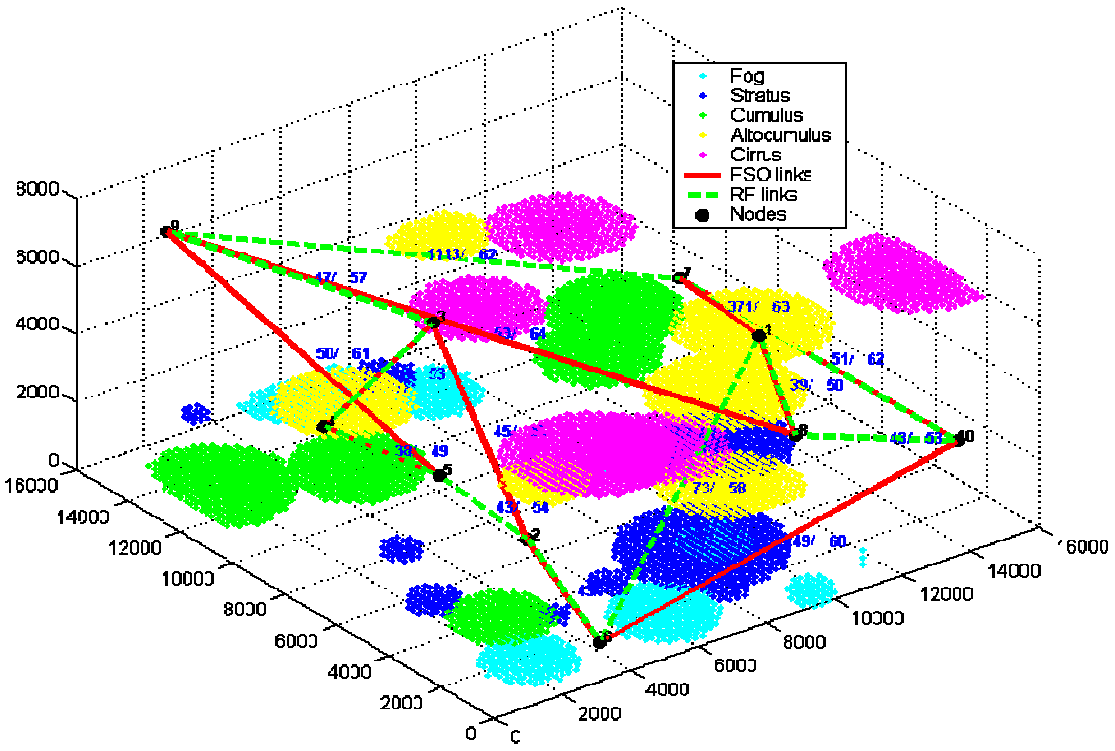

Figure 4.8: Snapshot of a dynamic 3-dimensional scenario with cloud layers at different altitudes and a 10 node directional wireless network using FSO and directional RF communication technologies.

As presented in section 4.4, the communication cost of a wireless link is defined as the transmitted power needed to assure the required link BER. In our definition, the link cost represents the energy per unit time needed to maintain a wireless link "alive" (given a QoS guarantee specified by the required link BER), which we relate to the potential energy of an analogous physical system.

Thus, the objective is to compute a set of communication cost matrices that define the evolution of the potential energy of the network system over the lifetime of the dynamic simulation scenario. Recall that the potential energy for a given link *(i,j)*

can be computed using Eq. 4.6 as $u_{ij} = P_{R0}^{j} \cdot \tau_{ij}$. Restating Eq. 4.6 in matrix form we obtain:

$$U = P_{R0} L , \tag{4.26}$$

where U is the potential energy matrix, P_{R0} the link margin matrix and L the path loss matrix. The communication cost matix U in dBm is obtained as

$$U(dBm) = P_{R0}(dBm) + L(dB) , \tag{4.27}$$

where P_{R0} is the link margin matrix in dBm and L the path loss matrix in dB. Fig. 4.9 illustrates this process.

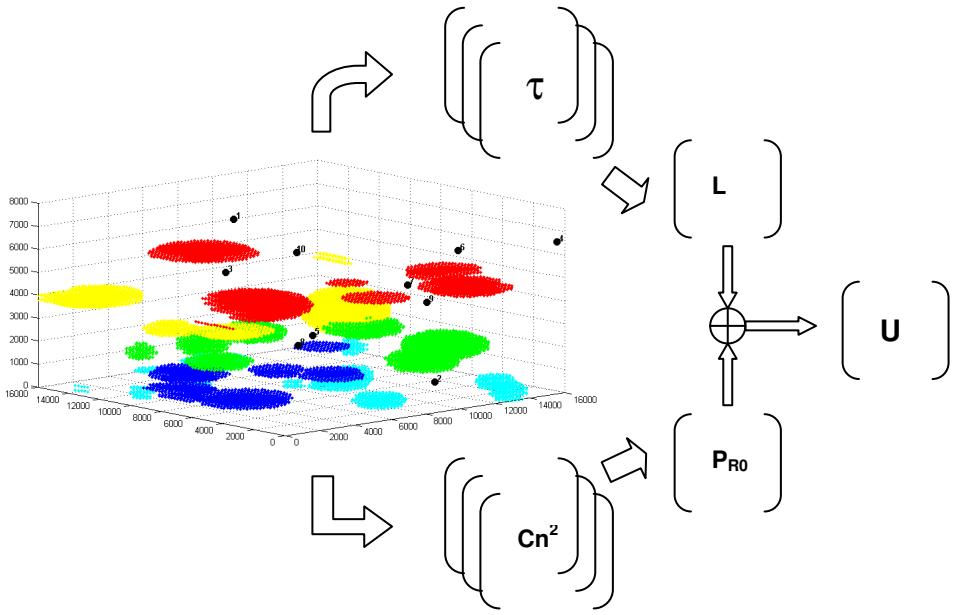

Figure 4.9: Modeling the network's communication cost. The atmospheric conditions of the 3D space determine the 3D obscuration matrix τ and the 3D turbulence strength matrix Cn^2. Given the location of the network nodes, the *NxN* path loss matrix L and the *NxN* link margin matrix P_{R0} are obtained from the 3D matrices τ and Cn^2 respectively. Finally, the potential energy matrix U, which contains the power needed at every potential link in the network is obtained using Eq. 4.27 as the aggregation of L and P_{R0}.

Chapter 5: Topology Reconfiguration

5.1 Introduction

Topology reconfiguration in DWB networks is defined as the process by which point-to-point links are broken and/or set-up to create a new physical network topology. Fig. 5.1 illustrates this process:

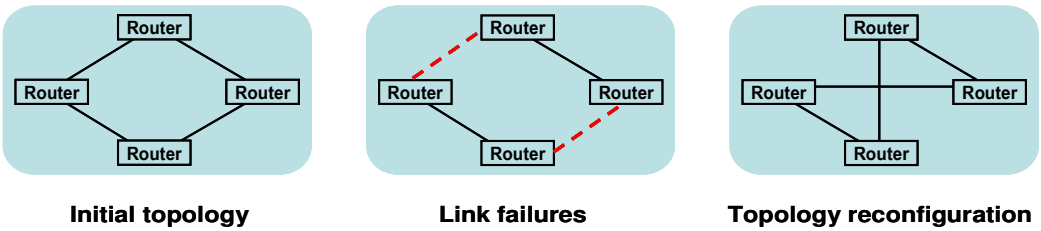

Figure 5.1: The topology reconfiguration process.

In this context, we define:

- *Topology optimization:* computation of an optimal topology from global network knowledge.
- *Bootstrapping:* initial configuration of a connected topology from disconnected network nodes with only local network knowledge.

5.2 Topology Optimization

5.2.1 Introduction

Topology reconfiguration may be designed to meet multiple objectives such as minimizing congestion, end-to-end delay or bit-error-rate (BER). Algorithms and heuristics are used for making efficient decisions about the choice of network topology to achieve a required level of performance. Fig. 5.2 shows the interaction between the topology control processes that provide the network with the autonomous reconfiguration capability.

Most physical layer topology control algorithms for multi-hop wireless networks attempt to optimize parameters such as power or bit error rate (BER). In FSO networks the critical factor affecting link performance at the physical layer is the atmospheric obscuration, which reveals the attenuation of the optical signal caused by the presence of atmospheric phenomena (clouds, fog, snow, etc) between the nodes trying to communicate. Thus, in [42], we considered the obscuration minimization problem.

A cost measure is assigned to every possible link in the network as a function of the link length and the obscuration factor. Minimum cost graph algorithms techniques are then used to construct optimized topologies. Constraints are imposed on the node degree (due to the limitation on the number of transceivers) and the network connectivity (specifically we will impose the network to be bi-connected,

which assures the existence of a communication path between any two nodes in the network even after a single link break).

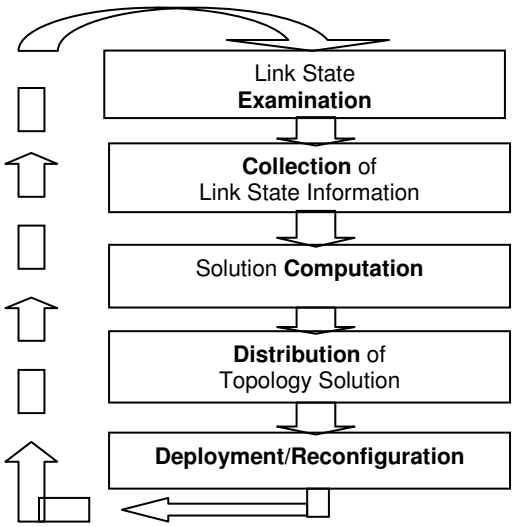

Link state examination: Link state is highly dynamic. Adverse weather conditions such as clouds, fog and snow may obscure optical links causing performance degradation manifested by increased BER, transmission delays, congestion, etc. These effects are even greater when allowing mobility of nodes. In such a dynamic environment, nodes should be continuously monitoring their link states and local topology information.

Collection of link state information: Upon degradation, link state information is reported to a designated node in order to keep track of the dynamics of the whole network and determine whether a topology change is needed.

Topology solution computation: If a new topology needs to be computed, the challenge is to develop efficient algorithms to find the optimal topology meeting a given objective while satisfying connectivity constraints. We have developed approximation algorithms to solve the problem in polynomial time as these algorithms must be scalable and be executed with low complexity to avoid significant loss of data. This issue becomes critical due to the extremely high data rates carried in optical wireless networks.

Distribution of topology solution: The new topology is sent to every node in the network in order to undergo reconfiguration.

Deployment/Reconfiguration: The deployment of the new topology takes place. Beam steering plus pointing-acquisition and tracking techniques are used in order to physically redirect the optical beams and quickly form a new topology [29].

Figure 5.2: Autonomous reconfiguration processes.

Topology optimization problems are typically NP-Complete and heuristics are needed in order to achieve scalable near-optimal solutions. Heuristics for topology optimization can be broadly classified into two categories as *link insertion* and *link deletion. Link insertion* heuristics insert links according to some sequence whenever interfaces are available. In *link deletion* heuristics the starting point is a maximally connected graph, and links are removed according to some sequence until no node has more links attached to it than it its number of interfaces.

Two centralized approaches to create an FSO topology with strong connectivity and short diameter with uniform degree bounds were presented in [43]. One is based on *link deletion,* and the other is based on *link insertion*. Their work does not take into account link cost and does not assure bi-connectivity. In [44], heuristics for minimizing BER and congestion, with bi-connectivity constraints, are described. All of them are based on *link insertion*.

In [42] we presented two heuristics for building minimum cost bi-connected topologies in the case of 2-degree (ring) networks as well as for 3-degree networks. All of them fit in the category of *link insertion*. The heuristics for ring networks were based on the Spanning Ring methodology presented in [44]. For 3-degree networks a new heuristic, 3-MST + Bridge Covering, was described, which achieves a closer to optimal solution with a slight increase in complexity compared to the 3-degree heuristic presented in [44].

5.2.1 Problem Statement

The topology optimization problem is stated as follows*:*

- *Given:* The network cost matrix *C* representing the cost of all possible links in the network.
- *Objective:* Find the network topology *T* minimizing the aggregate network cost *F*.
- $F(b_{ij}) = \sum_{i=1}^{N}\sum_{j=1}^{N} b_{ij}c_{ij}$, where $\begin{cases} b_{ij} = \begin{cases} 1 & \text{if } (i,j) \in T \\ 0 & \text{o.w} \end{cases} \\ c_{ij} = \text{cost of link } (i, j) \end{cases}$ (5.1)
- *Constraints:* node degree (which must not exceed the number of directional transceivers per node) and edge bi-connectivity (the network must remain connected even after a single link break).

Note that in the topology optimization problem above, the cost matrix *C* is given and the optimization is performed over the b_{ij} variables, which determine the connections between backbone nodes. The topology optimization problem is actually an instance of the general energy minimization problem stated in Eq. 3.3:

$$\min U(b_{ij}, \mathrm{R}_1, ..., \mathrm{R}_\mathrm{N}) = \eta \cdot \left(\sum_{i=1}^{N}\sum_{j=1}^{N} b_{ij} u(\mathrm{R}_\mathrm{i}, \mathrm{R}_\mathrm{j}) \right) + \left(\sum_{k=1}^{M} u(\mathrm{R}_{\mathrm{h}(k)}, \mathrm{r}_k) \right)$$

$$\text{s.t. } b_{ij} = \begin{cases} 1 & \text{if } (i,j) \in T \\ 0 & \text{o.w.} \end{cases}$$

Note that when the location of the backbone nodes $\mathrm{R}_1, ..., \mathrm{R}_\mathrm{N}$ is given and the optimization is done over the backbone connectivity variables b_{ij}, the network coverage term *G* is fixed and does not affect the optimization process. Only the backbone connectivity term *F* is considered and 3.3 reduces to:

$$\min U(b_{ij}) = \sum_{i=1}^{N}\sum_{j=1}^{N} b_{ij}u(\mathrm{R_i}, \mathrm{R_j}) \quad \text{s.t. } b_{ij} = \begin{cases} 1 & \text{if } (i,j) \in T \\ 0 & \text{o.w.} \end{cases}, \tag{5.2}$$

where now the energy function U is just the backbone connectivity term F. The topology optimization problem is thus a connectivity optimization problem formulated as an integer programming problem.

In our approach, a weighted graph is considered as the abstraction of the network. A weighted graph $G = (V, E)$ is a group of $|V|$ vertices connected through $|E|$ weighted edges. The vertices represent the nodes in the network and the edges the links between them. The weight of an edge describes the cost associated with the link represented by that edge. The problem becomes that of finding sub-graphs with minimum total cost while satisfying connectivity constraints. Specifically, heuristics have been developed to solve the problem of finding the minimum cost ring topology (suitable when nodes have 2 optical transceivers), which is NP-Complete [40]. Also, the problem of forming a bi-connected topology when nodes are allowed to have up to 3 optical transceivers has been considered. In this case heuristics have been developed to find a 3-degree minimum spanning tree (3-MST) (NP-Complete [40]), and augmenting the tree to achieve bi-connectivity (also an NP-Complete problem [40]).

5.2.2 Heuristics for ring networks

When all network nodes have 2 optical transceivers the only possible bi-connected topology is a ring. The problem is to find the minimum cost ring topology.

In graph algorithms theory, this is equivalent to the "traveling salesman problem", which is known to be NP-Complete [40]. A simple heuristic called Spanning Ring (SR) was introduced in [44]. This heuristic keeps forming a simple path by adding edges in increasing order of cost and closes the path into a ring when all nodes are included. SR uses Prim's MST algorithm [41] with the additional constraint of the node degree being equal to 2, which indeed builds a close-to-minimum spanning ring. Its running time complexity is $O(E \log V)$ (the complexity of Prim's MST algorithm [41]). Observing that $|E| = O(V^2)$ (the number of all possible links in the network grows with the square of the number of nodes), we can re-state the complexity of SR as $O(V^2 \log V)$. This heuristic follows a *greedy* approach, that is, it makes locally optimal choices in the hope that this choice will lead to a globally optimal solution. The main problem is that there may be conditions where no feasible link can be added to the path in either direction, and, thus, a feasible ring topology cannot be found.

In order to overcome this problem, a new heuristic was developed, Reconfigurable Spanning Ring (RSR). This heuristic forms a simple path by adding least cost links, but when the path cannot be extended in either direction, an attempt is made to close it in a temporary ring, either by the path endpoints or by breaking an already set-up link. Then, the ring is opened into a new simple path and an attempt is made to extend it again. The process continues until all nodes are included. The procedure is described as follows:

- Sort links in increasing order of cost.
- While not all nodes included,
  - Add links to path in increasing order of cost.
  - If the path cannot be extended in either direction,
    - *Reform path:*
      - If a connection between the path endpoints is possible, make it.

- Else,
  - Sort links in the temporary path (excluding both path-end links) in increasing order of cost.
  - Break highest cost link and attempt to close the path into a temporary ring by connecting the path endpoints to the broken link endpoints.
  - If no feasible connections exist, break next highest link and make a new attempt to form a temporary ring.
- If a temporary ring could be formed, break next highest cost link to open the ring into a new simple path.
- Else, no feasible solution.

The possibility of breaking already set-up links and reconfiguring the path as it is formed, gives the heuristic more flexibility to find a feasible solution. Intuitively we should expect additional time complexity as the algorithm needs to search for feasible ways to reform the path when getting into an infeasible situation (no feasible links can be added to extend the path). Specifically, the reforming process adds to the time complexity of the heuristic, in the worst case (that is when *reform path* needs to be executed at every step, and all intermediate path links need to be examined before a temporary ring can be formed), an $O(V^2 \log V)$ factor. This is because for each *reform path* call we need to sort the edges in the temporary path, which takes $O(i \log i)$ time (*heapsort* algorithm [41] is used), where i is the number of edges in the temporary path. In the worst case, we will have to reform the path for every link addition. Thus, the complexity of RSR is given by

$$\begin{aligned}\sum_{i=1}^{V} i \log i \le V \sum_{i=1}^{V} \log i &= V \log(V!) \\ &= V\, O(V \log V) \\ &= O(V^2 \log V).\end{aligned}$$

The overall running time of the RSR heuristic is therefore $O(V^2 \log V + V^2 \log V) = O(V^2 \log V)$. Despite the additional time used by the reforming process, RSR

maintains the same polynomial complexity and provides higher efficiency in finding feasible minimum cost ring topologies.

A simulation was developed to measure the performance of these heuristics. The simulation involved multiple runs in which the heuristics attempt to configure a minimum cost topology for a particular network scenario. Fig. 5.3 shows the performance of both heuristics. The dashed line shows the network cost for the topologies obtained using SR. The solid line represents the network cost for the topologies obtained by RSR. The white circles represent the instances where SR does not achieve a feasible solution (some of the active links have higher cost than the link cost threshold). In most of those cases, the RSR heuristic is able to find a feasible solution by reforming the temporary path. The black dots show the situations where not even RSR is able to configure a feasible topology.

Time complexity was also measured for both heuristics. Experiments were run in which the average time taken for computing a new topology was measured (average over a 100 runs in different scenarios) as a function of the number of nodes, for both heuristics. Fig. 5.4 shows the reconfiguration time for 8 to 60 nodes. As expected, RSR spends more time on average, but both heuristics follow a polynomial pattern. For a 30 node network, SR took an average of 1.7 ms, while RSR took almost 4 ms to compute the topology.

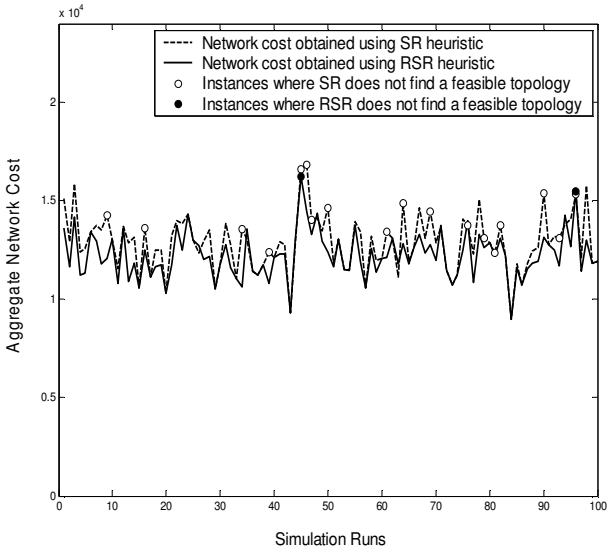

Figure 5.3: Performance of SR and RSR heuristics (20 nodes).

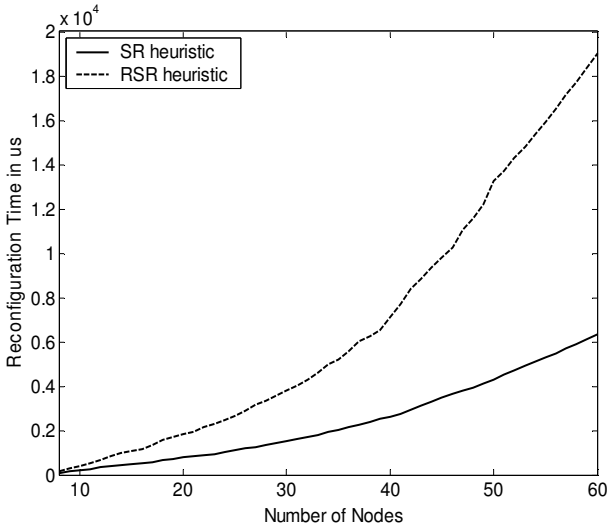

Figure 5.4: Average running time of SR and RSR heuristics in μs (8-60 nodes).

The Branch Exchange algorithm provides a way to incrementally move towards the optimal topology from an already established one. Branch exchange is a brute force approach that checks all possible configurations obtained by exchanging one or more links of the initial topology. The k-link Branch Exchange algorithm checks all configurations that can be formed by exchanging *k* links of the initial topology and keeps the one that meets the given objective (in our case, the one with minimum aggregate cost).

In the case of rings, at least 2 links must be exchanged by corresponding 2 new links to find a new ring topology. Thus the 2-link Branch Exchange algorithm can be used to find the ring topology with the minimum aggregate cost, differing from the existing topology by 2 links. The pseudo code for the 2-link Branch Exchange algorithm is as follows:

- Find all possible link pairs that can be exchanged by new link pairs to obtain another ring topology.
- Get the current link pair and remove both links.
- If the 2 links to be added in order to form the new ring topology have lower cost than the link cost threshold,
  - Add the 2 new links.
  - Compute the new aggregate network cost.
- Go to next link pair.
- If all link pairs are finished, stop.
- Find the minimum aggregate network cost and take the corresponding link pair.
- Exchange it for the new link pair.

Since there are $\frac{N(N-3)}{2}$ (N=|V|, the number of nodes) possible branch exchanges to obtain a new ring topology, which differs by two links from the existing ring topology, the time complexity of the 2-link Branch Exchange algorithm is $O(V^2)$.

After a link pair is exchanged by the corresponding new link pair, the Branch Exchange algorithm can be executed again upon this new topology to gain further improvement. Multiple iterations of the Branch Exchange algorithm successively find topologies with better performance (lower aggregate cost) at the expense of increased run time complexity.

In our simulation the 2-link Branch Exchange algorithm was applied to the topologies obtained by RSR in order to gain further improvement and achieve closer-to-optimal topologies. Fig. 5.5 shows how most of the performance improvement achieved by the Branch Exchange algorithm is accounted in the first iteration. Improvement increases with network size. Performance improvements range from 1% to 5% for networks of 10 to 20 nodes. This suggests that there is little room for improvement for the topologies obtained by RSR.

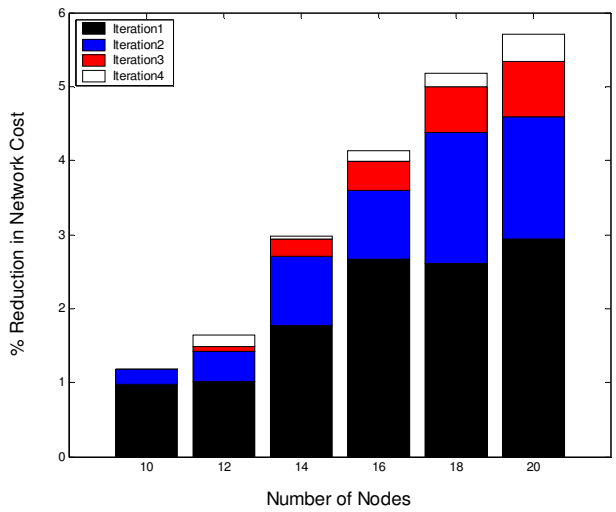

Figure 5.5: Average cost reduction with successive Branch Exchange iterations.

In order to determine the effectiveness of our heuristics we compared our results to the optimal solutions found via integer programming. The integer programming formulation for the optimal solution, in the case of ring networks, is as follows:

$$\text{min} \qquad F = \sum_{i=1}^{N}\sum_{j=1}^{N} b_{ij}c_{ij}\,, \qquad \text{where} \begin{cases} b_{ij} = \begin{cases} 1 & \text{if } (i,j) \in T \\ 0 & \text{o.w} \end{cases} \\ c_{ij} = \text{cost of link } (i,\ j) \end{cases}$$

$$\text{s.t.} \qquad \left.\begin{aligned} &\sum_{i=1}^{N} b_{ij} = 1, \forall j \\ &\sum_{j=1}^{N} b_{ij} = 1, \forall i \end{aligned}\right\} \text{ degree constraints}$$

$$\left.\begin{aligned} &u_1 = 1 \\ &2 \le u_i \le N, \forall i \ne 1 \\ &u_i - u_j + 1 \le (N-1)(1-b_{ij}), \forall \text{i} \ne 1\, \forall \text{j} \ne 1 \end{aligned}\right\} \text{ sub-tour elimination Constraints}$$

Fig. 5.6 shows the histogram of the optimality gap for our best performance heuristic for ring networks, RSR+BE [42].

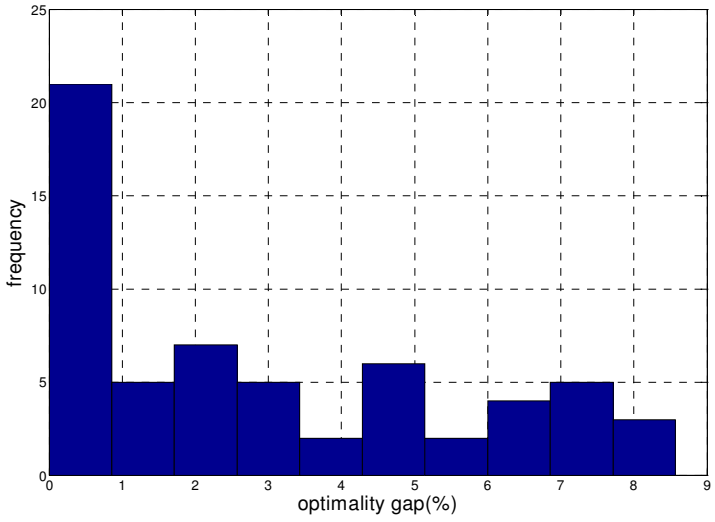

Figure 5.6: Histogram of the optimality gap for RSR+BE heuristic.

5.2.3 Heuristics for 3-degree networks

The possibility of having 3 optical transceivers per node allows greater flexibility and reduced complexity in forming or configuring networks with higher connectivity. Assuming every node has 3 optical transceivers and the cost matrix is known, the problem is to find the minimum cost bi-connected topology.

To solve this problem, a 2-step approach is proposed:

- Form a minimum connectivity graph, i.e. a spanning tree, with minimum cost.
- Augment the spanning tree to achieve bi-connectivity, also with minimum cost.

It is known that the problem of finding an MST when the node degree is bounded (which is the case as every node has 3 transceivers) is NP-Complete [40]. The 3-MST heuristic is used for step 1, which builds a close-to-minimum spanning tree with 3-degree bound. In this case we use Kruskal's MST approach [41], which picks edges in increasing order of cost independently of the already selected edges (Prim's approach makes sure the edges are added to the set of already selected edges). The time complexity is also $O(E \log V)$ [41]. Again $|E| = O(V^2)$, therefore 3-MST takes $O(V^2 \log V)$ time.

Step 2 is a bi-connectivity augmentation problem, which is also known to be NP-Complete [40]. The heuristic developed, Reconfigurable Spanning Path (RSP) uses RSR methodology to connect the nodes with degree 1, i.e. with just one active link. The only difference is that we do not need to form a ring, as a simple path connecting 1-degree nodes is sufficient to achieve bi-connectivity [41]. The heuristic

thus stops when all 1-degree nodes are connected through a simple path. The time complexity is the same as for RSR heuristic, i.e. $O(V^2 logV)$. Thus "3-MST + RSP" runs in $O(V^2 logV + V^2 logV) = O(V^2 logV)$ time. The problem of RSP is that we won't always be able to find a feasible path connecting 1-degree nodes. These nodes are the leaves of the tree constructed in step 1 (which may well be further apart) and connecting them through a path won't always be a good solution. A better approach should add edges between nodes with open interfaces (1 and 2-degree nodes) and stop as soon as bi-connectivity is achieved. We present the Bridge Covering (BC) heuristic, which is based on the just stated idea. Before going into the details of the heuristic we shall introduce the concept of a bridge in a graph, which is critical in our objective of achieving bi-connectivity. A bridge is an edge in a graph upon the removal of which, the graph becomes disconnected. Recall that a bi-connected graph is a graph that will remain connected after any single link break.

Following theorems connect the bridge concept with graph connectivity [41].

Theorem1: If a graph is said to be bi-connected, the graph contains no bridges.

Proof: If a graph is bi-connected we can remove any single edge of the graph and the graph will remain connected. Therefore a bi-connected graph cannot contain any bridge.

Theorem2: If a graph is said to be a tree, all the edges of the graph are bridges.

Proof: Since a tree is a connected graph with no cycles, by a single removal of any of its edges, the graph becomes disconnected. Therefore all the edges of a tree are bridges.

Based on theorem 2 we know that all the edges in the tree obtained in step 1 are bridges. The idea is to add edges to the tree in such a way that for each link addition, we cover as many bridges as possible. By theorem 1 we know that when all bridges are covered, the graph is already bi-connected. It is important to remind that our objective is to find a bi-connected graph with minimum cost, thus the cost of the edges to be added should be still taken into account. The BC heuristic adds edges in increasing order of "bridge covering capability", until the final graph contains no bridges. The "bridge covering capability" metric is defined so that both, the number of bridges covered and the link cost, are taken into account. Specifically, the "bridge covering capability" of a particular edge *e* is defined as the sum of the cost of all the bridges covered upon the addition of *e* minus the cost of *e*. The pseudo code for the BC heuristic is as follows:

- Build a *potential link set* with all possible links between nodes with open interfaces (nodes with degree 1 or 2).
- Build a *bridge set* for each of the potential links containing the bridges which would be covered upon the addition of the potential link to the tree.
- Compute the bridge covering capability for each potential link.
- Sort links in the potential link set in increasing order of bridge covering capability.
- Add the link with highest bridge covering capability.
- Update the potential link set, the corresponding bridge sets, and bridge covering capabilities.
- If no bridges left,
  - End.
- Else,
  - Go to step 3.

The critical task in the BC heuristic is to build and update the bridge sets. Initially we need to run BFS (Breadth First Search algorithm) [41] for every potential link in order to build their bridge sets. BFS on a tree takes *O(V)* time and we have

$O(E)= O(V^2)$ potential links. Therefore step1 takes $O(V^3)$ time. For the update steps, we need $O(E) = O(V^2)$ updates after each link addition. Each update takes $O(V)$ time and there are $O(V)$ link additions. Thus the updating process takes $O(V^4)$ time. The dominating factor is the updating process, which makes BC to run in $O(V^4)$ time. The whole "3-MST + BC" heuristic runs in $O(V^2 \log V + O(V^4)) = O(V^4)$ time.

The same simulation methodology described in section 3 was used to measure the performance of the 3-degree heuristics. Results are shown in Figs. 5.7 and 5.8. As in the case of ring topologies the graph in Fig. 5.7 shows the network cost after configuring an optimized topology by using "3-MST + RSP" (dashed line) and "3-MST + BC" (solid line) heuristics. The experiment shows how "3-MST + BC" obtains closer-to-minimum cost bi-connected topologies at the expense of a higher degree polynomial time complexity (Fig. 5.8). The average running time of 3-degree heuristics went into a few seconds range for very large networks (about 13 seconds for 60 nodes) but it was still less than 100 ms for 25 node networks. Also, BC is shown to be much more efficient in achieving bi-connectivity than RSP. The white dots in Fig. 5.7 show the instances where RSP fails to achieve a feasible path connecting 1-degree nodes, thus failing to achieve a bi-connected graph. In those cases BC finds a feasible set of edges to be added to the tree and achieve bi-connectivity. The black dot shows that for a particular scenario in our simulation not even a feasible tree could be obtained.

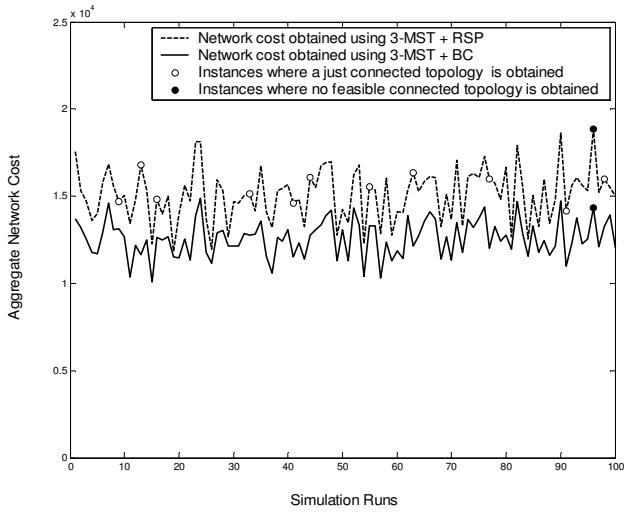

Figure 5.7: Performance comparison of 3-degree heuristics (20 nodes).

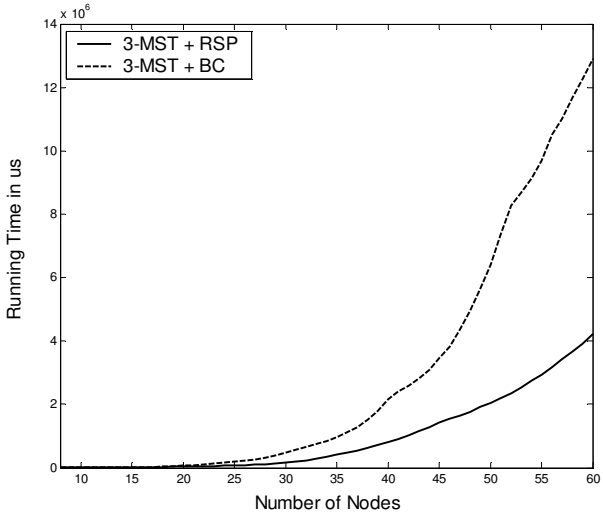

Figure 5.8: Average running time of 3-degree heuristics (8-60 nodes).

5.3 Bootstrapping

In this section, we address the problem of initial configuration of a directional wireless network topology, which is referred to as the bootstrapping problem. In this context, nodes are initially disconnected and only know about potential neighbor connectivity. Nodes therefore need to coordinate their local decisions and actions to collectively establish a connected topology. An efficient solution to the bootstrapping problem requires the design of a self-organized system in which the emergence of a system-wide adaptive structure such as global network connectivity is achieved through local interactions between individual entities (network nodes).

Our work on topology optimization [42] assumes the existence of a connected topology. The objective is to dynamically evaluate the current topology and reconfigure amidst degradation. Such an assumption makes the implementation of a centralized system very suitable, as overall network information can be used to efficiently obtain close-to-optimal solutions while avoiding agreement, coordination and synchronization problems. A Designated Topology Control Node (DTCN) [3] is responsible for gathering overall network information, evaluating the current topology, deciding upon reconfiguration and computing a new optimized topology. Moreover, the available high-bandwidth connectivity allows overcoming the scalability and response time limitations of centralized systems in low-bandwidth, unreliable networks.

The objective in bootstrapping is to provide fast initial connectivity rather than optimizing an existing topology. The problem of initially configuring a network topology is distributed in nature as nodes only know about potential neighbor

connectivity and need to coordinate their local decisions to collectively set up an initial connected topology.

A complete bootstrapping model requires the design of algorithms and protocols for:

- Determining the connections to be formed until a connected network is obtained.
- Exchanging information between nodes in the network.
- Guaranteeing coordination and synchronization.

The limitation on the number of transceivers per node imposes a constraint on the degree of the network topology being formed. The problem of achieving fast connectivity with limited number of transceivers per node can be modeled as the Minimum Degree Spanning Tree (MSDT) problem, which is known to be NP-Complete. In our previous work, a distributed approximation algorithm which constructs a spanning tree with maximal node degree at most one larger than that in the optimal solution was developed [41]. This work provides a bottom-up methodology to iteratively establish connections until a tree topology is formed, but does not address the problems of information exchange and synchronization which are essential in guaranteeing the efficient formation of a connected topology.

In [52] we presented the design, implementation and evaluation of a hybrid distributed/centralized bootstrapping model for directional wireless backbone networks. Our approach uses the advantages of a centralized computation and communication model as soon as high-bandwidth connectivity is available between a given set of nodes. The bootstrapping process iteratively transforms a completely

disconnected distributed network system into a set of connected centralized components, until a single connected network with a unique DTCN is formed. Our model uses a bottom-up distributed algorithm to determine connections between connected components, and adds the required communication and synchronization mechanisms in order to assure the efficient emergence of network connectivity from local interactions between connected components.

We have designed a process model in the form of a finite state machine, which can be integrated in any directional wireless network model in order to provide the bootstrapping functionality. Simulation experiments were run to test the efficiency and scalability of our model for different network systems, with varying size and signaling data rate.

Fig. 5.4 shows the average total delay for bootstrapping directional wireless networks of 10 to 100 nodes, for different signaling data rates. As expected, the total delay increases when decreasing the signaling data rate, but the linear time complexity is preserved, verifying the scalability of our model.

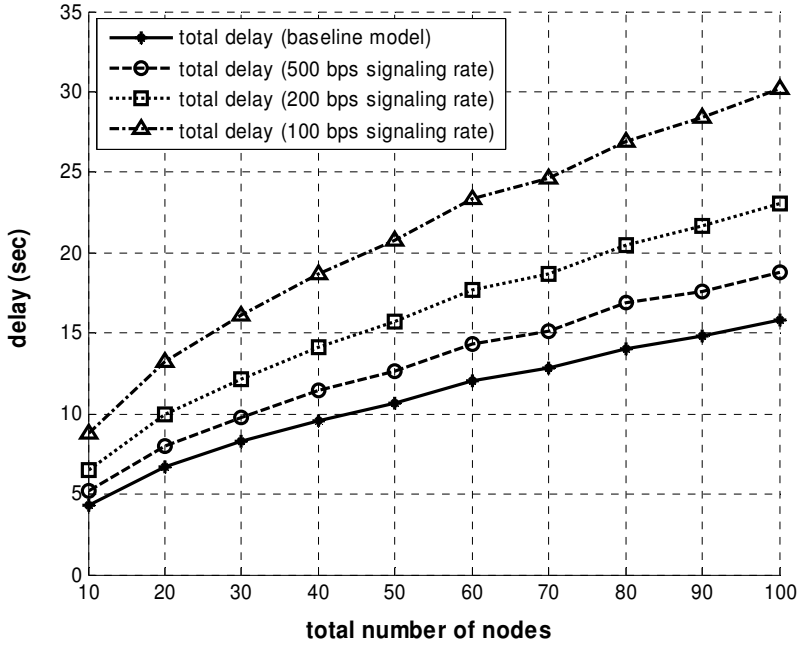

Figure 5.9: Average total delay of the bootstrapping process.

Chapter 6: Mobility Control

6.1 Introduction

As seen in Chapter 5, topology reconfiguration processes allow dynamic network performance optimization by physically changing directional wireless links among network nodes. This process involves temporary loss of data due to the unavailability of several source-to-destination paths during the reconfiguration process. In directional wireless networks, the degree constraints imposed on the nodes imply that during a topology change, unwanted links have to be removed before new links can be created. Whenever this is the case, the network topology will be in a transient state after the removal of unwanted links and before the establishment of new links. This transient state could exist for a small time interval, but it nevertheless exists and results in suboptimal network performance during this time.

Whenever topology reconfiguration cannot improve network performance due to a high reconfiguration cost, the physical DWB configuration can be adjusted by repositioning mobile base station nodes. Mobility control allows adjusting the backbone topology without breaking point-to-point links and thus avoiding temporary loss of data.

Recall that in our proposed architecture, a set of dynamic “service demand clusters” are to be connected by a set of directional wireless backbone nodes with limited coverage range (dotted circles Fig. 6.1). A service demand cluster is

essentially a connected set of hosts or terminals which demand for broadband connectivity (hexagons in Fig. 6.1).

In this architecture, a communication between two terminal nodes takes place by a multi-hop transmission scheme over the wireless nodes until the traffic of the source reaches one of the backbone nodes, then it travels over the backbone network until it reaches a backbone node which is close enough to the intended destination, and finally it travels over a few wireless nodes until it reaches its destination. Our problem is to find the optimal locations of the backbone nodes such that two main objectives are maximized: network coverage and backbone connectivity. A point that makes our problem distinct from traditional facility location problems is the fact that we need to make the backbone connected through FSO and/or RF links. This implies that backbone nodes need to stay within FSO/RF communication range and imposes further constraints than just covering the service demand areas. As a consequence, providing coverage to service demand areas and maintaining strong backbone connectivity results in a multi-objective optimization problem with two competing objectives**.** Maximizing backbone connectivity involves bringing backbone nodes together, which leads to strong backbone connectivity, but may incur in low network coverage (Fig. 6.1b). On the other hand, maximizing coverage involves spreading backbone nodes over to service demand areas, which may lead to a weaker (i.e., lower connectivity) backbone configuration (Fig. 6.1a).

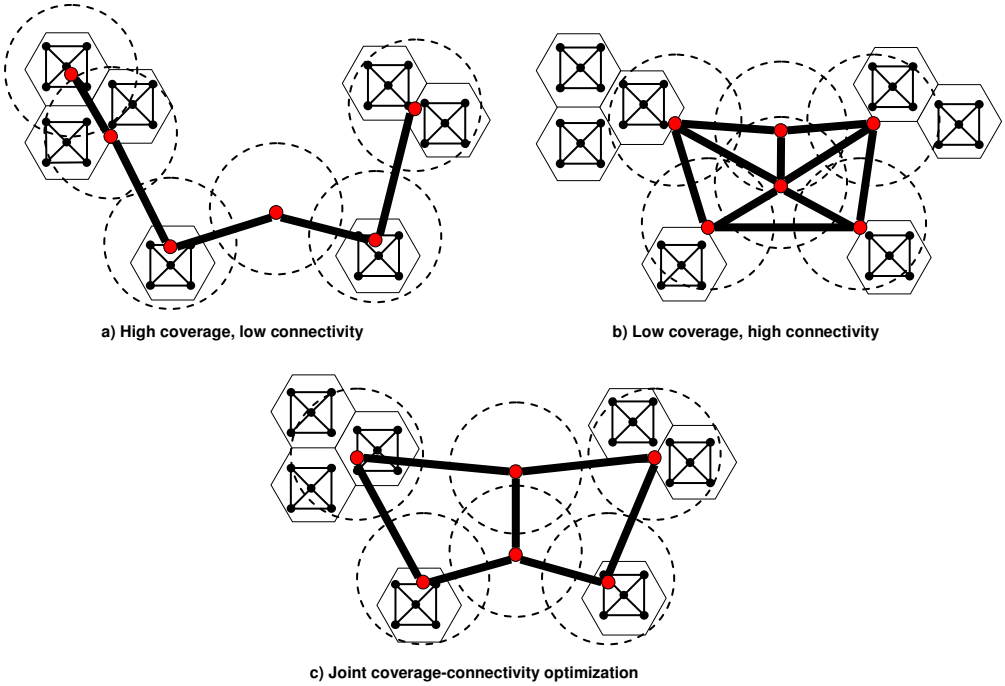

Figure 6.1: Trade-off between network coverage and backbone connectivity.

6.2 Potential energy minimization

This work proposes a novel approach to solve this problem by formulating it as an energy minimization problem in which the network is modeled as a system of particles in a potential field. The idea is to characterize the DWB configuration with a cost function that mimics the potential energy of an analogous particle system. Energy functions are typically convex, and thus suitable to minimize. Moreover, being able to characterize network configurations with energy functions allows the design of self-organized network systems which autonomously achieve energy minimizing configurations driven by local forces exerted on network nodes. Forces between nodes are defined based on network connectivity. Attraction forces are

defined between neighbor backbone nodes (for backbone connectivity) and between each backbone node and the terminals within their respective coverage range (for network coverage). The effects of the host layer (cluster mobility) and of the environment (atmospheric turbulence and obscuration) are modeled as external forces changing the potential energy of the network system. Mobility control algorithms are designed to autonomously readjust the DWB physical topology based on resulting forces to achieve energy minimizing configurations.

Physical systems naturally react to minimize their potential energy and thereby increase their robustness. Internal forces are responsible for bringing the network to an equilibrium condition where the total energy is minimized. Our approach models network control strategies as internal forces minimizing the energy of the network system. In this work, we present algorithms and protocols for mobility control that adjust the location of backbone nodes by computing internal forces at each backbone node as negative energy gradients. We show how the network can autonomously achieve energy minimizing configurations driven by local forces exerted on network nodes. The beauty of this physical energy model is that very complex systems can be characterized with continuous and convex energy functions which take into account the heterogeneity of the network system. We also show how the use of mobility control strategies that minimize the energy of the network system, ensure desirable network properties such as coverage, connectivity and power efficiency.

6.3 Coverage and connectivity optimization

Assume we have a network of *N* backbone nodes and *M* end terminals or hosts located in a geographical space $A \in \mathrm{R}_3$. The end hosts are at locations $\mathrm{r}_1, \mathrm{r}_2 ..., \mathrm{r}_\mathrm{M}$ in the network, in which $\mathrm{r}_\mathrm{i} = (x_i, y_i, z_i)$ represents the location of the i^{th} end host in *A*. Similarly, the backbone nodes are at locations $\mathrm{R}_1, \mathrm{R}_2 ..., \mathrm{R}_\mathrm{N}$ in the network, in which $\mathrm{R}_\mathrm{j} = (X_j, Y_j, Z_j)$ denotes location of the j^{th} backbone node in *A*. Each backbone node provides coverage to a group of end hosts in its proximity. In this scheme, a host *s* communicates with another host *d* in the following way: host *s* transmits its information to the closest backbone node; then the traffic traverses through the backbone network until it reaches the backbone node that is closest to the destination. Finally, the backbone node that is closest to the destination transports the traffic to the host *d*. As it can be observed, this scheme is based on two properties: first, the end hosts need to be well covered by the backbone nodes, and second, the backbone nodes must have good connectivity among themselves. We describe both aspects in our model in terms of the following two cost metrics:

- *Coverage cost*: takes into consideration the cost of covering the end hosts by the backbone network. This component of cost is defined as a function of the communications energy needed in order for the end hosts to communicate with their closest backbone node. The more the energy required, the higher the coverage cost. Assume that $h(k)$ represents the index of the backbone node that provides coverage to the end host node *k*.

Apparently, we have $1 \le h(k) \le N$. Now, we define the following form of coverage cost:

$$G = \sum_{k=1}^{M} u(\mathrm{R}_{\mathrm{h}(k)}, \mathrm{r}_k), \tag{6.1}$$

where G represents the coverage cost and it is computed as the summation of the energy stored in the wireless links connecting each end host to its closest backbone node.

– *Connectivity cost*: considers the cost of maintaining the backbone nodes connected. In the simplest form, backbone nodes may be connected forming a chain topology, which implies that a chain of links starts from a backbone node and passes through all the other backbone nodes. In many practical applications such a simple graph is vulnerable to link failures; if a single link fails the network becomes disconnected. In practice, it is desirable to achieve some degree of fault tolerance by superimposing a redundant connectivity graph among the backbone nodes. Samples of such connectivity patterns include ring topologies, or k-connected graphs (the graphs for which there are k disjoint paths between every arbitrary pair of backbone nodes). For a given connected topology, the connectivity term of the cost function models the energy used by the backbone network to keep its nodes connected. Similar to the coverage cost, we define the connectivity cost as follows:

$$F = \sum_{i=1}^{N} \sum_{j=1}^{N} b_{ij} u(\mathrm{R}_{\mathrm{i}}, \mathrm{R}_{\mathrm{j}}), \tag{6.2}$$

in which F represents the connectivity cost and it is computed as the summation of the energy stored in the links forming the backbone topology.

Based on the above cost components, we define the following composite cost function:

$$U = \eta \cdot F + G = \eta \cdot \left(\sum_{i=1}^{N} \sum_{j=1}^{N} b_{ij} u(\mathrm{R_i}, \mathrm{R_j}) \right) + \left(\sum_{k=1}^{M} u(\mathrm{R_{h(k)}}, \mathrm{r}_k) \right). \tag{6.3}$$

Note that the cost function above U integrates both coverage and connectivity cost terms and represents the total energy usage in the network system.

Thus, in this dissertation, the mobility control problem is formulated as an energy minimization problem, as follows:

$$\min U(\mathrm{R_1}, ..., \mathrm{R_N}) = \eta \cdot \underbrace{\left(\sum_{i=1}^{N} \sum_{j=1}^{N} b_{ij} u(\mathrm{R_i}, \mathrm{R_j}) \right)}_{F} + \underbrace{\left(\sum_{k=1}^{M} u(\mathrm{R_{h(k)}}, \mathrm{r}_k) \right)}_{G}. \tag{6.4}$$

$$\text{s.t.} \quad b_{ij} = \begin{cases} 1 & (\mathrm{i}, \mathrm{j}) \in \mathrm{T} \\ 0 & \text{o.w.} \end{cases}$$

Note that in this case the backbone topology T (b_{ij} variables) is given and the optimization is performed over the location of the backbone nodes $(\mathrm{R_1}, ..., \mathrm{R_N})$. Changing the location of the backbone nodes changes the link cost function u_{ij} for both backbone-to-backbone and backbone-to-terminal links. The objective is to find the location of the backbone nodes that jointly optimizes network coverage and backbone connectivity by minimizing the total energy of the network system.

The form of the above energy function depends on the communication cost model. As seen in section 4.1.3, the cost of a wireless link *(i,j)* is defined as the

communications energy per unit time used to send information at a specified BER between node *i* and node *j*, and it is described in terms of three main components: the link margin P_{R0}, the atmospheric attenuation τ_{obs} and the free space path loss τ_{fs}:

$$u_{ij} = \underbrace{\underbrace{\left(P_{R0}^{j}\right)}_{\text{link margin}} \underbrace{\left(e^{\alpha_{ij}\left\|\mathrm{R_i}-\mathrm{R_j}\right\|}\right)}_{\tau_{obs}} \underbrace{\left(\frac{4\pi}{D_T^i A_{eR}^j}\left\|\mathrm{R_i}-\mathrm{R_j}\right\|^n\right)}_{\tau_{fs}}}_{\tau}.$$

Note that the link energy function u_{ij} is the product of a polynomial and an exponential function of the link distance and thus is convex. In the following sections, we will introduce reasonable assumptions regarding atmospheric obscuration and free space path loss for the link cost function u_{ij} that will lead to different energy models, always maintaining the convexity property of the energy function. The mobility control algorithms developed will differ under the assumptions adopted, but the general methodology will remain the same. Forces will be computed at each backbone node as the negative energy gradient at the backbone node's location, which will drive their mobility and thus the network topology. In sections 6.3 and 6.4 we present the general force-driven mobility control methodology that will apply on all scenarios and for all energy models developed. In section 6.5 we present results for the specific case of clear atmospheric conditions in which the network system is shown to behave like a spring system. In section 6.6 the effects of atmospheric obscuration are introduced. In section 6.7 the model is extended to include power limitations arising in practical scenarios.

6.4 Force-driven mobility control

Our approach to solve the optimization problem described in Eq. 6.4 is to use iterations on the placement of the backbone nodes. In each iteration, forces are computed at each backbone node that determine the backbone nodes' relocation directions. In the following section, we define the notion of the force acting on a communications network node based on the gradient of the energy function U with respect to the node's location.

6.4.1 Communication-defined forces

Using Eq. 6.3 we can compute the gradient of the energy function U with respect to R_i as:

$$\nabla U_i = \begin{bmatrix} \frac{\partial U}{\partial X_i} \\ \frac{\partial U}{\partial Y_i} \\ \frac{\partial U}{\partial Z_i} \end{bmatrix} = \eta \begin{bmatrix} \frac{\partial F}{\partial X_i} \\ \frac{\partial F}{\partial Y_i} \\ \frac{\partial F}{\partial Z_i} \end{bmatrix} + \begin{bmatrix} \frac{\partial G}{\partial X_i} \\ \frac{\partial G}{\partial Y_i} \\ \frac{\partial G}{\partial Z_i} \end{bmatrix} = \eta \begin{bmatrix} \sum_{j=1}^{N} b_{ij} \frac{\partial u_{ij}}{\partial X_i} \\ \sum_{j=1}^{N} b_{ij} \frac{\partial u_{ij}}{\partial Y_i} \\ \sum_{j=1}^{N} b_{ij} \frac{\partial u_{ij}}{\partial Z_i} \end{bmatrix} + \begin{bmatrix} \sum_{k=1}^{M} 1(h_{(k)} = i) \frac{\partial u_{ik}}{\partial X_i} \\ \sum_{k=1}^{M} 1(h_{(k)} = i) \frac{\partial u_{ik}}{\partial Y_i} \\ \sum_{k=1}^{M} 1(h_{(k)} = i) \frac{\partial u_{ik}}{\partial Z_i} \end{bmatrix}. \quad (6.5)$$

in which $1(.)$ is the indicator function; it takes value one if the statement within its argument is true, and it is zero otherwise.

As it can be observed, ∇U is a three dimensional vector that represents the maximum variation of the energy function U with respect to the location of the backbone node i. Since the gradient is the direction of the steepest ascent of the cost function U, relocation of a backbone node in the opposite direction of the gradient

gives the steepest descent of the cost function U. Therefore, we define the following notion of the net force at the location of the i^{th} backbone node:

$$\mathrm{F_i} = -\nabla U_i = \begin{bmatrix} -\frac{\partial U}{\partial X_i} \\ -\frac{\partial U}{\partial Y_i} \\ -\frac{\partial U}{\partial Z_i} \end{bmatrix} = \eta \begin{bmatrix} \sum_{j=1}^{N} b_{ij}\left(-\frac{\partial u_{ij}}{\partial X_i}\right) \\ \sum_{j=1}^{N} b_{ij}\left(-\frac{\partial u_{ij}}{\partial Y_i}\right) \\ \sum_{j=1}^{N} b_{ij}\left(-\frac{\partial u_{ij}}{\partial Z_i}\right) \end{bmatrix} + \begin{bmatrix} \sum_{k=1}^{M} 1(h_{(k)} = i)\left(-\frac{\partial u_{ik}}{\partial X_i}\right) \\ \sum_{k=1}^{M} 1(h_{(k)} = i)\left(-\frac{\partial u_{ik}}{\partial Y_i}\right) \\ \sum_{k=1}^{M} 1(h_{(k)} = i)\left(-\frac{\partial u_{ik}}{\partial Z_i}\right) \end{bmatrix}. \qquad (6.6)$$

Note that the net force on node i is a three dimensional vector pointing in the direction of the steepest descent of the energy function U at the location of backbone node i. Thus, relocating a backbone node in the direction of the force results in the steepest decrease of the cost function.

Eq. 6.6 can be restated in terms of the link energy gradient ∇u_{ij} as:

$$\begin{aligned} \mathrm{F_i} &= \eta \sum_{j=1}^{N} b_{ij} \begin{bmatrix} -\frac{\partial u_{ij}}{\partial X_i} \\ -\frac{\partial u_{ij}}{\partial Y_i} \\ -\frac{\partial u_{ij}}{\partial Z_i} \end{bmatrix} + \sum_{k=1}^{M} 1(h_{(k)} = i) \begin{bmatrix} -\frac{\partial u_{ik}}{\partial X_i} \\ -\frac{\partial u_{ik}}{\partial Y_i} \\ -\frac{\partial u_{ik}}{\partial Z_i} \end{bmatrix}, \qquad (6.7) \\ &= \eta \sum_{j=1}^{N} b_{ij}\left(-\nabla^i u_{ij}\right) + \sum_{j=1}^{M} 1(h_{(k)} = i)\left(-\nabla^i u_{ik}\right) \end{aligned}$$

where the vector $\nabla^i u_{ij}$ represents the gradient of the link cost function u_{ij} with respect to the location $\mathrm{R_i}$. Now, we can introduce the notion of the force acting at location $\mathrm{R_i}$ due to the interaction of node i with its neighbor node j, as the negative gradient of the potential energy stored at link *(i,j)*, u_{ij}, with respect to the location $\mathrm{R_i}$, as:

$$\mathrm{f_{ij}} = -\nabla^{i} u_{ij} = \begin{bmatrix} -\dfrac{\partial u_{ij}}{\partial X_i} \\ -\dfrac{\partial u_{ij}}{\partial Y_i} \\ -\dfrac{\partial u_{ij}}{\partial Z_i} \end{bmatrix} = \begin{bmatrix} f_{ij,x} \\ f_{ij,y} \\ f_{ij,z} \end{bmatrix}, \tag{6.8}$$

where $f_{ij,x}$, $f_{ij,y}$ and $f_{ij,z}$ are the *x, y* and *z* components of the force acting on node *i* due to its interaction with node *j*.

Using Eq. 6.8, we can compute the net force acting at location $\mathrm{R_i}$ as the aggregation of the forces resulting from the interaction of node *i* with all its neighbor nodes as:

$$\mathrm{F_i} = \eta \sum_{j=1}^{N} b_{ij} \mathrm{f_{ij}} + \sum_{k=1}^{M} 1(h_{(k)} = i) \mathrm{f_{ik}} \tag{6.9}$$

which in parametric form becomes:

$$\begin{bmatrix} F_{i,x} \\ F_{i,y} \\ F_{i,z} \end{bmatrix} = \eta \sum_{j=1}^{N} b_{ij} \begin{bmatrix} f_{ij,x} \\ f_{ij,y} \\ f_{ij,z} \end{bmatrix} + \sum_{k=1}^{M} 1(h_{(k)} = i) \begin{bmatrix} f_{ik,x} \\ f_{ik,y} \\ f_{ik,z} \end{bmatrix}. \tag{6.10}$$

Using the general link cost model u_{ij} in Eq. 4.8, the three components of the force $\mathrm{f_{ij}}$ that results at node *i* due to its interaction with nod *j*, can be computed as:

$$f_{ij,x} = -\frac{\partial u_{ij}}{\partial X_i} = -P_{R0}^j \frac{4\pi}{D_T^j A_{eR}^j} \left[\begin{array}{l} \left(\alpha_{ij} e^{\alpha_{ij} \left\| \mathrm{R_i} - \mathrm{R_j} \right\|} \left\| \mathrm{R_i} - \mathrm{R_j} \right\|^n \frac{\left(X_i - X_j \right)}{\left\| \mathrm{R_i} - \mathrm{R_j} \right\|} \right) + \\ \left(n e^{\alpha_{ij} \left\| \mathrm{R_i} - \mathrm{R_j} \right\|} \left\| \mathrm{R_i} - \mathrm{R_j} \right\|^{n-1} \frac{\left(X_i - X_j \right)}{\left\| \mathrm{R_i} - \mathrm{R_j} \right\|} \right) \end{array} \right]$$

$$f_{ij,y} = -\frac{\partial u_{ij}}{\partial Y_i} = -P_{R0}^j \frac{4\pi}{D_T^j A_{eR}^j} \left[\begin{array}{l} \left(\alpha_{ij} e^{\alpha_{ij} \left\| \mathrm{R_i} - \mathrm{R_j} \right\|} \left\| \mathrm{R_i} - \mathrm{R_j} \right\|^n \frac{\left(Y_i - Y_j \right)}{\left\| \mathrm{R_i} - \mathrm{R_j} \right\|} \right) + \\ \left(n e^{\alpha_{ij} \left\| \mathrm{R_i} - \mathrm{R_j} \right\|} \left\| \mathrm{R_i} - \mathrm{R_j} \right\|^{n-1} \frac{\left(Y_i - Y_j \right)}{\left\| \mathrm{R_i} - \mathrm{R_j} \right\|} \right) \end{array} \right]$$

$$f_{ij,z} = -\frac{\partial u_{ij}}{\partial Z_i} = -P_{R0}^j \frac{4\pi}{D_T^j A_{eR}^j} \left[\begin{array}{l} \left(\alpha_{ij} e^{\alpha_{ij} \left\| \mathrm{R_i} - \mathrm{R_j} \right\|} \left\| \mathrm{R_i} - \mathrm{R_j} \right\|^n \frac{\left(Z_i - Z_j \right)}{\left\| \mathrm{R_i} - \mathrm{R_j} \right\|} \right) + \\ \left(n e^{\alpha_{ij} \left\| \mathrm{R_i} - \mathrm{R_j} \right\|} \left\| \mathrm{R_i} - \mathrm{R_j} \right\|^{n-1} \frac{\left(Z_i - Z_j \right)}{\left\| \mathrm{R_i} - \mathrm{R_j} \right\|} \right) \end{array} \right]. \quad (6.11)$$

Combing the above equations, the vector force $\mathrm{f_{ij}}$ can be expressed as:

$$\mathrm{f_{ij}} = \left[\begin{array}{l} f_{ij,x} \\ f_{ij,y} \\ f_{ij,z} \end{array} \right]$$

$$\mathrm{f_{ij}} = -P_{R0}^j \frac{4\pi}{D_T^j A_{eR}^j} \left[\begin{array}{l} \left(\alpha_{ij} e^{\alpha_{ij} \left\| \mathrm{R_i} - \mathrm{R_j} \right\|} \left\| \mathrm{R_i} - \mathrm{R_j} \right\|^{n-1} + n e^{\alpha_{ij} \left\| \mathrm{R_i} - \mathrm{R_j} \right\|} \left\| \mathrm{R_i} - \mathrm{R_j} \right\|^{n-2} \right) \left(X_i - X_j \right) \\ \left(\alpha_{ij} e^{\alpha_{ij} \left\| \mathrm{R_i} - \mathrm{R_j} \right\|} \left\| \mathrm{R_i} - \mathrm{R_j} \right\|^{n-1} + n e^{\alpha_{ij} \left\| \mathrm{R_i} - \mathrm{R_j} \right\|} \left\| \mathrm{R_i} - \mathrm{R_j} \right\|^{n-2} \right) \left(Y_i - Y_j \right) \\ \left(\alpha_{ij} e^{\alpha_{ij} \left\| \mathrm{R_i} - \mathrm{R_j} \right\|} \left\| \mathrm{R_i} - \mathrm{R_j} \right\|^{n-1} + n e^{\alpha_{ij} \left\| \mathrm{R_i} - \mathrm{R_j} \right\|} \left\| \mathrm{R_i} - \mathrm{R_j} \right\|^{n-2} \right) \left(Z_i - Z_j \right) \end{array} \right].$$

$$\mathrm{f_{ij}} = -\left(P_{R0}^j \frac{4\pi}{D_T^j A_{eR}^j} \right) \left(\alpha_{ij} e^{\alpha_{ij} \left\| \mathrm{R_i} - \mathrm{R_j} \right\|} \left\| \mathrm{R_i} - \mathrm{R_j} \right\|^{n-1} + n e^{\alpha_{ij} \left\| \mathrm{R_i} - \mathrm{R_j} \right\|} \left\| \mathrm{R_i} - \mathrm{R_j} \right\|^{n-2} \right) \left[\begin{array}{l} X_i - X_j \\ Y_i - Y_j \\ Z_i - Z_j \end{array} \right]$$

(6.12)

Using the notion of the displacement vector R_{ji}, defined as:

$$\mathrm{R}_{ji} = \begin{bmatrix} X_i - X_j \\ Y_i - Y_j \\ Z_i - Z_j \end{bmatrix}, \tag{6.13}$$

Eq. 6.12 becomes:

$$\mathrm{f}_{ij} = -\left(P_{R0}^{j} \frac{4\pi}{D_T^j A_{eR}^j} \right) \left(n \left\| \mathrm{R}_i - \mathrm{R}_j \right\|^{n-2} e^{\alpha_{ij} \left\| \mathrm{R}_i - \mathrm{R}_j \right\|} + \alpha_{ij} \left\| \mathrm{R}_i - \mathrm{R}_j \right\|^{n-1} e^{\alpha_{ij} \left\| \mathrm{R}_i - \mathrm{R}_j \right\|} \right) \mathrm{R}_{ji} . \tag{6.14}$$

Finally, noting that $\mathrm{R}_{ji} = -\mathrm{R}_{ij}$, we have that the vector force acting on node *i* from its interaction with node *j* is described as:

$$\mathrm{f}_{ij} = \left(P_{R0}^{j} \frac{4\pi}{D_T^j A_{eR}^j} \right) \left(n \left\| \mathrm{R}_i - \mathrm{R}_j \right\|^{n-2} e^{\alpha_{ij} \left\| \mathrm{R}_i - \mathrm{R}_j \right\|} + \alpha_{ij} \left\| \mathrm{R}_i - \mathrm{R}_j \right\|^{n-1} e^{\alpha_{ij} \left\| \mathrm{R}_i - \mathrm{R}_j \right\|} \right) \mathrm{R}_{ij} . \tag{6.15}$$

where now the R_{ji} is the displacement vector starting at the location of node *i* and ending at the location of node *j*.

From Eq. 6.15, it can be observed that the net force acting on a given backbone node *i* can be computed using local information only, that is, information about node *i* itself and its neighbors. Thus, distributed solutions to the mobility control problem can be developed in which each backbone node reacts locally based on forces exerted by neighbor nodes. No centralized global information is needed. Each backbone node can make movement decisions by itself informed by purely local information. The distributed nature of our force-driven mobility control approach is

of key importance in our attempt to provide a scalable and self-organized control system for network performance optimization in dynamic scenarios.

Note that the vector force f_{ij} has the direction of R_{ij} and the amplitude is given by a function of the link distance $L = \left\| \mathrm{R}_i - \mathrm{R}_j \right\|$ and the atmospheric attenuation factor α_{ij}. Thus, the interaction of a given node *i* with its neighbors results in attraction forces acting at the location of node *i*, R_i, which pull node *i* towards the location of its neighbors for improved communications performance. In the following sections, we will study how the amplitude of the force varies under different scenario conditions determined by the path loss exponent and the atmospheric attenuation.

Finally, note from Eq. 6.9 that the net force F_i can be described in terms of two main groups of forces. We use F_i^b to describe the force acting on node *i* coming from its interaction with all its neighbor backbone nodes as:

$$\mathrm{F}_i^b = \sum_{j=1}^{N} b_{ij} \begin{bmatrix} f_{ij,x} \\ f_{ij,y} \\ f_{ij,z} \end{bmatrix}, \tag{6.16}$$

and F_i^c to describe the force acting on node *i* coming from its interaction with all the terminal nodes covered by backbone node *i,* as:

$$\mathrm{F}_i^c = \sum_{k=1}^{M} 1(h_{(k)} = i) \begin{bmatrix} f_{ik,x} \\ f_{ik,y} \\ f_{ik,z} \end{bmatrix}. \tag{6.17}$$

As it can be observed F_i^b is a force that tries to minimize the potential energy stored in the links connecting the backbone nodes, thus driving the backbone nodes to

stick together for backbone connectivity optimization. On the other hand, F_i^c is a force that tries to minimize the potential energy stored in the links connecting the backbone node *i* with its covered end hosts, thus pulling backbone node *i* close to its terminals, for network coverage optimization. Thus, the net for acting on backbone node *i* can be described as a balancing force for joint coverage-connectivity optimization, as:

$$F_i = \eta F_i^b + F_i^c , \tag{6.18}$$

with F_i^b and F_i^c as described din Eqs. 6.16 and 6.17 respectively.

In the next section we present an algorithm for relocating the backbone nodes based on the value of the net force at the backbone nodes' locations. This algorithm also gives a method that assigns each end host to one of the backbone nodes.

6.4.2 Force-driven optimization algorithm

The mathematical formulation of the previous section gives us a method for relocating each backbone node in the direction of the net force such that the cost function shows the steepest descent. In this method, we use a set of iterations that both relocate the backbone nodes iteratively, and reassign the end hosts to the backbone nodes in each iteration.

Two operations are used for each iteration: in the first operation, the values of the forces are used to relocate the backbone nodes; in the second operation, the new locations of the backbone nodes are used to reassign the end hosts to the backbone nodes. These operations can be stated in a more accurate way as follows:

- *Relocation*: this operation uses the value of the force on each backbone node to find the backbone node's new location. Such a relocation process can be done as follows:

$$\mathrm{R}_{\mathrm{i}}^{\mathrm{n+1}} = \mathrm{R}_{\mathrm{i}}^{\mathrm{n}} + \delta \mathrm{F}_{\mathrm{i}} \tag{6.19}$$

in which $\mathrm{R}_{\mathrm{i}}^{\mathrm{n}}$ denotes the location of the backbone node *j* at iteration *n* and δ is a small step size, and we have $\delta > 0$.

- *Reassignment*: this operation assigns each end host node *k* to the backbone node *i* that minimizes the link cost function u_{ik} for all $1 \le i \le N$. For this purpose, we find the following value for each end host node *k*:

$$\begin{aligned} & h^n(k) = \arg\min_{\mathrm{i}} u(\mathrm{R}_i, \mathrm{r}_k), \\ & 1 \le i \le N \end{aligned} \tag{6.20}$$

in which $h^n(k)$ represents the backbone node that provides coverage to the end host node *k* at iteration *n*, and $\arg\min_{\mathrm{i}}$ represents the index *i* that corresponds to the minimum of $u(\mathrm{R}_i, \mathrm{r}_k)$ for all $1 \le j \le N$.

Our main conjecture regarding the above iterations is that in each step of each type of the above iterations, the cost function remains constant or decreases. Note that the first operation decreases the cost function because it relocates a backbone node in the direction of the force, which is the opposite direction of the gradient of the cost function (Eq. 6.6). The second operation further reduces the cost because it reassigns a terminal node *k* from a backbone node *i* to another backbone node i' only if $u(\mathrm{R}_i, \mathrm{r}_k) \ge u(\mathrm{R}_{i'}, \mathrm{r}_k)$, and such an operation either reduces the cost function or does not change its current value.

Also note that if we form the a sequence $U_{(1)}, U_{(2)}, ..., U_{(n)}, ...$ with $U_{(n)}$ representing the values of cost function during the above iterations, then the above sequence is non-increasing and lower bounded (because $U_{(n)} > 0$). Therefore, this sequence has to converge to a value as n increases. Thus, the convergence criterion is stated as follows:

$$U_{(n+1)} - U_{(n)} < \varepsilon, \tag{6.21}$$

in which ε is a small positive constant.

Note from Eq. 6.21 that convergence is met when the variation of the energy function *U* is negligible, which implies that the overall net force acting on the system is also negligible. In analogy with physical systems, we refer to this condition as the equilibrium condition of the network system. In equilibrium, the net forces acting on the backbone nodes must converge to zero. Thus, an algorithm based on relocating backbone nodes in the direction of the net forces at each node stops when the amplitude of the force at all backbone nodes is small enough. We use the following criterion to stop the algorithm iterations:

$$\left\|\mathrm{F_i}\right\| < \varsigma \quad \text{for } 1 \le \mathrm{i} \le \mathrm{N} \tag{6.22}$$

where ς is a small positive constant.

In Fig. 6.2, we show a completely distributed force-driven mobility control algorithm, where every backbone node executes a simple protocol based on the two operations described above: reassignment and relocation.

For each backbone node *i*

While $(\|F_i\| > \varsigma)$

Update terminal neighbor set *t(i)*

Compute net force $\mathrm{F_i}$

Relocate to $\mathrm{R_i^{n+1}} = \mathrm{R_i^{n}} + \delta \mathrm{F_i}$

End

Figure 6.2: Force-driven mobility control algorithm.

Note that the reassignment operation is executed by the terminal nodes, which send their decisions to their chosen backbone nodes. The backbone nodes then use this information to update their respective terminal neighbor sets. We use *t(i)* to refer to the set of terminal nodes assigned to backbone node *i*.

Our last remark is on the value of η. Recall that this value determines the relative importance of the two terms of the cost function. For example, if the backbone nodes run on batteries, long range power transmissions between neighbor backbone nodes is very power consuming and therefore a large value of η is desirable. On the other hand, if we have plenty of power for each backbone node, for example through connection to the main power, a smaller value of η should be used in the optimization problem. Also, the dynamics of the scenario have a strong influence on the choice of the value of η. That is, when atmospheric obscuration is highly present and rapidly changing, a high value of η allows for stronger backbone connectivity and robustness against failures which could disconnect the backbone network. On the other hand, in clear sky conditions a smaller value of η can be used to improve network coverage while maintaining good backbone connectivity. Indeed,

in either case the mathematical formulation of the cost function and our optimization scheme is capable of modeling the problem.

6.5 Spring System

In this section we present a quadratic optimization method for coverage and connectivity control in DWB-based networks in clear atmospheric conditions. We show that when the effects of atmospheric obscuration can be neglected, the cost function U for the network system is analogous to the potential energy of a spring system where wireless links are replaced by physical springs exerting forces on network nodes. We show that Hooke-type forces [53] can be defined at each backbone node, which drive the network topology to achieve energy minimizing configurations.

6.5.1 Quadratic optimization

In clear atmospheric conditions we can neglect the effects of atmospheric obscuration ($\alpha_{ij} = 0$) and assume a path loss exponent of $n = 2$. Then the link cost u_{ij} becomes:

$$u_{ij} = \underbrace{P_{R0}^{j} \frac{4\pi}{D_T^i A_{eR}^j}}_{k_{ij}} L^2 , \tag{6.23}$$

which is a quadratic function of L, the link distance. The link margin P_{R0} is determined by the receiver sensitivity and the turbulence induced fading as defined in

section 4.2.2. Initially, we assume the deployment area of the backbone nodes to share the same turbulence conditions and thus P_{R0} will not change with the location of the backbone nodes. The $\frac{4\pi}{D_T A_{eR}}$ constant will also be independent of the backbone nodes' locations and will be determined by the directivity of the transmitter antenna D_T and the effective receiver area A_{eR}. Thus, we can reformulate the link cost function as:

$$u_{ij} = k_{ij}\left\|R_i - R_j\right\|^2, \text{ where } k_{ij} = P_{R0}^{j}\frac{4\pi}{D_T^i A_{eR}^j}, \tag{6.24}$$

which is analogous to the potential energy of a spring with spring constant k_{ij} and displacement $\mathrm{R_i} - \mathrm{R_j}$ [53]. Using this link cost function (Eq. 6.24), we can model wireless links as springs which exert attraction forces between network nodes for energy minimization. The beauty of this model is that given the link margin P_{R0} and the receiver area A_{eR}, the spring constant is inversely proportional to the transmitter directivity D_T. Thus, directional wireless links which have high directivities translate into springs with low spring constants, which allow for higher link distances. On the other hand, omnidirectional wireless links use low directivity antennas associated with high spring constants that require much more energy to elongate. This result is very much in accordance with our network architecture, where directional wireless links are used to connect backbone nodes over large distances, whereas omnidirectional wireless links are used to connect each terminal node to its assigned base station.

Using the spring link cost model 6.13, the mobility control problem formulation becomes:

$$\min\left\{ U(\mathrm{R}_1,...,\mathrm{R}_\mathrm{N}) = \eta \cdot \underbrace{\left(\sum_{i=1}^{N} \sum_{j=1}^{N} b_{ij} k_{ij} \left\| \mathrm{R}_\mathrm{i} - \mathrm{R}_\mathrm{j} \right\|^2 \right)}_{F} + \underbrace{\left(\sum_{k=1}^{M} k_{h(k)k} \left\| \mathrm{R}_{\mathrm{h}(k)} - \mathrm{r}_k \right\|^2 \right)}_{G} \right\}$$

$$\text{where} \qquad k_{ij} = P_{R0}^{j} \frac{4\pi}{D_T^i A_{eR}^j}, \tag{6.25}$$

$$\text{and} \qquad b_{ij} = \begin{cases} 1 & \text{if } (i,j) \in T \\ 0 & \text{o.w.} \end{cases}$$

The goal of the optimization problem is to find the locations of all the backbone nodes that minimize the above cost function. A very interesting property of the above cost function is that due to its quadratic form it can be solved analytically, and the locations found by solving the optimization problem are always inside the network, given the convexity of the feasible region. Moreover, this cost function is analogous to the potential energy of an equivalent network with edges replaced by springs, with spring constants as defined in Eq. 6.24. Thus, we can model the DWB network as a spring system whose potential energy is analogous to the communication cost of the DWB network. In a spring system, nodes move according to the forces exerted by the springs attached to them until reaching an equilibrium configuration where the net force on each node is equal to zero [53]. The equilibrium configuration is also the configuration that minimizes the potential energy of the spring system.

Note that the above cost function is not mutually convex. Thus, to increase the confidence margin of optimality of the solution, a perturbation method is used. The perturbation is applied several times after each time that the algorithm converges. If

the force-driven algorithm converges to the same solution after a certain number of times (typically, 2-3 times) the corresponding solution is chosen as a global optimal solution with a high degree of confidence.

In the following section, we derive the force-driven mobility control algorithm for the spring system model.

6.5.2 SPRING algorithm

As explained in section 6.3, the value of the net force at backbone node *i* is computed as the gradient of the energy function *U* with respect to the location the backbone node R_i and can be described as:

$$\mathrm{F_i} = \eta \mathrm{F_i^b} + \mathrm{F_i^c} = \eta \sum_{j=1}^{N} b_{ij} \mathrm{f_{ij}} + \sum_{k=1}^{M} 1(h_{(k)} = i) \mathrm{f}_{ik} \tag{6.26}$$

where $\mathrm{f_{ij}}$ is described using Eq. 6.15 as:

$$\mathrm{f_{ij}} = \left(P_{R0}^{j} \frac{4\pi}{D_T^j A_{eR}^j} \right) \left(2e^{\alpha_{ij} \left\| \mathrm{R_i} - \mathrm{R_j} \right\|} + \alpha_{ij} \left\| \mathrm{R_i} - \mathrm{R_j} \right\| e^{\alpha_{ij} \left\| \mathrm{R_i} - \mathrm{R_j} \right\|} \right) \mathrm{R_{ij}} \tag{6.27}$$

Note that in the case of the spring system, $\alpha_{ij} = 0$ for all *i, j*, thus $\mathrm{f_{ij}}$ becomes:

$$\mathrm{f_{ij}} = \left(P_{R0}^{j} \frac{4\pi}{D_T^j A_{eR}^j} \right) 2\mathrm{R_{ij}} = 2k_{ij} \mathrm{R_{ij}} \tag{6.28}$$

with k_{ij} as described in 6.24. Note that the force $\mathrm{f_{ij}}$ in 6.28 is a weighted average of the distance vectors between backbone node *i* and its neighbors. This result is in agreement with the behavior of an analogous spring system, where nodes react based

on forces exerted by neighbor nodes and move in the direction of the weighted average position of its neighbors.

Note that the force on a given backbone node only depends on the location of its neighbors. Thus, a completely distributed algorithm can be designed where each backbone node reacts locally to the forces exerted by neighbor nodes, providing scalability and robustness. No centralized global information is needed. Each backbone node can make movement decisions by itself informed by purely local information and the overall network achieves global optimal configurations.

The SPRING optimization algorithm can be derived from the general methodology described in section 6.3, which is based on two main operations: relocation and reassignment. Recall that the relocation operation uses the value of the force to find the node's new location, as:

$$\mathrm{R}_{\mathrm{i}}^{\mathrm{n+1}} = \mathrm{R}_{\mathrm{i}}^{\mathrm{n}} + \delta \mathrm{F}_{\mathrm{i}} .$$

Using Eq. 6.9 for the net force on backbone node i, F_{i}, the relocation operation is described as:

$$\mathrm{R}_{\mathrm{i}}^{\mathrm{n+1}} = \mathrm{R}_{\mathrm{i}}^{\mathrm{n}} + \delta \left[\eta \sum_{j=1}^{N} b_{ij} f_{ij} + \sum_{k=1}^{M} 1(h_{(k)} = i) f_{ik} \right]. \tag{6.29}$$

For the spring system case, using Eq. 6.28, the above operation becomes:

$$\mathrm{R}_{\mathrm{i}}^{\mathrm{n+1}} = \mathrm{R}_{\mathrm{i}}^{\mathrm{n}} + 2\delta \left[\eta \sum_{j=1}^{N} b_{ij} k_{ij} \mathrm{R}_{ij}^{\mathrm{n}} + \sum_{k=1}^{M} 1(h_{(k)} = i) k_{ik} \mathrm{R}_{ik}^{\mathrm{n}} \right] \tag{6.30}$$

Note that the new location found using 6.30 is one step size in the path between the current location of node i and the weighted average of the location of its neighbors, with weights defined by the spring constants k_{ij}.

The reassignment operation was also described in section 6.3 as:

$h^n(k) = \arg\min_i u(\mathrm{R}_i, \mathrm{r}_k),\ \text{for}\ 1 \le i \le N$, where *h(k)* denotes the index of the backbone node assigned to terminal node *k*. Using the expression for the link cost in Eq. 6.24, the reassignment operation for the spring algorithm becomes:

$$h^n(k) = \arg\min_i k_{ik} \left\| \mathrm{R}_i - \mathrm{r}_k \right\|^2 \qquad 1 \le i \le N \tag{6.31}$$

The SPRING algorithm thus follows the same form as the general force-driven mobility control algorithm illustrated in Fig. 6.2:

For each backbone node *i*

While $(\|F_i\| > \varsigma)$

Update terminal neighbor set *t(i)*

Compute net force F_i

Relocate to $\mathrm{R}_i^{n+1} = \mathrm{R}_i^{n} + \delta \mathrm{F}_i$

End

where now the force F_i is defined by Eqs. 6.9-6.15.

6.5.3 Simulation results

In order to gain more insight on the problem and verify the performance of our optimization algorithm, we present results from simulation studies with different design parameters.

In our initial simulations, *N* terminal nodes are distributed in a 100x100 two dimensional plane. Terminal nodes are organized in clusters. The first terminal node is placed in the plane according to a uniform random distribution. Each other terminal is placed within *clusterRange* of the previous terminal node with probability *p_cluster*, and uniformly in the 100x100 plane with probability *1-p_cluster*. Next, *M* backbone nodes are placed at random in the plane and an initial ring topology is built connecting all backbone nodes. Then, the SPRING algorithm is executed to make backbone nodes adjust their position until convergence to the optimal backbone configuration.

Before we report quantitative results, we first present several figures to visually illustrate the effectiveness of the mobility control algorithm. Fig. 6.3 shows results for a network with 100 terminal nodes and 10 backbone nodes. The values used for the variables *clusterRange* and *p_cluster* are 10 and 0.2 respectively. The backbone nodes are labeled and the links between them are shown in thick dotted lines. Links from each terminal node to its closest backbone node are shown in thinner dotted lines.

Fig. 6.3a shows the initial non-optimal network configuration. Fig. 6.3b shows the resulting network configuration after running the mobility control algorithm with a balancing factor $\eta = 1$. In this case, the low value of η allows backbone nodes to move close to the terminal nodes to optimize network coverage at the expense of low backbone connectivity. Figs. 6.3c and 6.3d show the resulting network configurations with $\eta = 5$ and $\eta = 10$ respectively. The higher value of η the more weight is put on the backbone connectivity objective thus making the backbone nodes move closer to

each other. Finally, Figs. 6.3e and 6.3f show the resulting network configurations for $\eta = 20$ and $\eta = 30$, where stronger backbone networks are produced at the expense of lower network coverage.

In Fig. 6.4 we show a network with 20 backbone nodes. The number of terminals remains 100 and they are randomly placed according to the procedure explained above. As seen in Fig. 6.4, the increased number of backbone nodes allows more flexibility to optimize network coverage with less penalization on backbone connectivity, and vice versa.

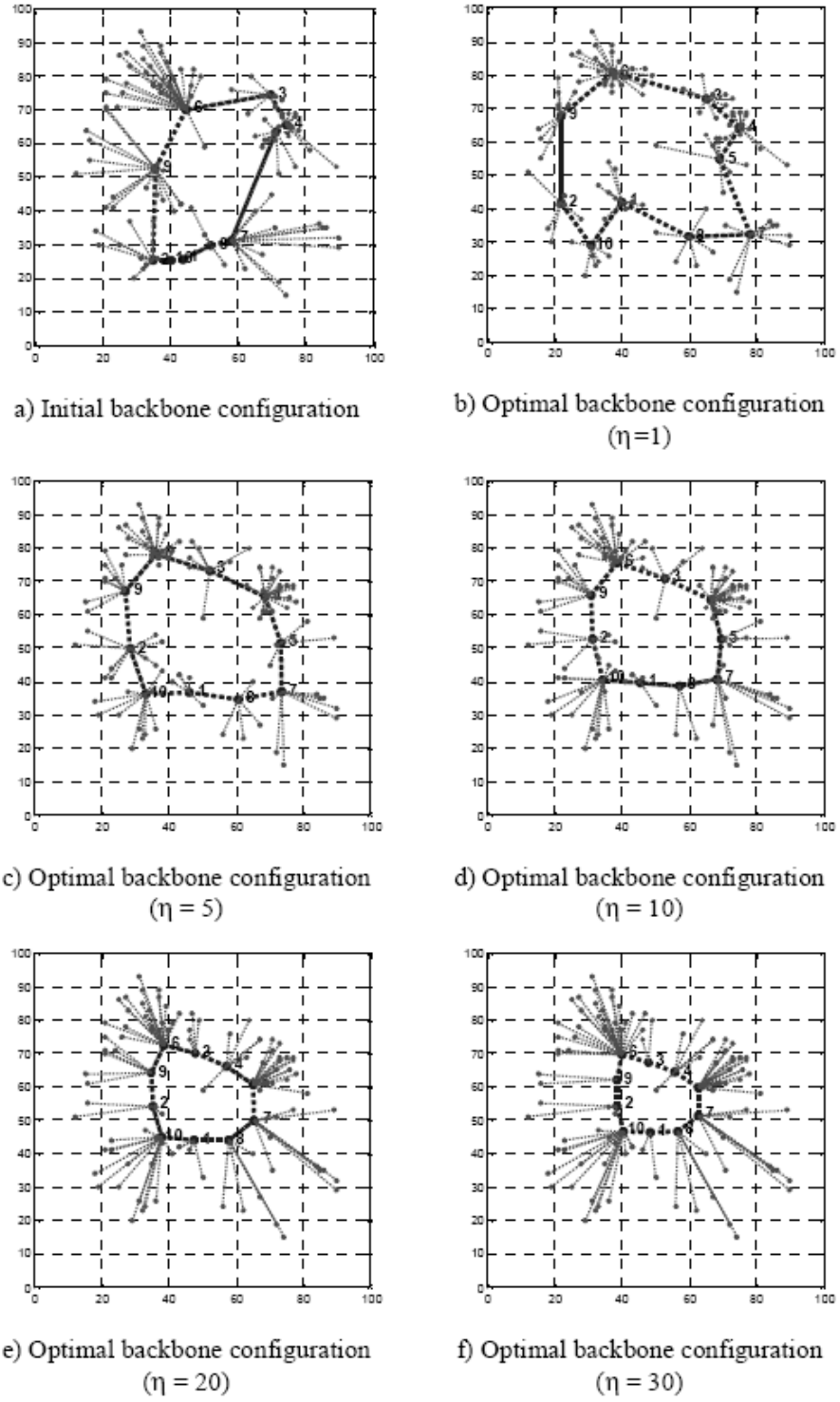

a) Initial backbone configuration

b) Optimal backbone configuration (η=1)

c) Optimal backbone configuration (η = 5)

d) Optimal backbone configuration (η = 10)

e) Optimal backbone configuration (η = 20)

f) Optimal backbone configuration (η = 30)

Figure 6.3: Initial non-optimal configuration (a) and optimal network configurations (b, c, d, e) after running the SPRING mobility control algorithm for different values of η (10 backbone nodes).

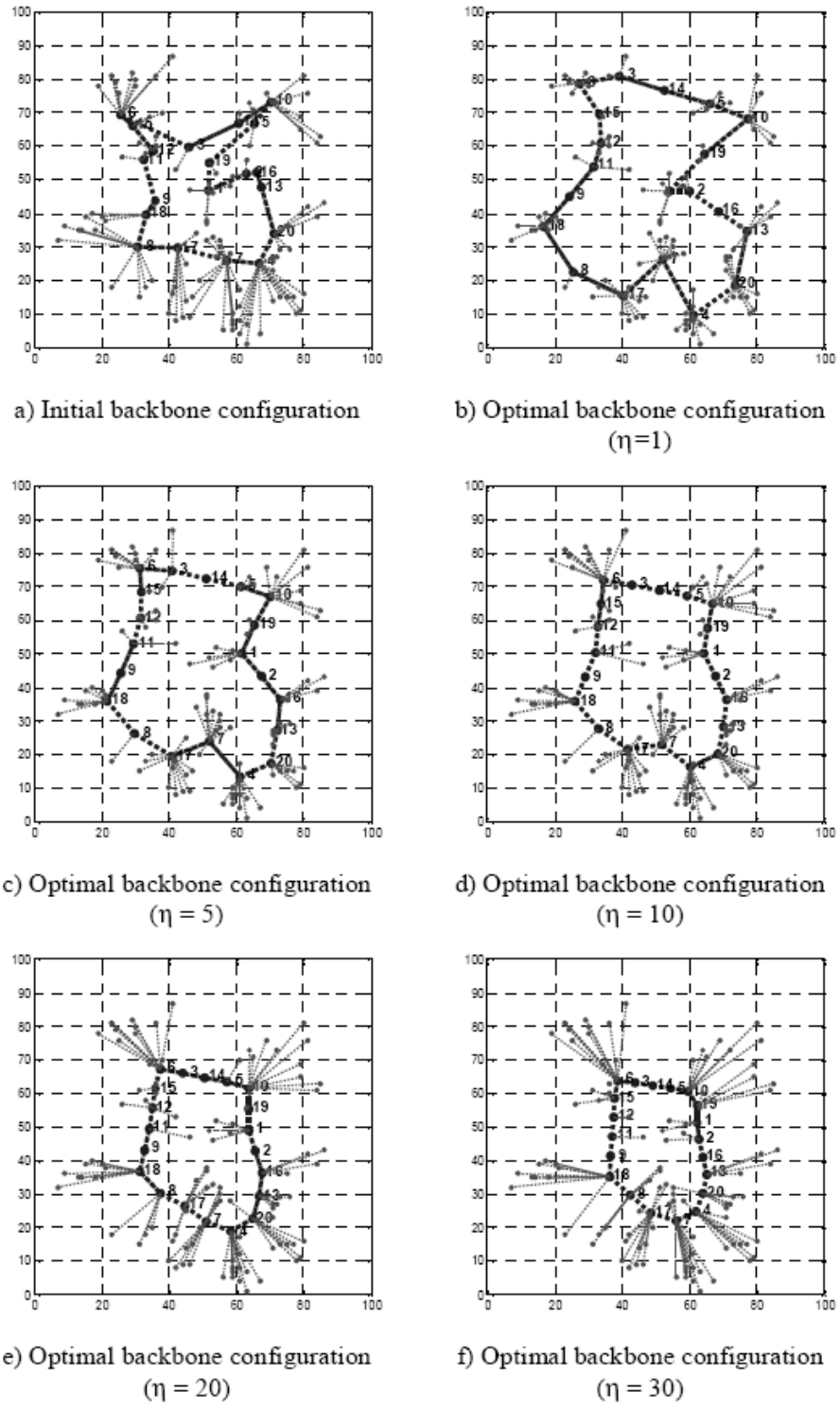

a) Initial backbone configuration

b) Optimal backbone configuration (η=1)

c) Optimal backbone configuration (η = 5)

d) Optimal backbone configuration (η = 10)

e) Optimal backbone configuration (η = 20)

f) Optimal backbone configuration (η = 30)

Figure 6.4: Initial non-optimal configuration (a) and optimal network configurations (b, c, d, e) after running the SPRING mobility control algorithm for different values of η (20 backbone nodes).

In order to quantitatively show the performance of our mobility control algorithm, we computed the coverage and connectivity cost metrics for the Pareto optimal network configurations obtained. Again, we considered networks with 100 terminal nodes and with 10 and 20 backbone nodes respectively. We used the following set of weights: 0.01, 0.3, 1, 3, 5, 10, 15, 20, 25, and 30, to generate 10 Pareto optimal solutions for the networks under study. Fig. 6.5 shows the Pareto optimal curves obtained. The *x* axis represents the coverage cost metric *G*, while the *y* axis represents de connectivity cost metric *F*. We used FSO links for the backbone-to-backbone links with 2 mrad half beam divergence and RF links for the terminal-to-backbone links with $\pi/4$ rad half beam divergence. The minimum required received power used was -45 dBm (31.6 nW) for all network nodes. The values of *F* and *G* obtained were normalized and scaled for the plot in Fig. 6.5.

Since the algorithm is solving a multi-objective optimization problem, optimal solutions, which combine low values of both cost metrics, must lie in the south-west corner of the solution space, as shown in Fig. 6.5. Note that the increased number of resources (base stations or backbone nodes) allows for improved Pareto optimization, as shown by the deeper south-west configuration of the Pareto optimal curve associated with the 20 backbone node network in the solution space. Fig. 6.5 also shows the limit on the network coverage cost metric. As we lower the weight on backbone connectivity, the network coverage cost decreases until reaching a point where no further improvement is possible for the given number of backbone nodes. As expected, when using 20 backbone nodes, network coverage can be further optimized due to the increased number of resources. The backbone connectivity cost

metric, on the other hand, can be brought to zero by increasing the balancing factor η, which would lead to a network configuration where all backbone nodes converge into a single point. As seen in Fig. 6.5, both curves tend to zero as the weight on backbone connectivity is increased.

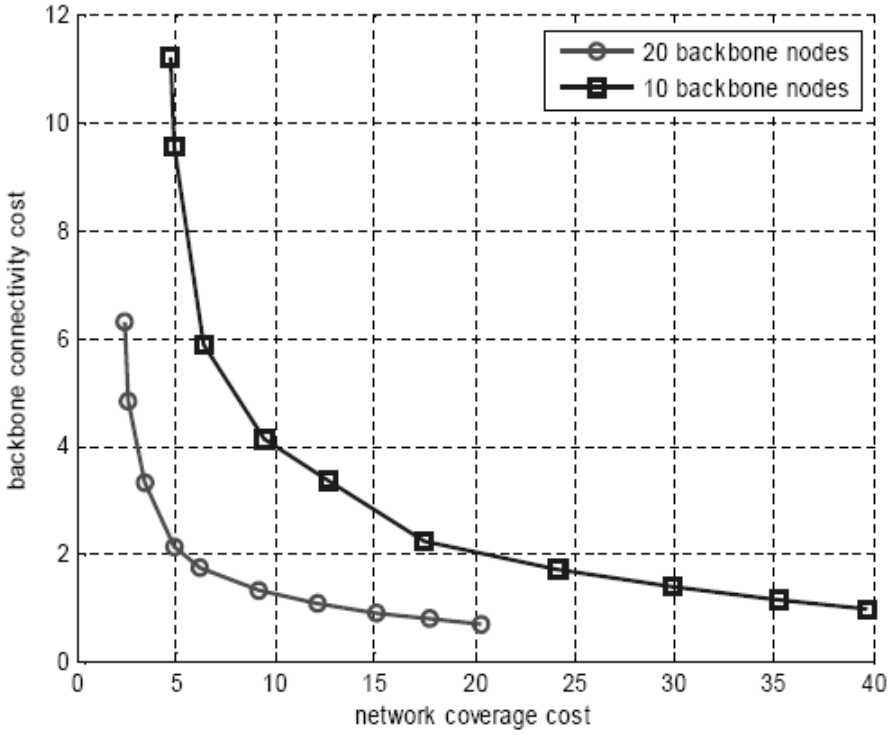

Figure 6.5: Pareto Optimal set of solutions (10 and 20 backbone nodes).

In order to show the self-organizing capability of our network system, we developed a simulation environment that outputs video sequences of dynamic network scenarios. The objective is to show that our self-organized network system is able to track the network dynamics.

As explained in Chapter 3, uncontrollable parameters such as the mobility of the terminal nodes and the atmospheric conditions constitute the network dynamics, which are modeled as external excitations to the network system. In this section, we assume clear atmospheric conditions and thus the scenario dynamics is based on the mobility of the terminal nodes. We first place *N* terminal nodes organized in clusters in a two dimensional plane following the procedure introduced earlier in this section. We then use the Reference Point Group Mobility (RPGM) model [54] to move the terminal clusters in the plane and show how the backbone system is able to react to the mobility of the terminal nodes driven by local forces that minimize the energy of the network system.

First, in Fig. 6.6, we show a sequence of snapshots of the evolution of the network form an initial non-optimal configuration to the optimal configuration driven by local forces computed using the SPRING algorithm. In 6.6a we show the initial placement of the terminal nodes. In this case, 100 terminal nodes are placed in a 50km x 50km plane. These terminal nodes constitute the demand for broadband connectivity. For that purpose, a "squat team" of backbone nodes are dropped in the area in order to form a backbone network to interconnect the terminal nodes. Fig. 6.6b shows the initial placement of the backbone nodes. The backbone nodes are deployed at an altitude of 0.5km. Fig. 6.6 shows 2D projections of the 3D scenario. Next, in Fig. 6.6c the backbone nodes form an initial backbone topology. We use ring topologies to assure resilience through bi-connectivity (as explained in Chapter 5). Fig. 6.6d shows the result of the initial reassignment step and the computation of the forces that arise at each backbone node. The green solid lines at each backbone node

represent the amplitude and direction of the force. Figures 6.6e through 6.6h show the resulting backbone configurations after several iterations of the force-driven mobility control algorithm. Note how the backbone nodes move in the direction of the net force at their respective locations until the net force is small enough. Recall that the SPRING algorithm converges when $\|F_i\| < \varsigma$ for $1 \le i \le N$ (see section 6.4.2). In this simulation we used $\varsigma = 1$. At this point, shown in Fig. 6.6i, the network has reached the equilibrium configuration which minimizes the energy function *U*.

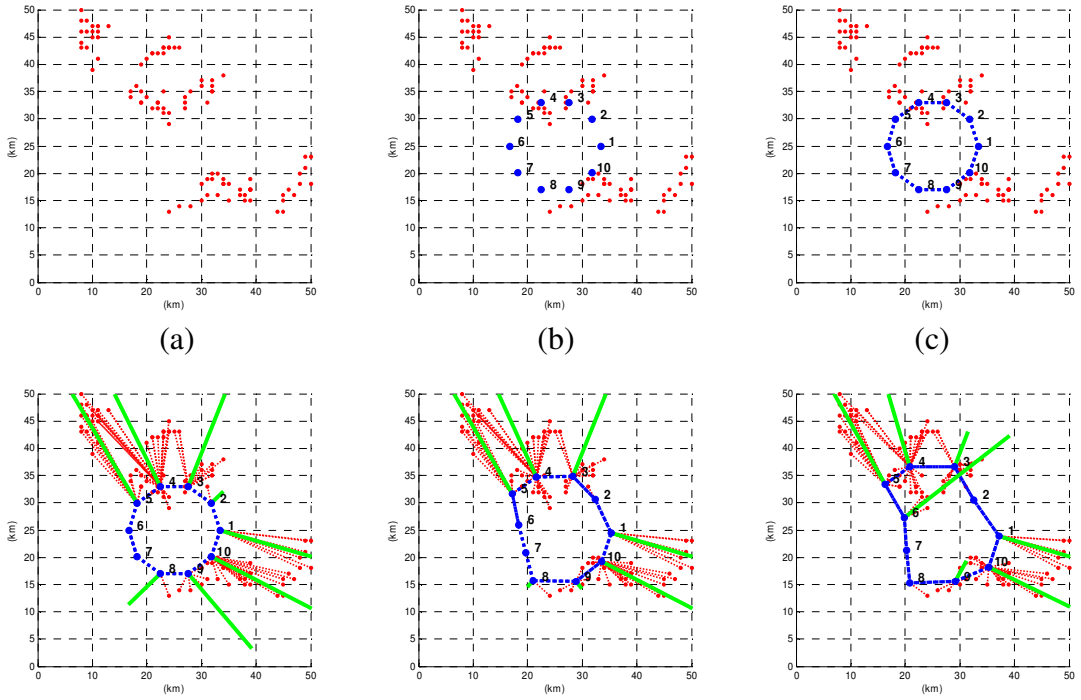

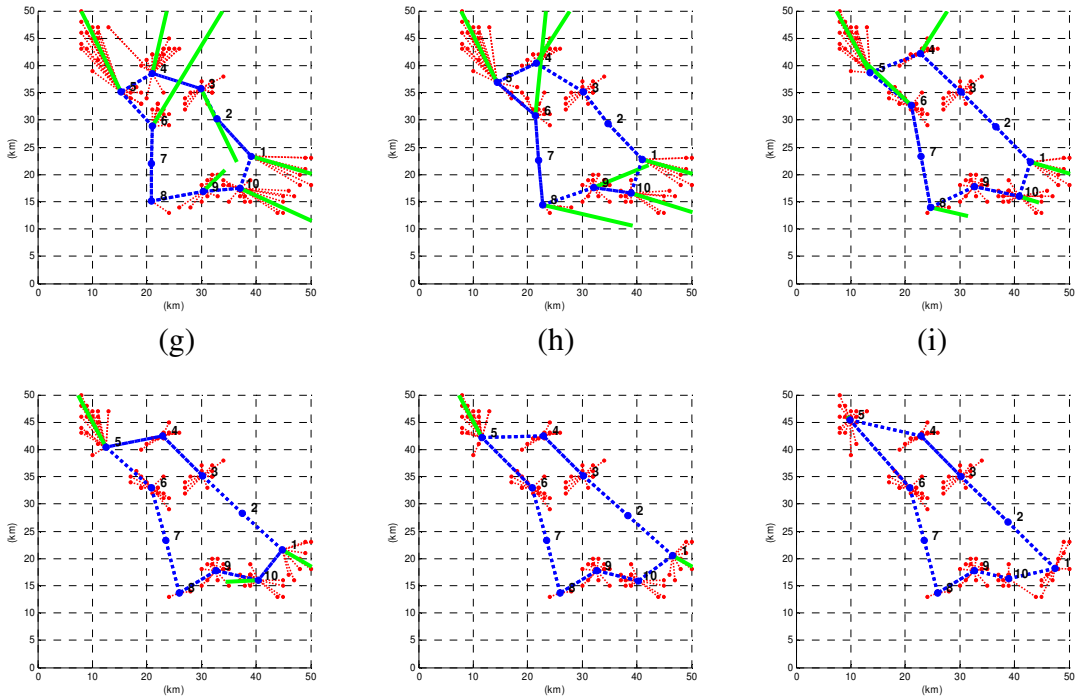

Figure 6.6: Network evolution from initial placement to equilibrium for a fixed terminal nodes' position scenario.

In Fig. 6.7 we show a sequence of snapshots of a simulation where terminal nodes move based on the RPGM model. Figs. 6.7a-6.7c show the evolution of the backbone network until the equilibrium configuration for the initial placement of the network nodes. Note that in Fig. 6.7 we also show the 3D view of the network (upper left corner), the evolution of the energy function U, as well as the energy cost functions for coverage (G) and connectivity (F) (lower left corner), and the amplitude of the forces at each backbone node (lower right corner). With these four plots in each figure, we can obtain a really good understanding of the network dynamics and the system's self-organizing capability. In this simulation we again used FSO links for the backbone-to-backbone links with 2 mrad half beam divergence and RF links for

the terminal-to-backbone links with $\pi/4$ rad half beam divergence. The minimum required received power used was also -45 dBm (31.6 nW) for all network nodes.

As it can be observed in Fig. 6.7a, the initial non-optimal configuration is characterized by a high potential energy value U = 5557.24W. This energy cost is mainly due the coverage cost G = 5557.22W. The backbone connectivity cost is fairly small (F = 0.02W) since the backbone nodes are initially placed close to each other. Note that the amplitudes of the forces are very large indicating the need for a topology adjustment in order to minimize the energy of the system. Fig. 6.7b shows the resulting network configuration after 1.5 minutes of backbone reaction using the SPRING algorithm (the velocity of the backbone nodes used is 4 km/min). Note how the backbone topology has stretched driven by the forces acting at each backbone node and the total energy of the system has dropped to U = 2012.7W. The coverage cost has also reduced to G = 2012.6W and the connectivity cost (F = 0.10W) has slightly increased due to the increased distances between backbone nodes. Fig. 6.7c shows the optimal configuration obtained after the equilibrium condition is met. The amplitudes of the forces are now $\|F_i\| < 1 \quad \text{for } 1 \le i \le N$ and the energy of the system has reduced to U = 372.57W. In this case, the network took 5 minutes to converge to the optimal configuration from the initial placement shown in Fig. 6.7a.

After this point the RPGM model is used to move the terminal nodes. The velocity of the terminals is chosen to be 2 km/min and the location of the terminal nodes is updated every 1 minute. Fig. 6.7d shows the new state of excitation of the network system caused by the first update on the mobility of the terminal nodes. Note that as soon as the update is received, a new reassignment operation is executed and

new forces appear at each backbone node. The energy of the system has increased to U = 424.89W and new forces arise to make the network react to the external excitation. Thus in this simulation (Fig. 6.7), the excitation caused by the terminal nodes mobility is illustrated in the following ways:

1) The total energy of the system *U* increases.
2) The coverage energy cost increases: this is due to the additional energy needed to communicate with terminal nodes that have moved out of their optimal positions with respect to the backbone network.
3) The connectivity energy cost remains constant. The backbone nodes have yet to move and thus this cost function does not change.
4) New forces appear at the backbone nodes as a result of the excitation to the network system.

Fig. 6.7e shows the resulting configuration after 0.5 minutes of reaction. Note how in Fig. 6.7e, after 0.5 minutes of reaction, the network has converged to an optimal configuration where the total energy *U* has decreased from 424.89W to 369.04W and the amplitudes of the net forces acting on each backbone node are close to zero.

Fig. 6.7f shows a new excitation to the network system caused by the terminals' mobility. The total energy of the system goes up to 503.51W and new forces arise at each backbone node that make the network adjust its topology. Figs. 6.7g and 6.7h show two snapshots of the backbone reaction after 0.5 and 1 minute respectively. In this case, the network is able to reduce the energy to U = 409.70W, but does not reach equilibrium before a new update is received (Fig. 6.7i).

Note how in the rest of the sequence (Figs. 6.7j-6.7t) the network is able to continue reacting to the excitations by following the local forces computed at each backbone node.

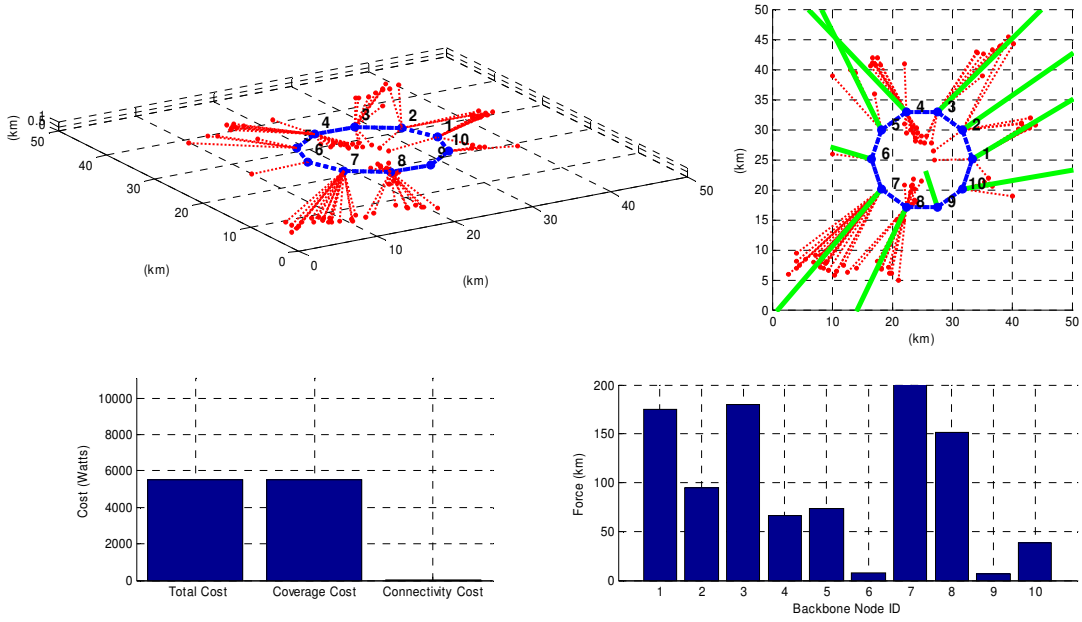

(a) Initial placement (0 min):
U = 5557.24W; G = 5557.22W; F = 0.02W

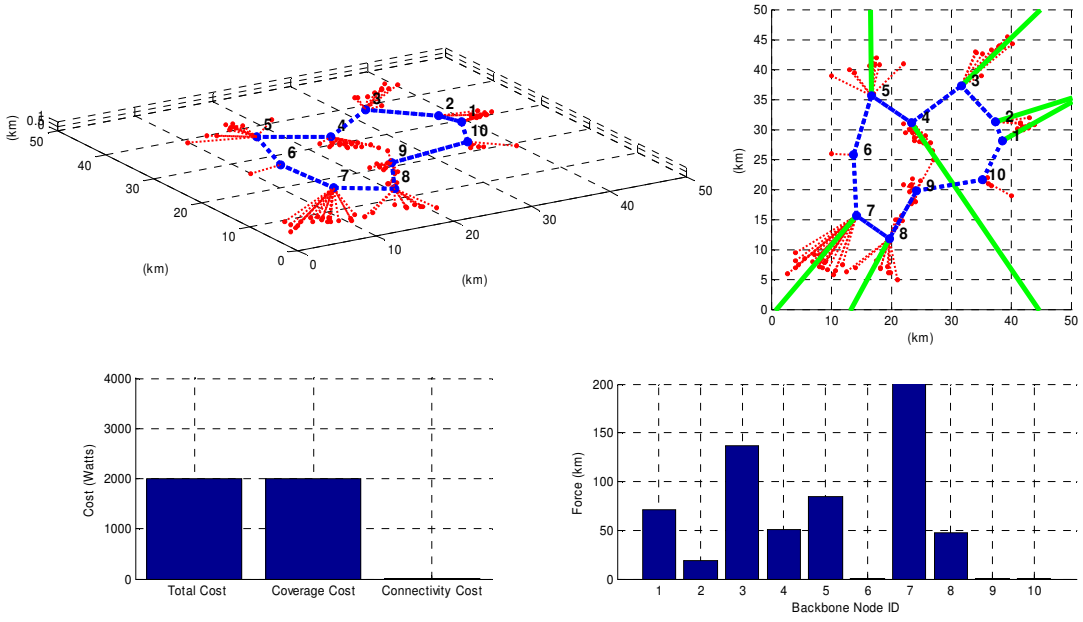

(b) Backbone reaction (1.5 min):
U = 2012.7W; G = 2012.6W; F = 0.10W

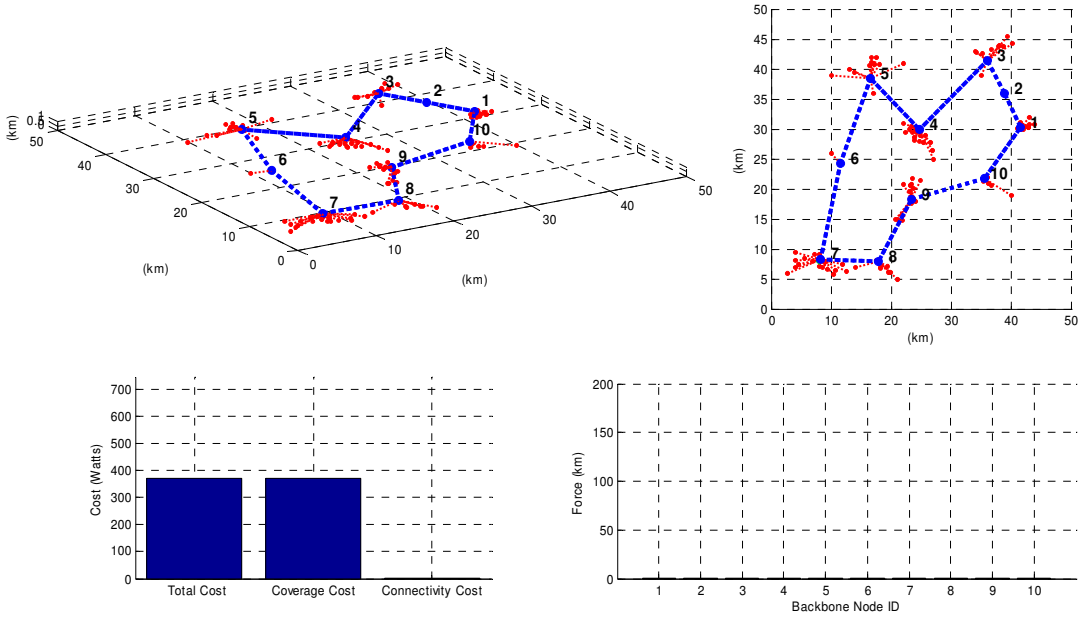

(c) Backbone reaction (5 min):
Equilibrium: U = 372.57W; G = 372.42W; F = 0.15W

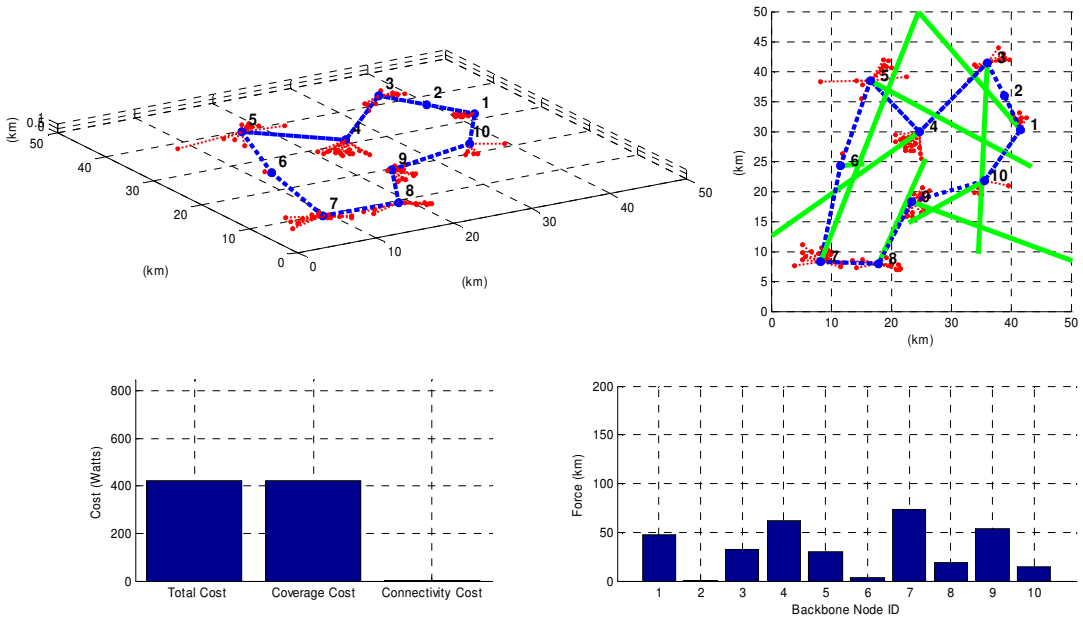

(d) Terminals location update (5 min):
U = 424.89W; G = 424.74W; F = 0.15W

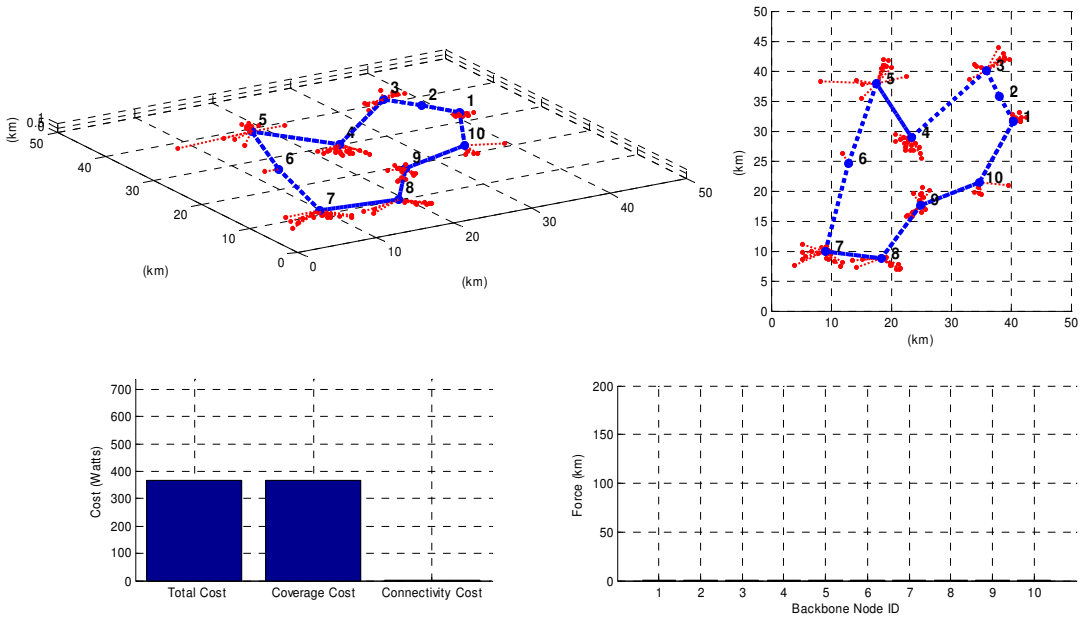

(e) Backbone reaction (5.5 min):
Equilibrium: U = 369.04W; G = 368.91W; F = 0.13W

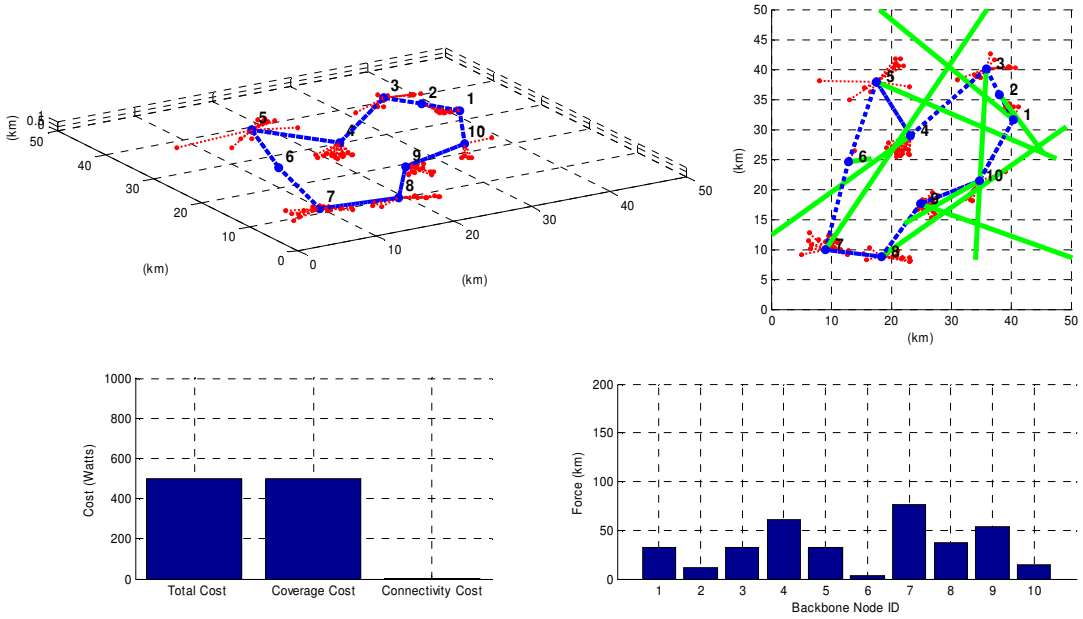

(f) Terminals location update (6 min):
U = 503.51W; G = 503.38W; F = 0.13W

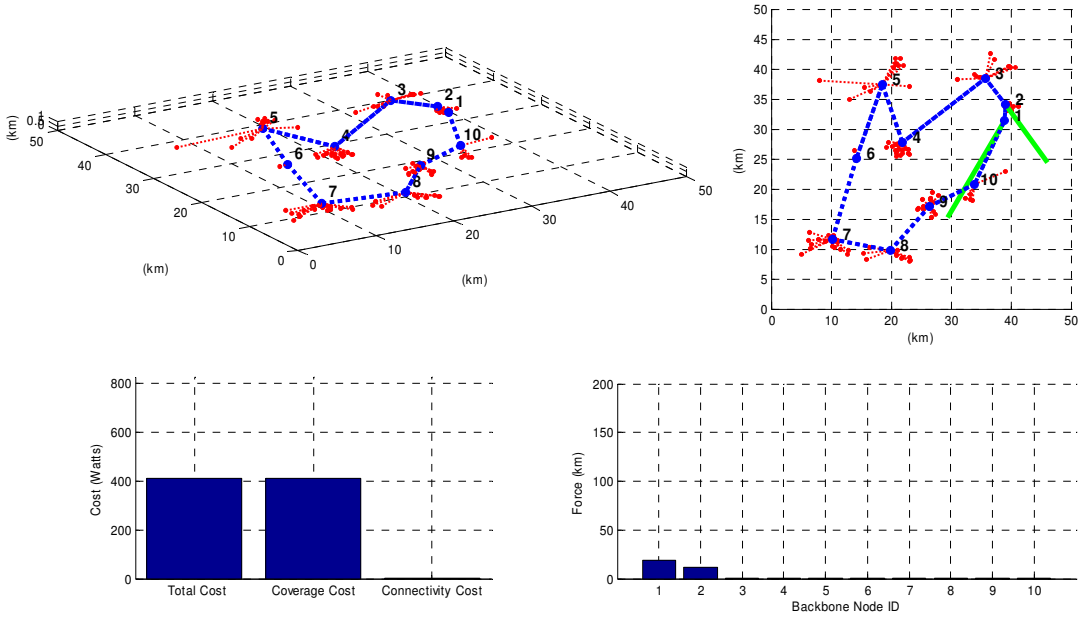

(g) Backbone reaction (6.5 min):
U = 413.30W; G = 413.18W; F = 0.12W

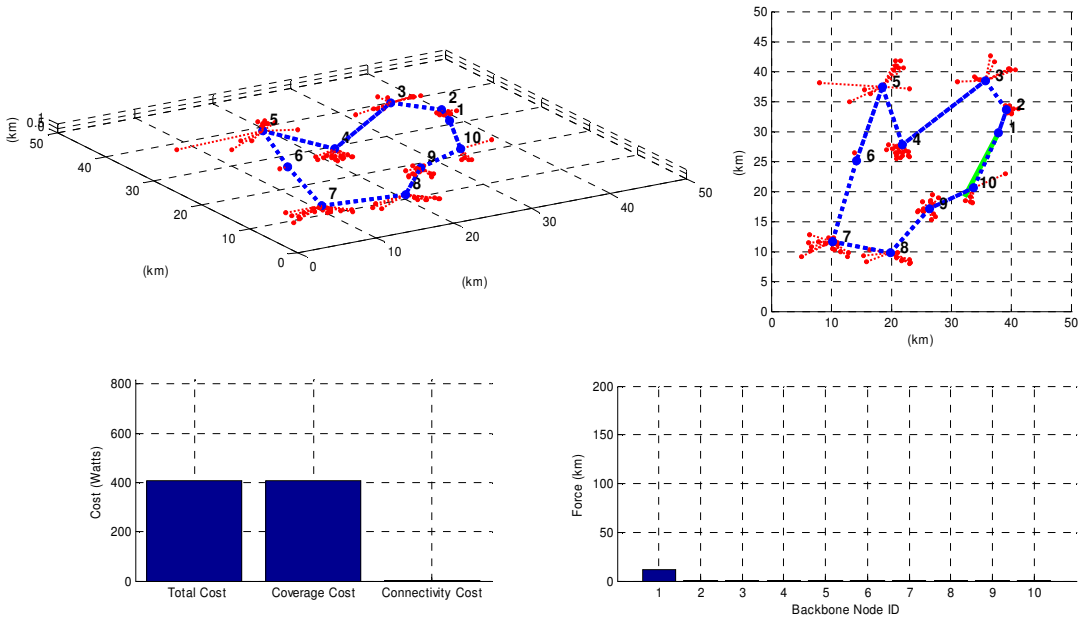

(h) Backbone reaction (7 min):
U = 409.70W; G = 409.58; F = 0.12W

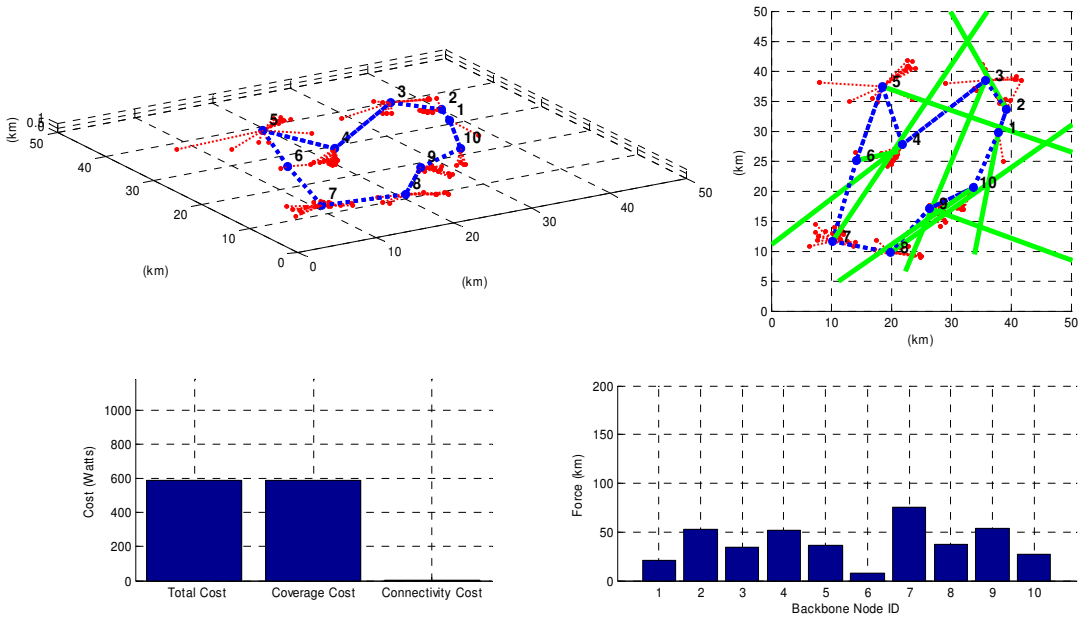

(i) Terminals location update (7 min):
U = 591.81W; G = 591.69W; F = 0.12W

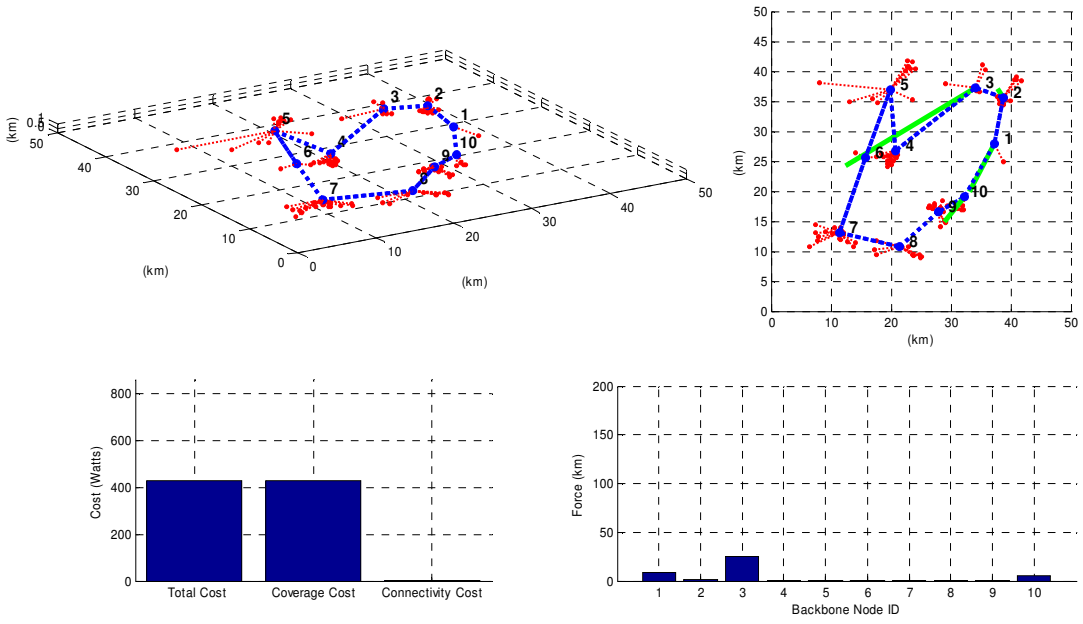

(j) Backbone reaction (7.5 min):
U = 429.84W; G = 429.73W; F = 0.11W

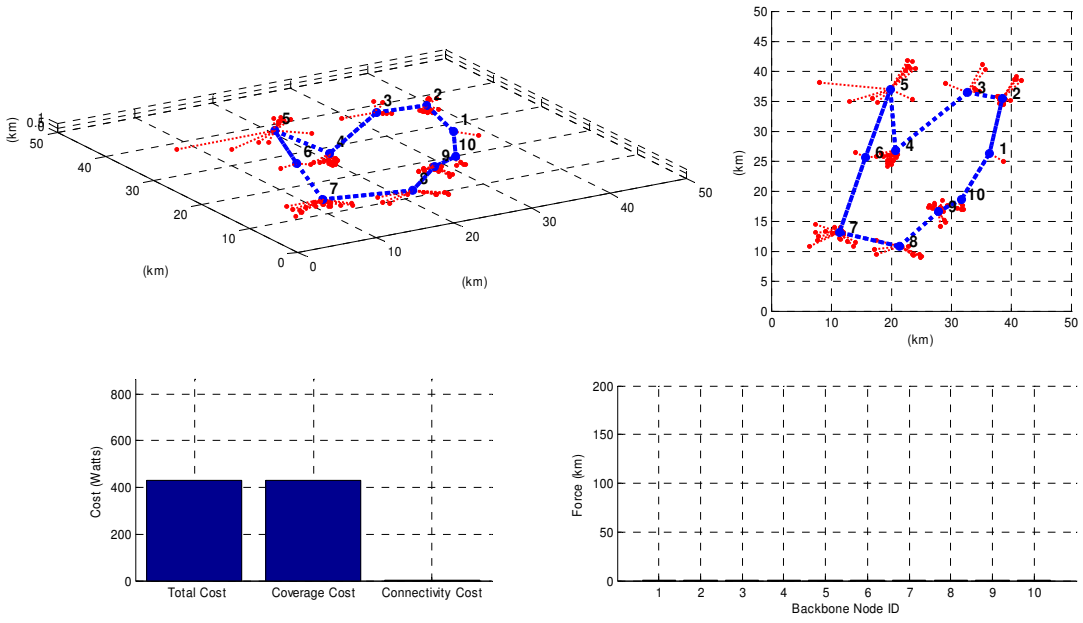

(k) Backbone reaction (8 min):
Equilibrium: U = 432.83W; G = 432.72W; F = 0.11W

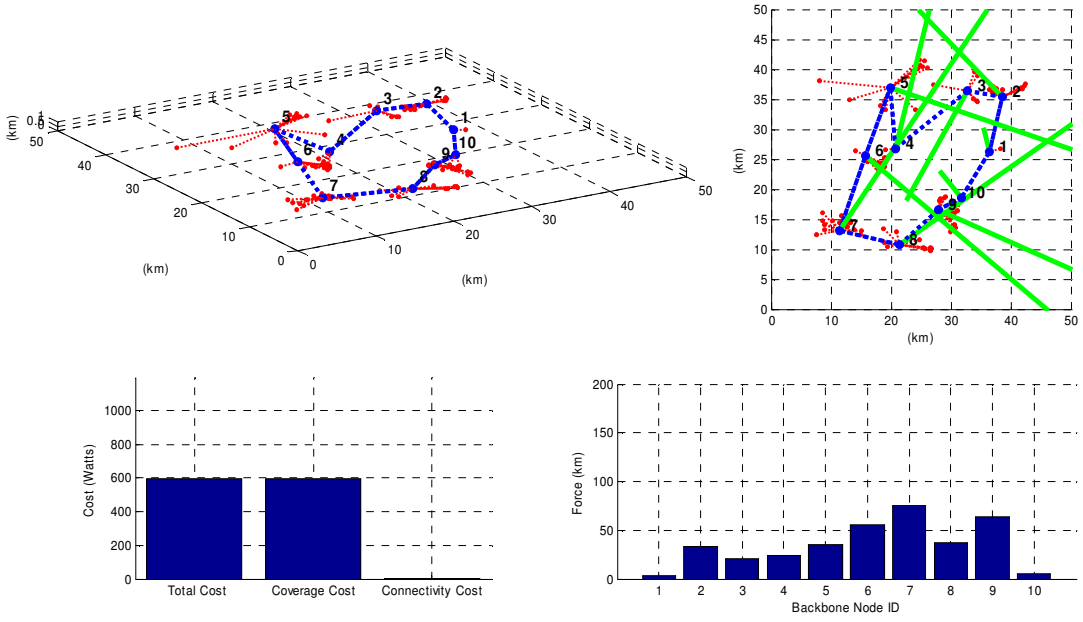

(l) Terminals location update (8 min):
U = 598.54W; G = 598.43W; F = 0.11W

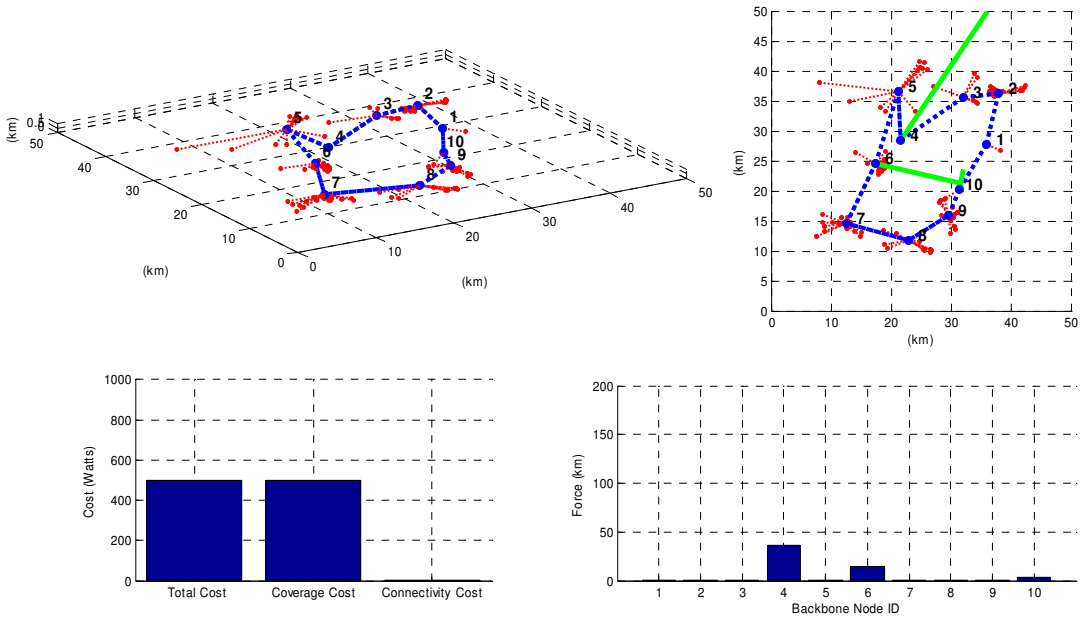

(m) Backbone reaction (8.5 min):
U = 502.12W G = 502.03W; F = 0.09W

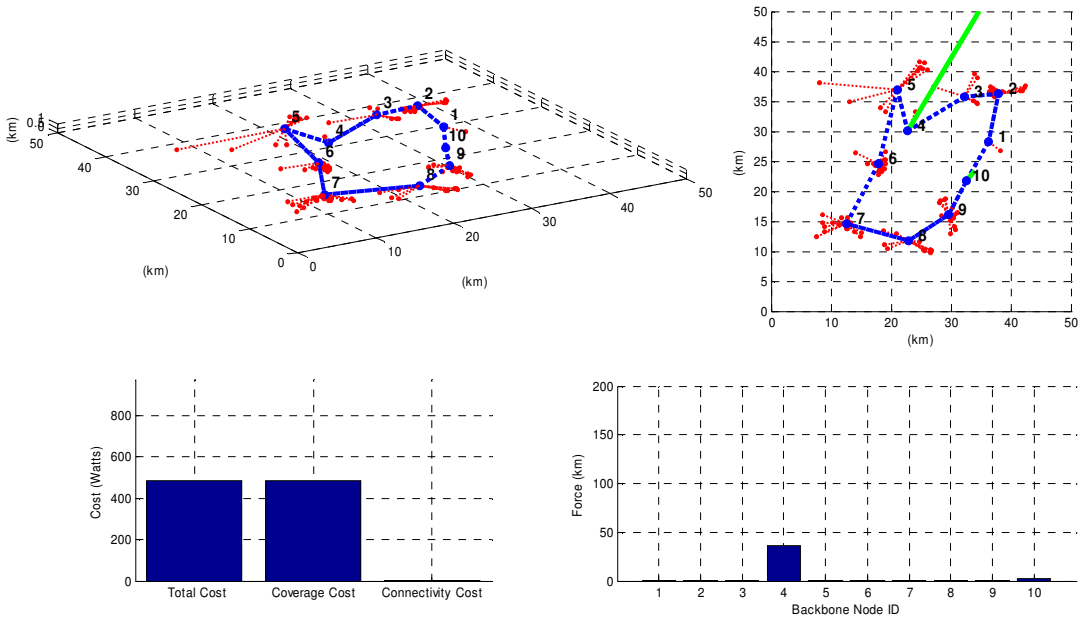

(n) Backbone reaction (9 min):
U = 487.78W; G = 487.69W; F = 0.09W

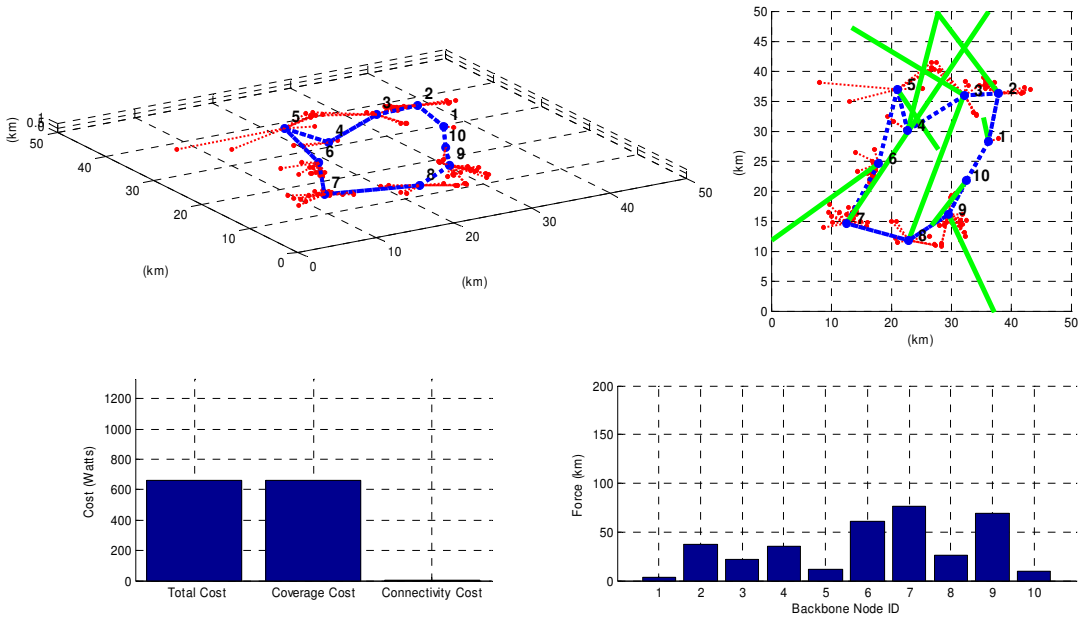

(o) Terminals location update (9 min):
U = 665.31W; G = 665.22W; F = 0.09W

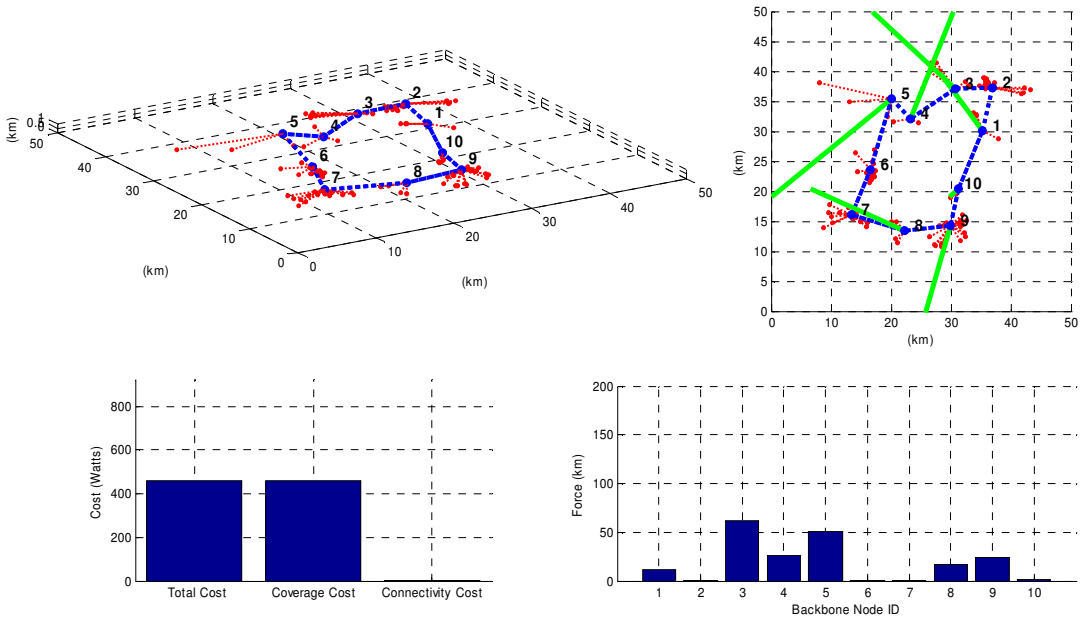

(p) Backbone reaction (9.5 min):
U = 461.73W; G = 461.66W; F = 0.07W

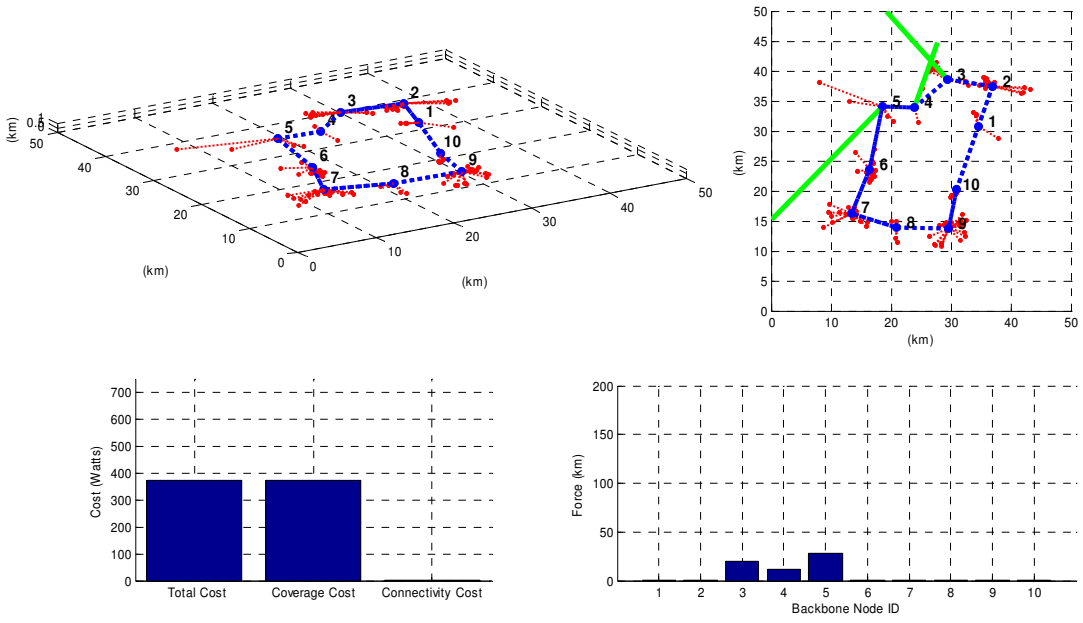

(q) Backbone reaction (10 min):
U = 374.67W; G = 374.60W; F = 0.07W

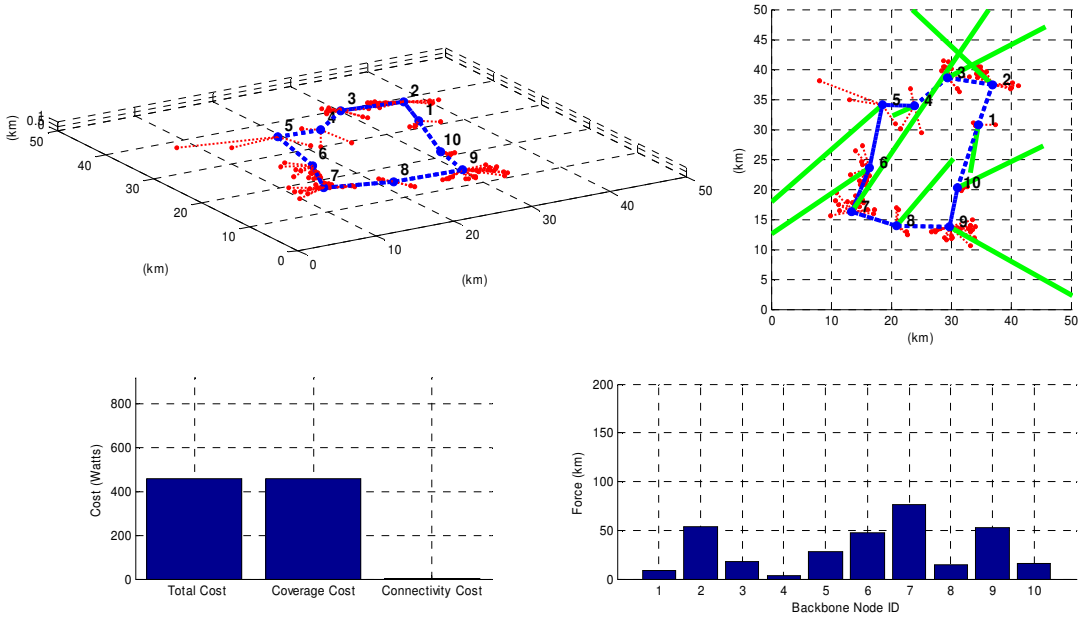

(r) Terminals location update (10 min):
U = 459.90W; G = 459.83W; F = 0.07W

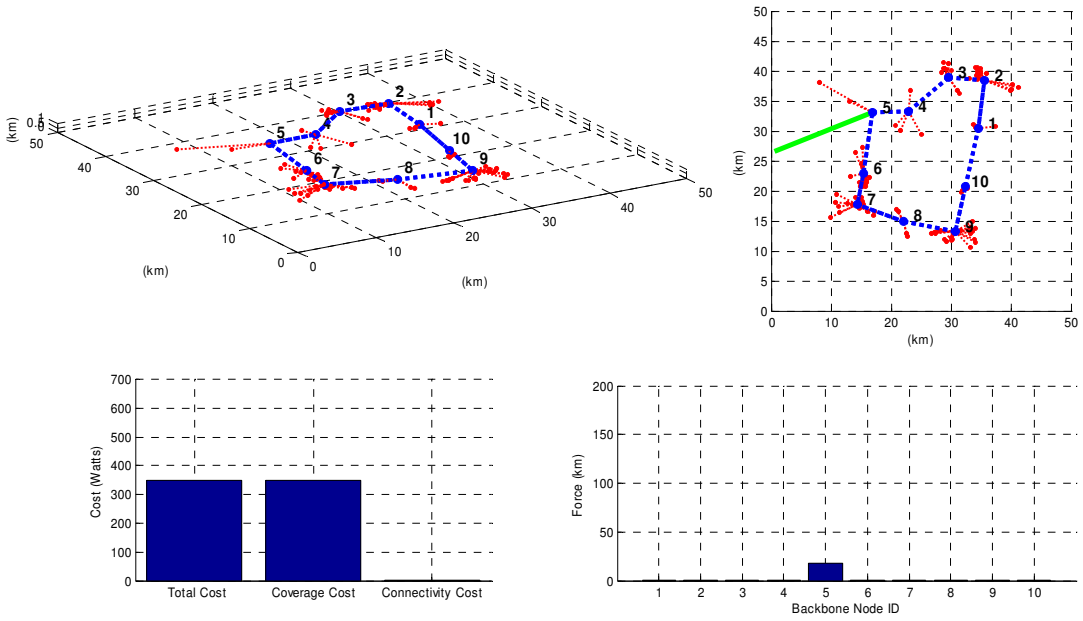

(s) Backbone reaction (10.5 min):
U = 350.71W; G = 350.65W; F = 0.06W

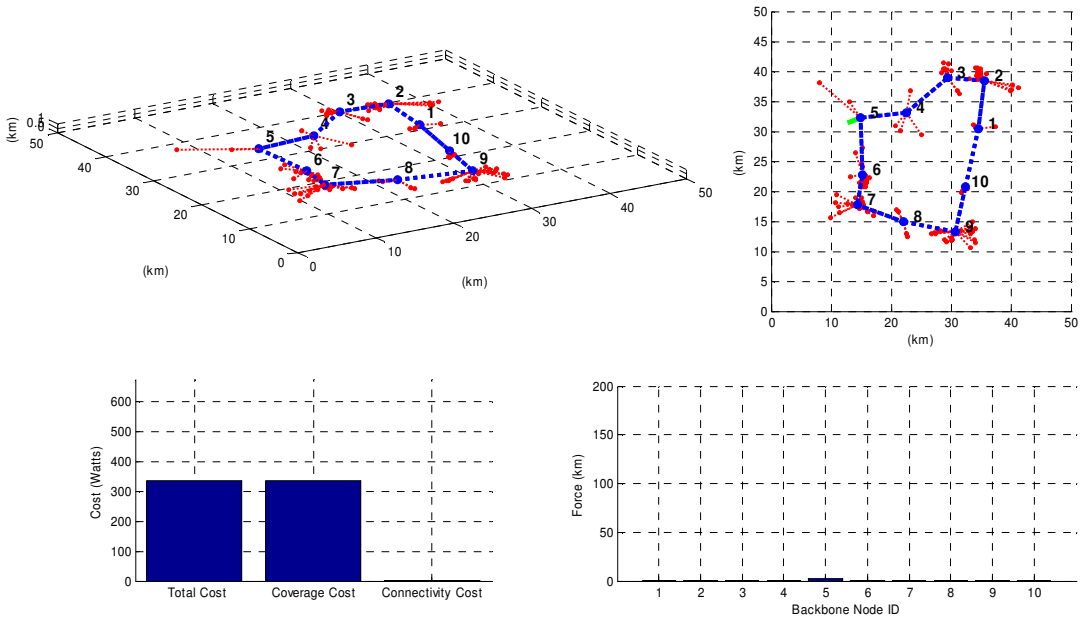

(t) Backbone reaction (11 min):
U = 336.79W; G = 336.72W; F = 0.07W

Figure 6.7: Network evolution with terminal clusters moving according to the RPGM model and backbone reacting using the SPRING algorithm.

In order to show the performance of the SPRING algorithm, we compared the average energy per unit time used in networks using the SPRING mobility control algorithm, with respect to: 1) networks with the base stations fixed at the initial optimal configuration and 2) networks using and average algorithm where the base stations move to he average position of its neighbors. We executed simulations for 10 and 20 backbone node networks, and for 10 different 1 hour scenario patterns (involving different terminal node placement and mobility patterns).

Table 6.1 shows the results obtained. As expected, when using fixed base stations, high energy values are needed to maintain network performance. The

continuous excitation produced by the network dynamics (terminal nodes' mobility) is not balanced due to the lack of a self-organizing capability.

One intuitive way of moving backbone nodes is to move them in the direction of the average position of its neighbors. We will refer to this method as the AVG algorithm. As seen in section 6.5, the solution to the energy minimization problem for the SPRING system makes nodes move in the direction of the weighted average of their neighbor's positions with weights defined based on the wireless technologies used. Thus, the AVG algorithm is an instance of the SPRING algorithm in the case of a homogeneous network architecture, where all communication nodes have the same communication capabilities. Our network scenarios are characterized by a heterogeneous architecture and thus the SPRING algorithm is able to outperform the AVG algorithm by taking into account the different behavior of wireless links using different communication technologies. Recall that in this simulation the backbone-to-backbone links are FSO links with $\theta = 2$ mrad and the terminal-to-backbone links are RF links with $\theta = \pi / 4$ rad. The SPRING algorithm is able to minimize the energy of the network system by driving the network topology in the direction of the steepest decrease of the global energy function. Note from table 6.1 that the SPRING algorithm uses on average 41% less energy than the AVG algorithm when using 10 backbone nodes, and a 58% reduction is obtained for 20 backbone nodes networks.

	10 backbone nodes	**20 backbone nodes**
No mobility control	2391 W	1750 W

AVG algorithm	543 W	249 W
SPRING algorithm	318 W	104 W
Percentage improvement (SPRING v.s. No mobility)	87 %	94 %
Percentage improvement (SPRING v.s. AVG)	41 %	58 %

Table 6.1: Average percentage improvement in total average power usage using the SPRING mobility control algorithm versus using the AVG algorithm and versus no mobility control, for networks with 10 and 20 backbone nodes.

6.6 Mobility control under atmospheric obscuration

As it has been shown throughout this dissertation, mobility control strategies modeled as energy minimization problems strongly depend on the link cost models used. As seen in the previous section, when no atmospheric obscuration effects are taken into account the energy function to be minimized mimics the potential energy of a spring system. If we introduce the effects of atmospheric obscuration, then the link cost model becomes that of Eq. 4.8:

$$u_{ij} = \left(P_{R0}^{j}\right)\left(e^{\alpha_{ij}\left\|\mathrm{R_i}-\mathrm{R_j}\right\|}\right)\left(\frac{4\pi}{D_T^j A_{eR}^j}\left\|\mathrm{R_i}-\mathrm{R_j}\right\|^2\right).$$

If the obscuration factor α is assumed to be constant in the area where the backbone nodes are distributed, then the link cost becomes a function of the type

$f = kx^2 e^{\alpha x}$, where x is the link length $L = \left\| \mathrm{R_i} - \mathrm{R_j} \right\|$. This type of function, although not quadratic, is still convex and an exponential function of the link distance.

In this section we use our general force-driven mobility control methodology described in section 6.2 to derive the solution to the mobility control problem in the presence of atmospheric obscuration.

6.6.1 Convex optimization

In this section we extend our link energy model to include the effects of atmospheric attenuation. Eq. 4.8 can be restated as follows:

$$u_{ij} = k_{ij} \left\| \mathrm{R_i} - \mathrm{R_j} \right\|^2 e^{\alpha_{ij} \left\| \mathrm{R_i} - \mathrm{R_j} \right\|}, \tag{6.32}$$

which is the product of a quadratic function and an exponential function of the link distance $L = \left\| \mathrm{R_i} - \mathrm{R_j} \right\|$. The constant k_{ij} was defined in Eq. 6.24 as $k_{ij} = P_{R0}^j \frac{4\pi}{D_T^i A_{eR}^j}$.

This link cost function in Eq. 6.32 is thus defined in terms of two main components:

1) $k_{ij} \left\| \mathrm{R_i} - \mathrm{R_j} \right\|^2$: this component models the energy needed to overcome the effects of the free space path loss, as described in section 4.4.1. This is quadratic function of the link distance analogous to the potential energy of a spring with spring constant defined by the link directivity (refer to section 4.4.1).

2) $e^{\alpha_{ij} \left\| \mathrm{R_i} - \mathrm{R_j} \right\|}$: this component models the energy needed to overcome the effects of atmospheric attenuation, as described in section 4.4.2. This is an exponential function of the link distance which models the scattering of electromagnetic radiation through the atmosphere in the presence of clouds and fog

(refer to section 4.4.2). Note that in clear atmospheric conditions, when the scattering coefficient α is small enough, this component can be neglected and the link cost function becomes that of a spring system. As α increases due to the presence of cloud layers in the atmosphere, this component imposes an exponential increase on the energy needed to maintain the specified link BER.

Using the link energy model in Eq. 6.32, the potential energy function for the network system becomes:

$$U(\mathrm{R}_1,...,\mathrm{R}_N) = \eta \cdot \underbrace{\left(\sum_{i=1}^{N} \sum_{j=1}^{N} b_{ij} k_{ij} \left\| \mathrm{R}_i - \mathrm{R}_j \right\|^2 e^{\alpha_{ij} \left\| \mathrm{R}_i - \mathrm{R}_j \right\|} \right)}_{F} + \underbrace{\left(\sum_{k=1}^{M} k_{h(k)k} \left\| \mathrm{R}_{h(k)} - \mathrm{r}_k \right\|^2 e^{\alpha_{h(k)k} \left\| \mathrm{R}_{h(k)} - \mathrm{r}_k \right\|} \right)}_{G} \quad . \quad (6.33)$$

And thus the mobility control problem formulation is stated as follows:

$$\min \left\{ \begin{array}{l} U(\mathrm{R}_1,...,\mathrm{R}_N) = \eta \cdot \underbrace{\left(\sum_{i=1}^{N} \sum_{j=1}^{N} b_{ij} k_{ij} \left\| \mathrm{R}_i - \mathrm{R}_j \right\|^2 e^{\alpha_{ij} \left\| \mathrm{R}_i - \mathrm{R}_j \right\|} \right)}_{F} + \\ \qquad \underbrace{\left(\sum_{k=1}^{M} k_{h(k)k} \left\| \mathrm{R}_{h(k)} - \mathrm{r}_k \right\|^2 e^{\alpha_{ij} \left\| \mathrm{R}_{h(k)} - \mathrm{r}_k \right\|} \right)}_{G} \end{array} \right\}$$

$$\text{where} \quad k_{ij} = P_{R0}^{j} \frac{4\pi}{D_T^i A_{eR}^j}, \quad (6.34)$$

$$\text{and} \quad b_{ij} = \begin{cases} 1 & \text{if } (i,j) \in T \\ 0 & \text{o.w.} \end{cases}$$

Again, the goal of the optimization problem is to find the locations of all the backbone nodes that minimize the above cost function. In this case the energy function *U* is not quadratic, but it is still continuous and convex.

In the following section we derive the force-driven mobility control algorithm for network systems under atmospheric obscuration.

6.6.2 FORCE algorithm

Recall that in our force-driven mobility control methodology, the value of the net force at backbone node *i* is computed as the gradient of the energy function *U* with respect to the location the backbone node R_i, described in Eq. 6.9 as:

$$\mathrm{F_i} = \eta \mathrm{F_i^b} + \mathrm{F_i^c} = \eta \sum_{j=1}^{N} b_{ij} \mathrm{f_{ij}} + \sum_{k=1}^{M} 1(h_{(k)} = i) \mathrm{f_{ik}} \ ,$$

where $\mathrm{f_{ij}}$ is the force exerted on node *i* due the its interaction with node *j*, defined as the negative gradient of the link energy function u_{ij} with respect to R_i, as:

$$\mathrm{f_{ij}} = -\nabla^i u_{ij} = \begin{bmatrix} -\dfrac{\partial u_{ij}}{\partial X_i} \\ -\dfrac{\partial u_{ij}}{\partial Y_i} \\ -\dfrac{\partial u_{ij}}{\partial Z_i} \end{bmatrix}.$$

Using Eq. 6.24 for the link energy function u_{ij}, $\mathrm{f_{ij}}$ is described as:

$$\mathrm{f_{ij}} = \begin{bmatrix} f_{ij,x} \\ f_{ij,y} \\ f_{ij,z} \end{bmatrix} = -k_{ij} \left(2e^{\alpha_{ij} \left\| \mathrm{R_i} - \mathrm{R_j} \right\|} + \alpha_{ij} e^{\alpha_{ij} \left\| \mathrm{R_i} - \mathrm{R_j} \right\|} \left\| \mathrm{R_i} - \mathrm{R_j} \right\| \right) \begin{bmatrix} X_i - X_j \\ Y_i - Y_j \\ Z_i - Z_j \end{bmatrix}, \tag{6.35}$$

which in vector form becomes:

$$\mathrm{f_{ij}} = k_{ij} \left(2e^{\alpha_{ij} \left\| \mathrm{R_i} - \mathrm{R_j} \right\|} + \alpha_{ij} \left\| \mathrm{R_i} - \mathrm{R_j} \right\| e^{\alpha_{ij} \left\| \mathrm{R_i} - \mathrm{R_j} \right\|} \right) \mathrm{R_{ij}} \, . \tag{6.36}$$

As it can be observed from Eq. 6.36, in the presence of atmospheric obscuration, the force on a given backbone node still depends on local information only. Thus, a completely distributed algorithm can be designed where each backbone

node reacts locally to the forces exerted by neighbor nodes, maintaining the scalability and robustness of the control system.

Note that in this case the direction of the force is still given by the displacement vector R_{ij}, but the amplitude is a more complicated function of the link distance as compared to the spring system scenario. In this case, an exponential function of the link distance dictates the additional force exerted on network nodes in areas of significant atmospheric obscuration. This extra force arises to bring backbone nodes even closer to each other in order to overcome the signal power attenuation caused by the scattering of electromagnetic radiation due to the presence of atmospheric obscurants in the form of clouds or fog.

The optimization algorithm can be derived from the general methodology described in section 6.4.2, which is based on two main operations: relocation and reassignment. Recall that the relocation operation uses the value of the force to find the node's new location, as: $\mathrm{R}_{\mathrm{i}}^{\mathrm{n+1}} = \mathrm{R}_{\mathrm{i}}^{\mathrm{n}} + \delta \mathrm{F}_{\mathrm{i}}$. In the presence of atmospheric obscuration, using Eq. 6.36, the relocation operation becomes:

$$\mathrm{R}_{\mathrm{i}}^{\mathrm{n+1}} = \mathrm{R}_{\mathrm{i}}^{\mathrm{n}} + \delta \left[\begin{array}{l} \eta \sum_{j=1}^{N} b_{ij} k_{ij} \left(2e^{\alpha_{ij} \left\| \mathrm{R_i - R_j} \right\|} + \alpha_{ij} \left\| \mathrm{R_i - R_j} \right\| e^{\alpha_{ij} \left\| \mathrm{R_i - R_j} \right\|} \right) \mathrm{R}_{\mathrm{ij}} \\ + \sum_{k=1}^{M} 1(h_{(k)} = i) k_{ik} \left(2e^{\alpha_{ik} \left\| \mathrm{R}_i - \mathrm{r_k} \right\|} + \alpha_{ik} \left\| \mathrm{R}_i - r_k \right\| e^{\alpha_{ik} \left\| \mathrm{R}_i - \mathrm{r_k} \right\|} \right) \mathrm{R}_{ik} \end{array} \right]. \quad (6.37)$$

The reassignment operation was also described in section 6.3 as: $h^n(k) = \arg\min_{\mathrm{i}} u(\mathrm{R}_i, \mathrm{r}_k), \text{ for } 1 \le i \le N$, where *h(k)* denotes the index of the backbone node assigned to terminal node *k*. Using the expression for the link cost in Eq. 6.32, the reassignment operation for the spring algorithm becomes:

$$h^n(k) = \arg\min_i k_{ik} \left\| \mathrm{R_i} - \mathrm{r_k} \right\|^2 e^{\alpha_{ik} \left\| \mathrm{R_i} - \mathrm{r_k} \right\|} \quad 1 \le i \le N \tag{6.38}$$

The mobility control algorithm based on these two operations follow the same form as in Fig. 6.2, but using the updated operations described above which take into account the effects of atmospheric obscuration in the network. We refer to this extended force-driven mobility control algorithm as the FORCE algorithm.

6.6.3 Simulation results

As we did in section 6.5.3 to validate the SPRING algorithm, in this section we present simulation results to validate the performance of the FORCE algorithm.

Fig. 6.8 shows a sequence of snapshots of a dynamic network simulation. In this first simulation the terminal nodes are not moving. The excitation to the network system is caused by the presence of atmospheric obscuration. The obscuration pattern is represented by and array that contains the average attenuation factor in km^{-1} for the backbone FSO links, for every minute of the simulation.

In Fig. 6.8a the network is at equilibrium. Fig. 6.8b shows a first excitation to the system caused by the presence of atmospheric obscuration. At this point, the average atmospheric attenuation factor is 0.4 km^{-1} and thus forces appear that make backbone nodes start moving closer to each other. No nodes have yet changed their positions, but the energy of the system has increased from U = 308.88W to U = 347.07W due to the effects of atmospheric attenuation. Fig. 6.8c shows the resulting configuration after 1 minute of reaction. The network has reached an equilibrium configuration with a total energy value of U = 341.67W. Fig. 6.8d shows the effects

of the new update on the atmospheric attenuation coefficient which has increased to 0.6 km^{-1}. The backbone connectivity cost increases to F = 517.94W indicating the extra energy needed at the FSO links forming the backbone network in order to maintain connectivity. Fig. 6.8e shows the equilibrium configuration obtained after 1 minute of reaction. In the sequence 6.8f-6.8r the backbone network keeps reacting to the increasing atmospheric attenuation coefficient by pulling its nodes closer to each other. In Fig. 6.8q (minute 7), the attenuation coefficient increases to 1.6 km^{-1} and the network is able to reach an equilibrium configuration at minute 7.5 where the total energy of the system is U = 2369.6W (Fig. 6.8r). At minutes 8 and 9, the attenuation coefficient remains at 1.6 km^{-1} and thus the network remains at the same optimal configuration (Figs. 6.8s-6.8v). At minute 10, the attenuation coefficient starts decreasing. Fig. 6.8w shows the resulting forces after α has dropped to 1.4 km^{-1}. Note how now the forces make the backbone topology stretch back in the direction of the terminal nodes as more energy can be used for coverage due to the reduction in connectivity cost, caused by the lower atmospheric attenuation. The final sequence (Figs. 6.8x-6.8dd) shows the reaction of the backbone topology as the atmospheric attenuation decreases from 1.4 km^{-1} to 0 km^{-1}. Note how at minute 17 of the simulation (Fig. 6.8dd), the backbone topology has converged back to the initial optimal configuration of Fig. 6.8a.

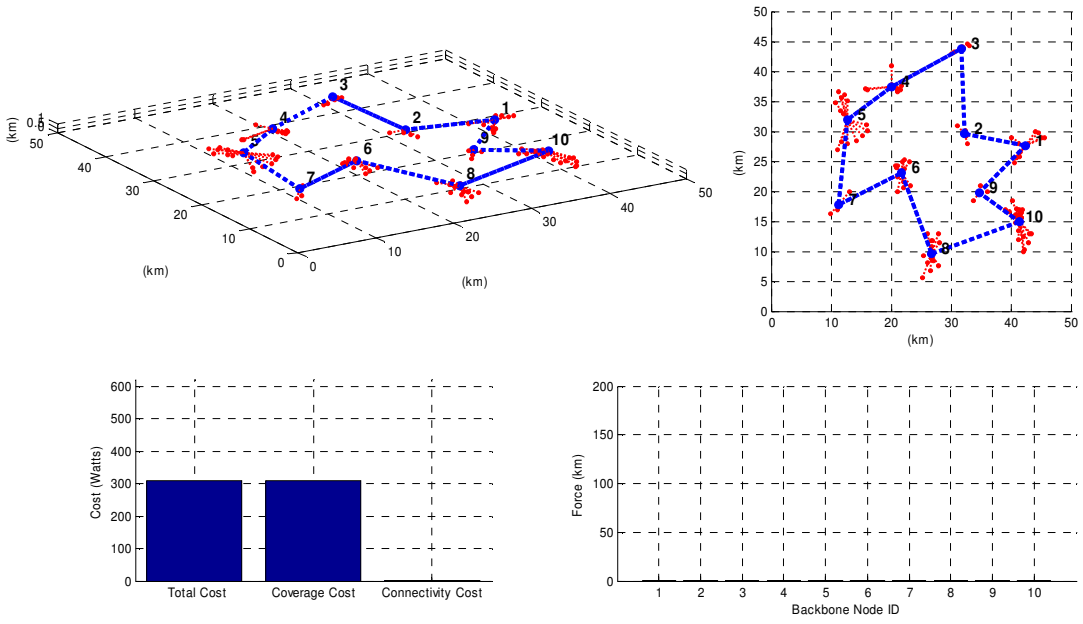

(a) Initial placement (0 min):
Equilibrium: U = 308.88W; G = 308.73W; F = 0.15W

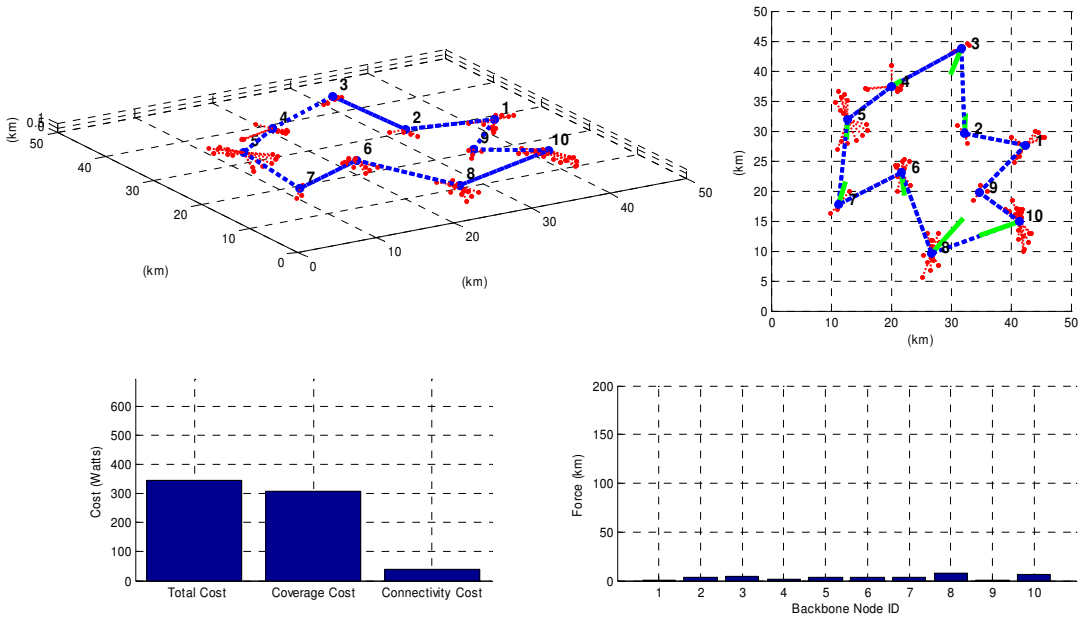

(b) Atmospheric attenuation update ($\alpha = 0.4\ km^{-1}$) (1 min):
U = 347.07W; G = 308.73W; F = 38.34W

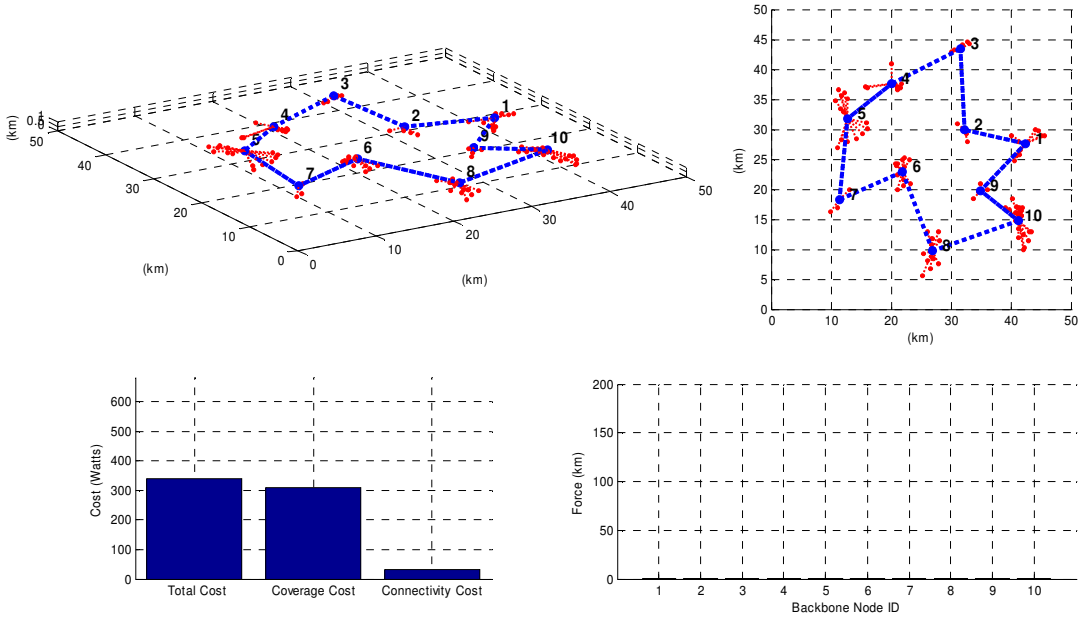

(c) Backbone reaction (1.5 min):
Equilibrium: U = 341.67W; G = 310.38W; F = 31.29W

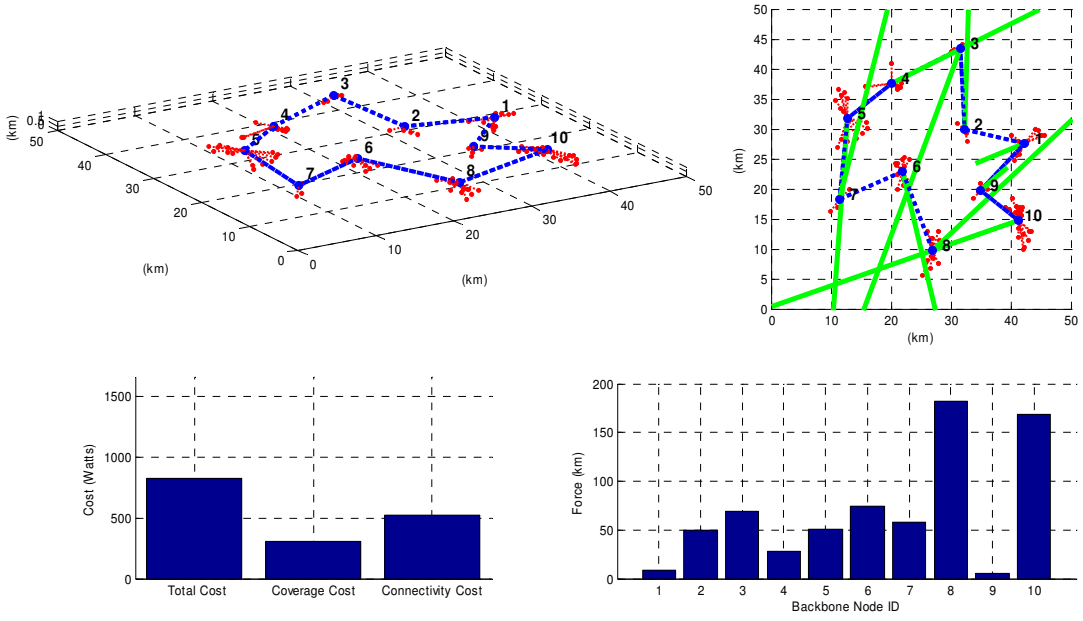

(d) Atmospheric attenuation update ($\alpha = 0.6\ km^{-1}$) (2 min):
U = 828.36W; G = 310.41W; F = 517.94W

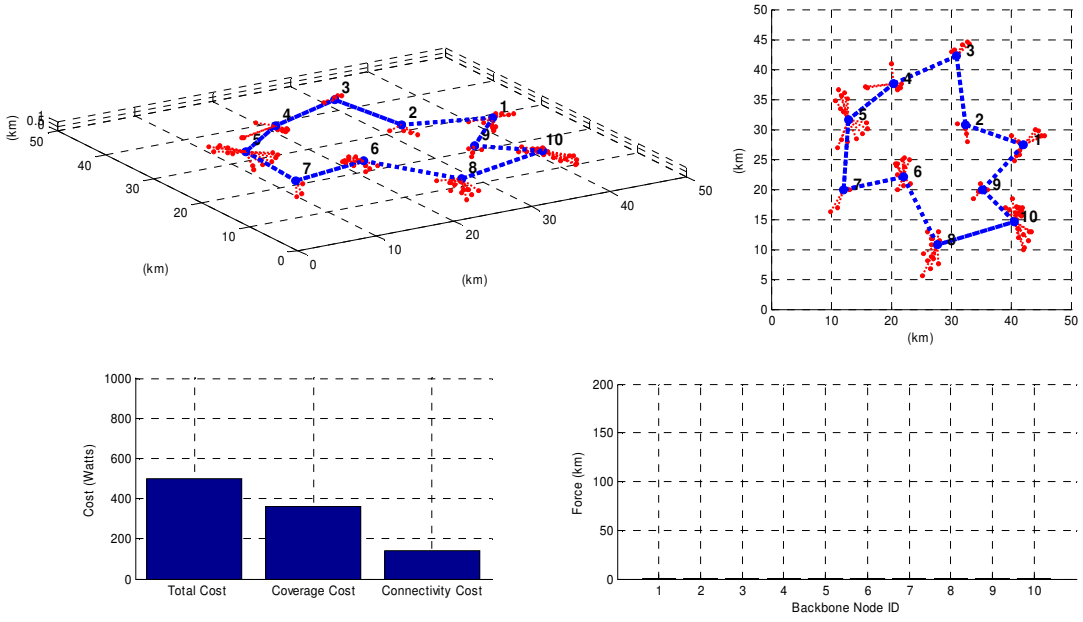

(e) Backbone reaction (2.5 min):
Equilibrium: U = 503.50W; G = 361.22W; F = 142.28W

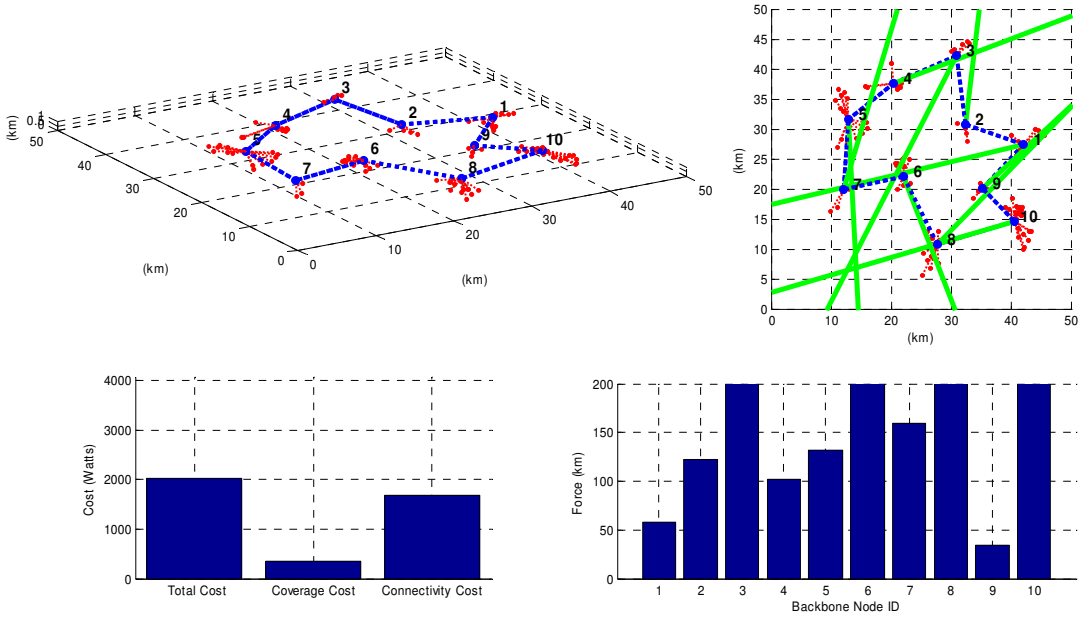

(f) Atmospheric attenuation update ($\alpha = 0.8\ km^{-1}$) (3 min):
U = 2034.7W; G = 361.4W; F = 673.3W

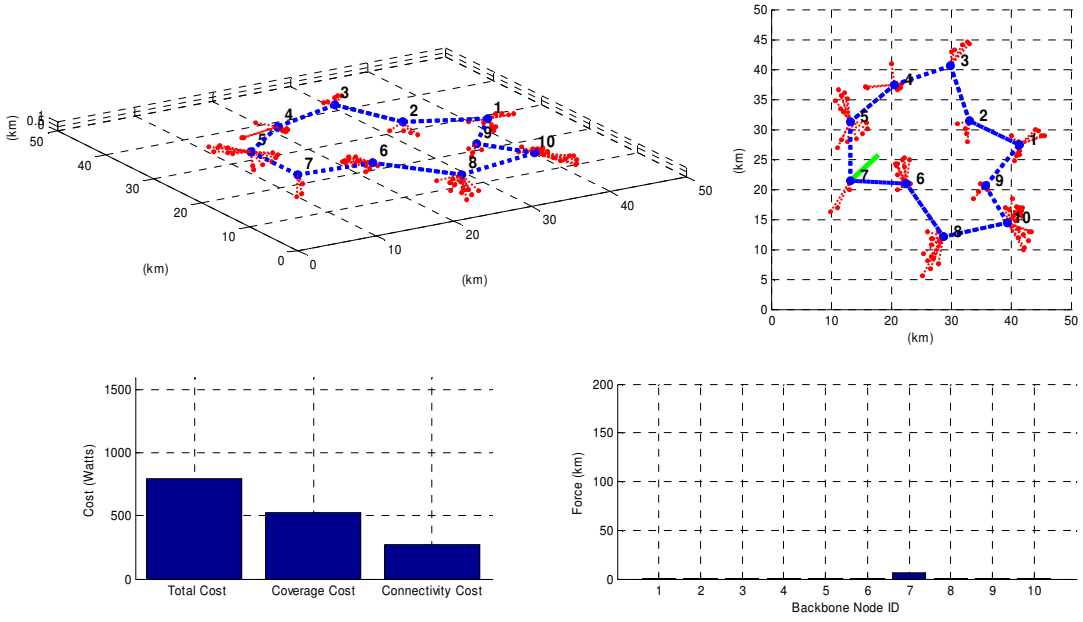

(g) Backbone reaction (3.5 min):
U = 800.4W; G = 523.8W; F = 276.6W

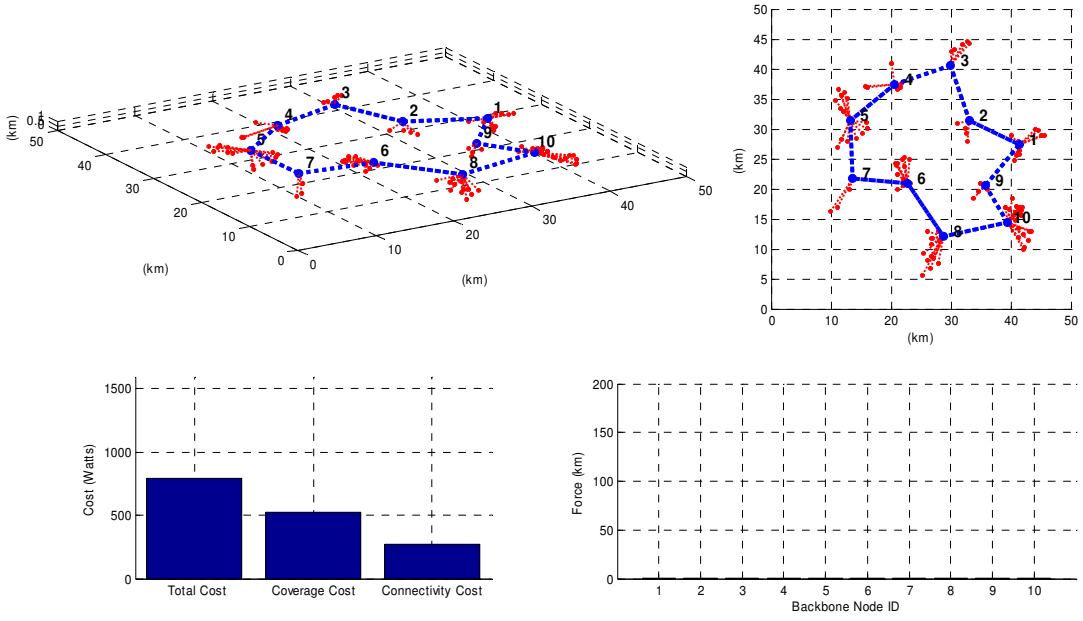

(h) Backbone reaction (4 min):
Equilibrium: U = 796.6W; G = 526.7W; F = 269.9W

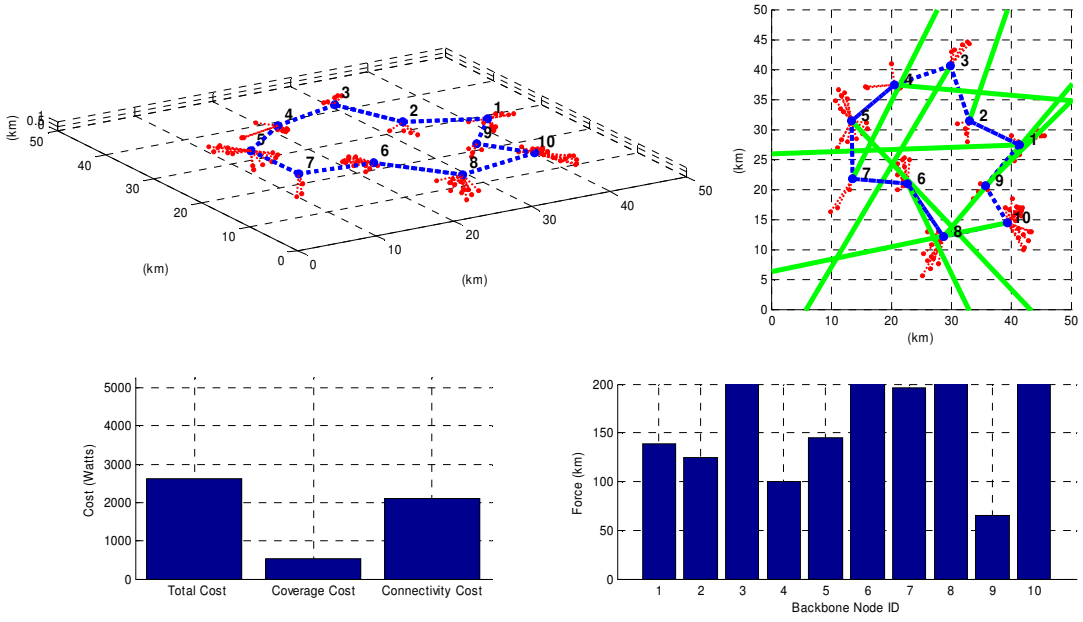

(i) Atmospheric attenuation update ($\alpha = 1.0\ km^{-1}$) (4 min):
U = 2637.6W; G = 527.1W; F = 2110.5W

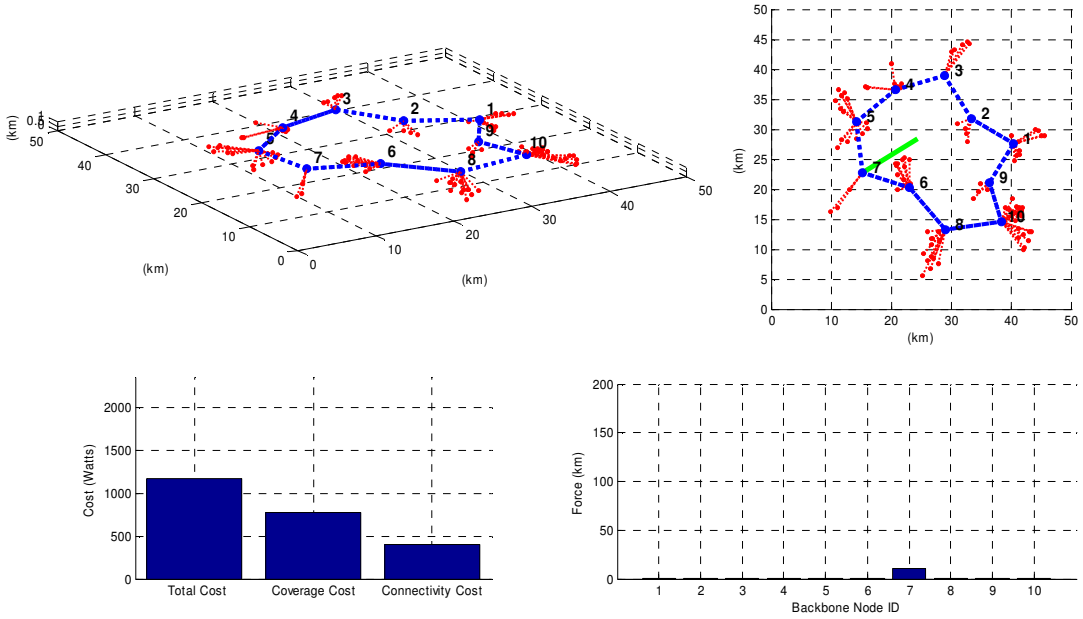

(j) Backbone reaction (4.5 min):
U = 1176.1W; G = 773.1W; F = 403.0W

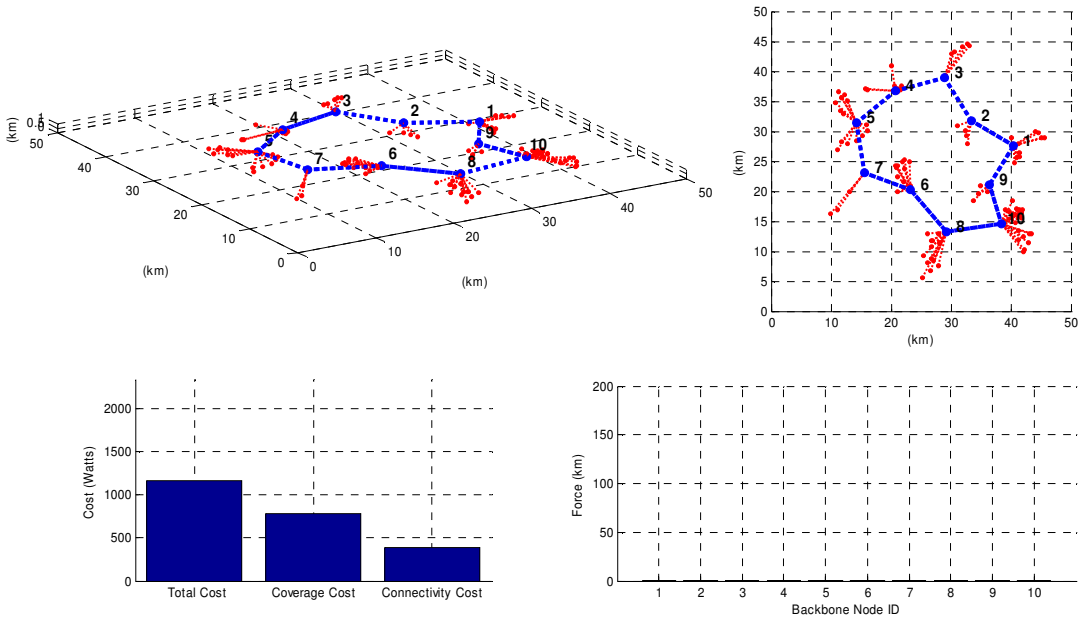

(k) Backbone reaction (5 min):
Equilibrium: U = 1168.8W; G = 778.4W; F = 390.4W

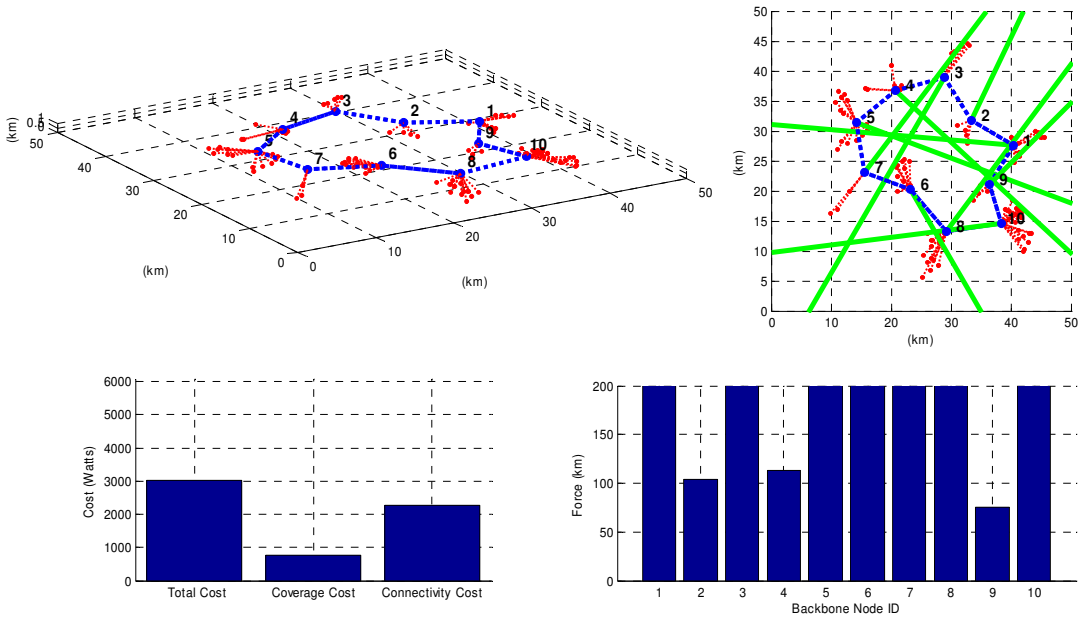

(l) Atmospheric attenuation update ($\alpha = 1.2\ km^{-1}$) (5 min):
U = 3040.0W; G = 778.9W; F = 2261.1W

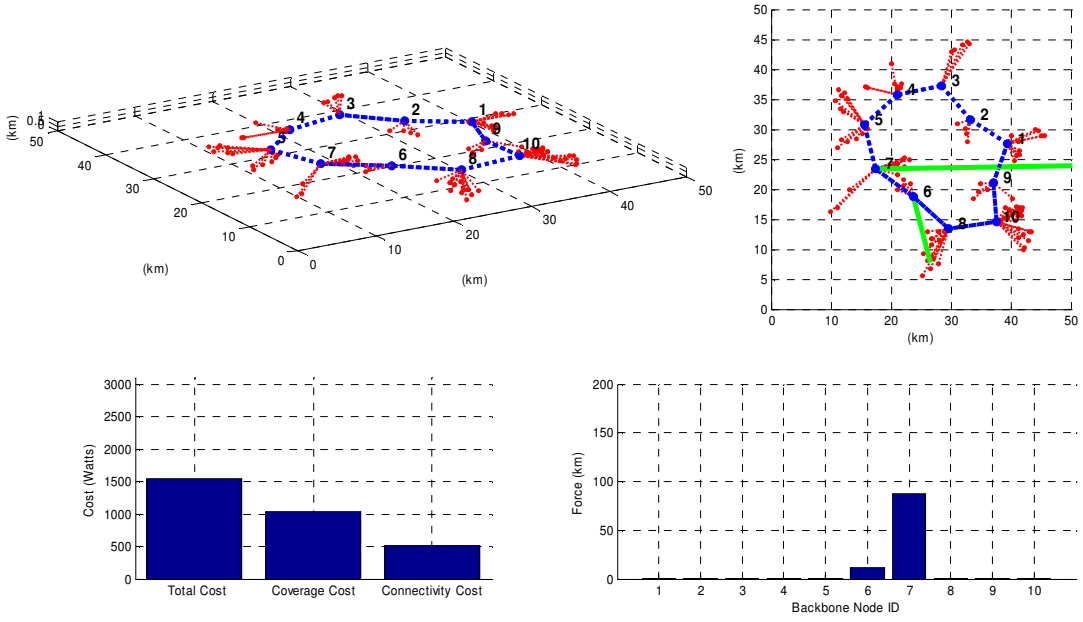

(m) Backbone reaction (5.5 min):
U = 1558.1W; G = 1042.4W; F = 515.7W

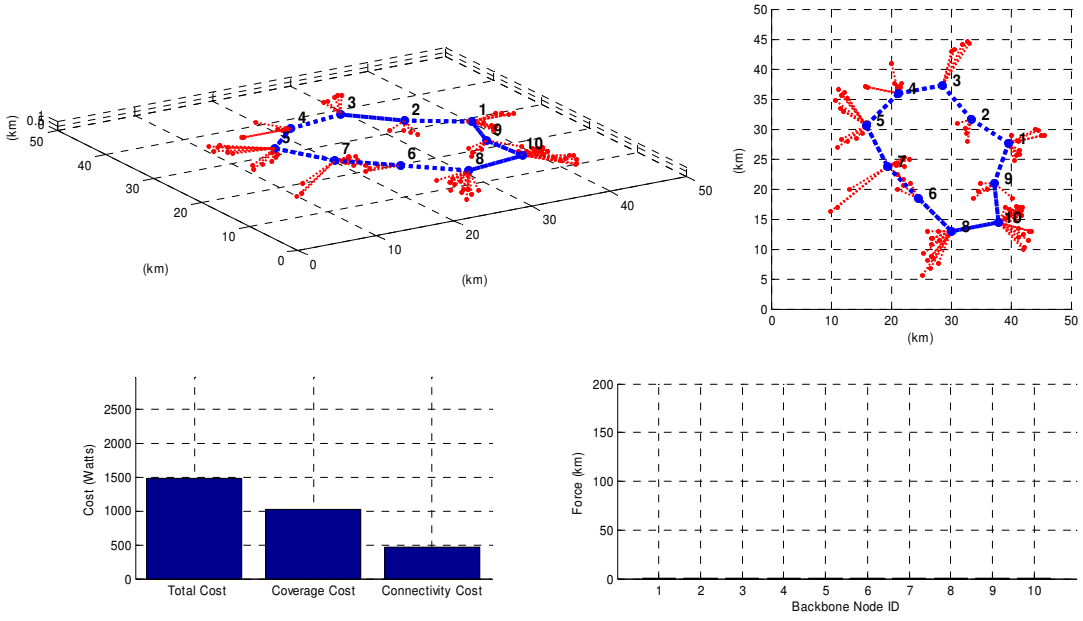

(n) Backbone reaction (6 min):
Equilibrium: U = 1493.2W; G = 1029.4W; F = 463.9W

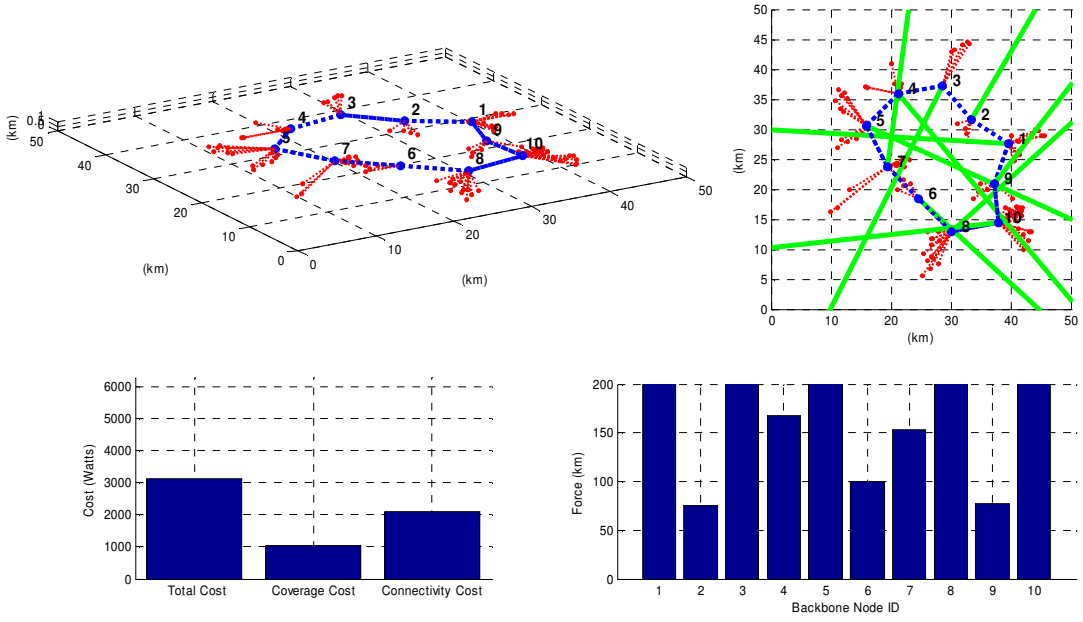

(o) Atmospheric attenuation update ($\alpha = 1.4\ km^{-1}$) (6 min):
U = 3142.9W; G = 1030.0W; F = 2112.9W

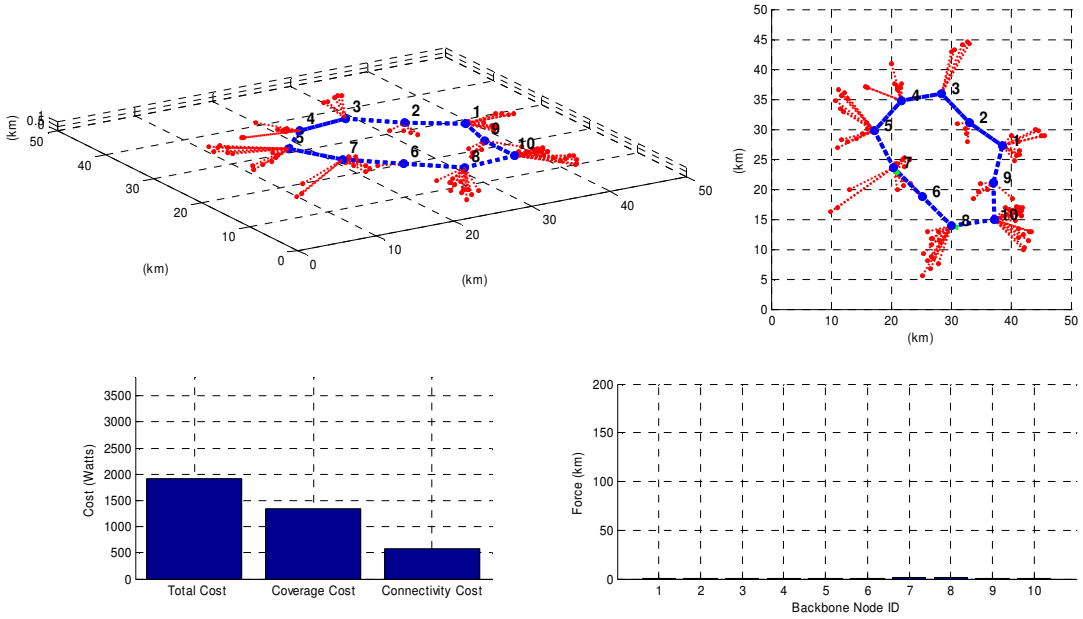

(p) Backbone reaction (6.5 min):
Equilibrium: U = 1928.0W; G = 1346.9W; F = 581.1W

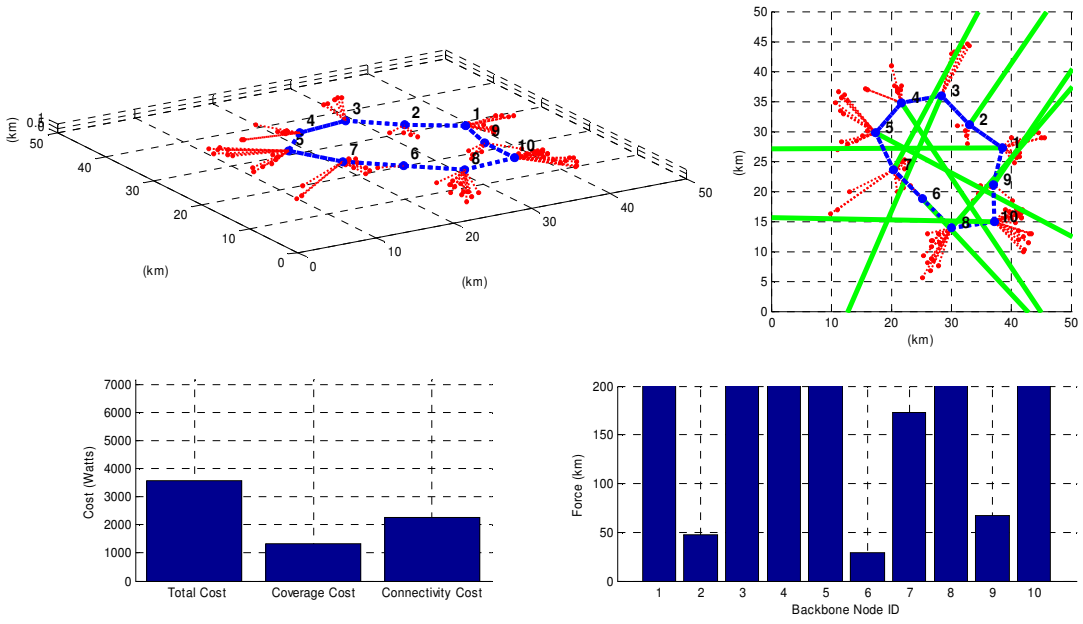

(q) Atmospheric attenuation update ($\alpha = 1.6\ km^{-1}$) (7 min):
U = 3604.5W; G = 1347.6W; F = 2256.9W

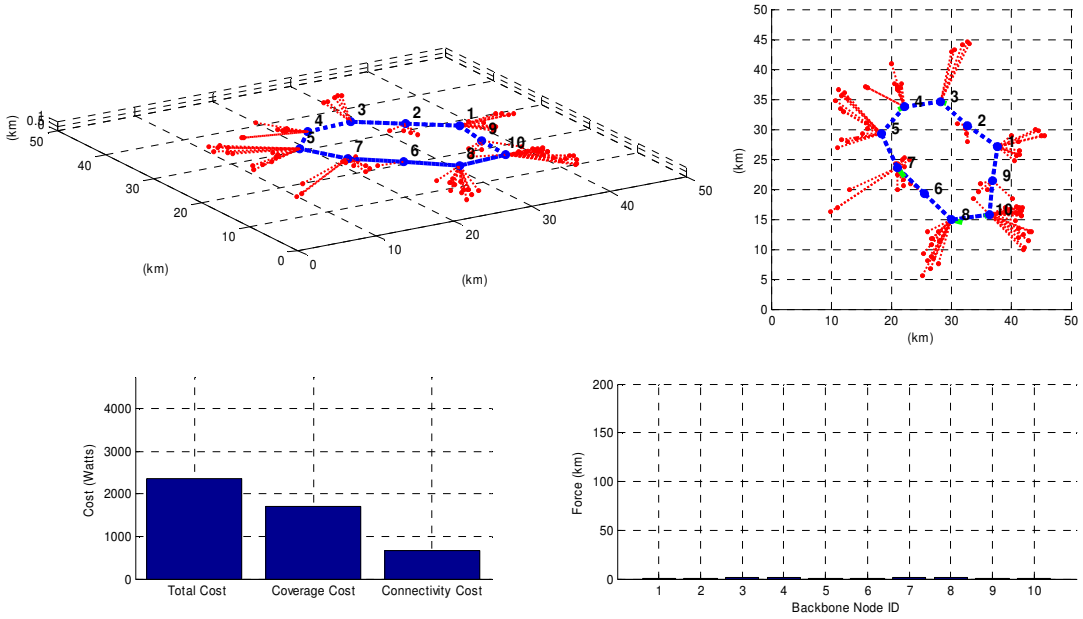

(r) Backbone reaction (7.5 min):
Equilibrium: U = 2369.6W; G = 1708.9W; F = 660.7W

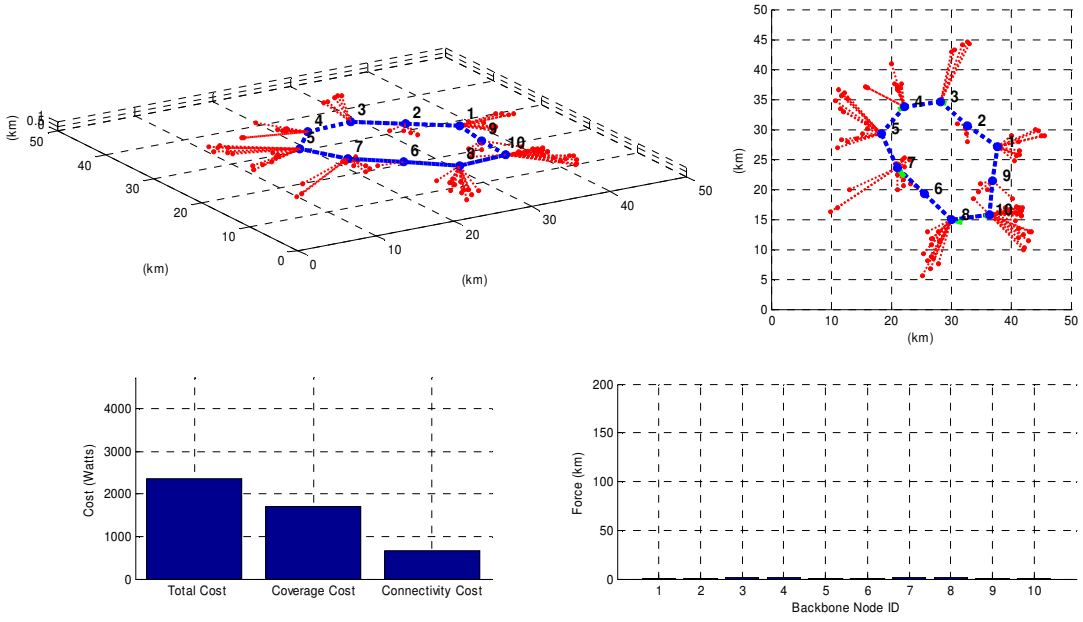

(s) Atmospheric attenuation update ($\alpha = 1.6\ km^{-1}$) (8 min):
Equilibrium: U = 2369.6W; G = 1708.9W; F = 660.7W

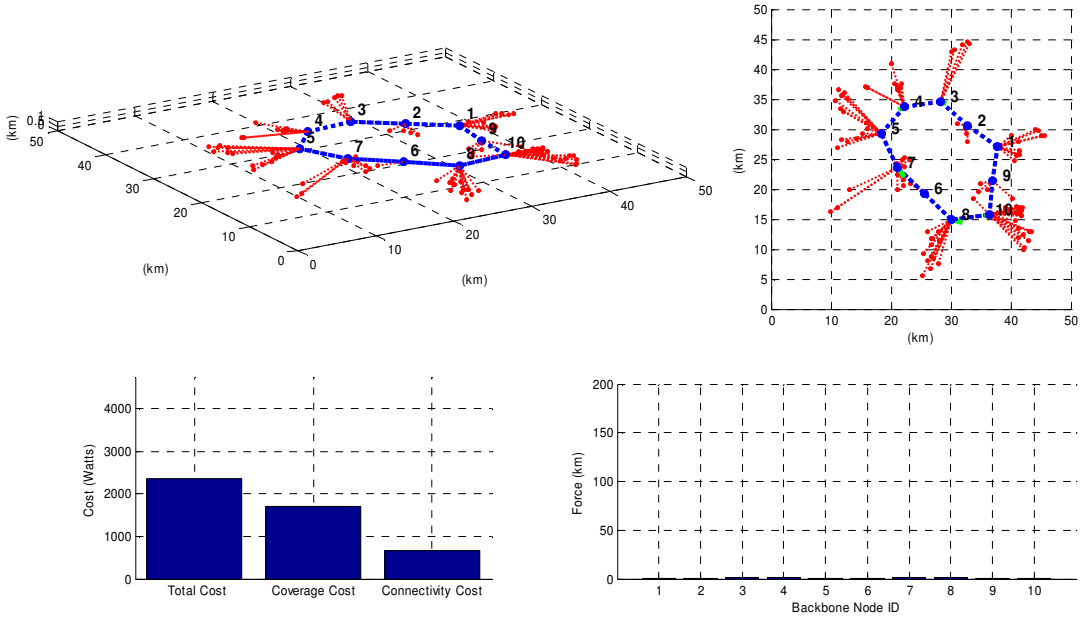

(t) Backbone reaction (8.5 min):
Equilibrium :U = 2369.6W; G = 1708.9W; F = 660.7W

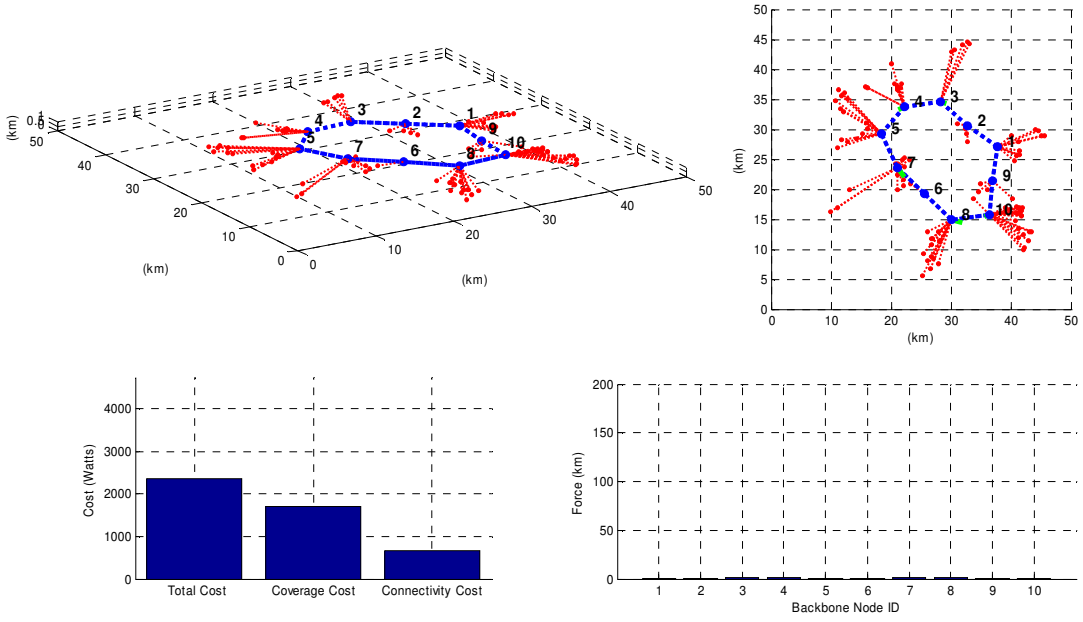

(u) Atmospheric attenuation update ($\alpha = 1.6\ km^{-1}$) (9 min):
Equilibrium: U = 2369.6W; G = 1708.9W; F = 660.7W

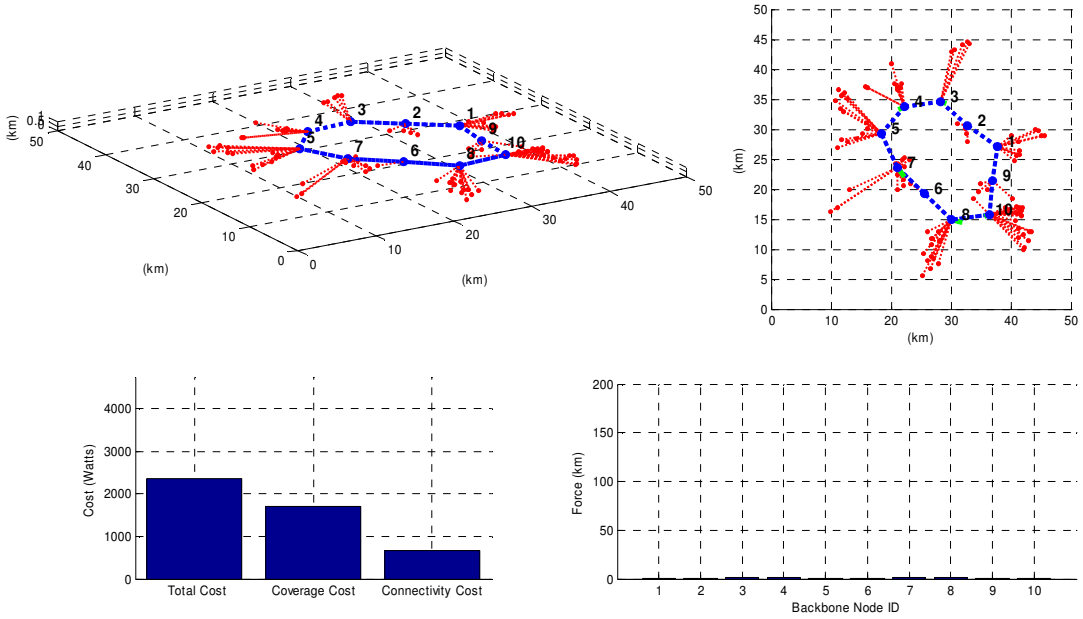

(v) Backbone reaction (9.5 min):
Equilibrium: U = 2369.6W; G = 1708.9W; F = 660.7W

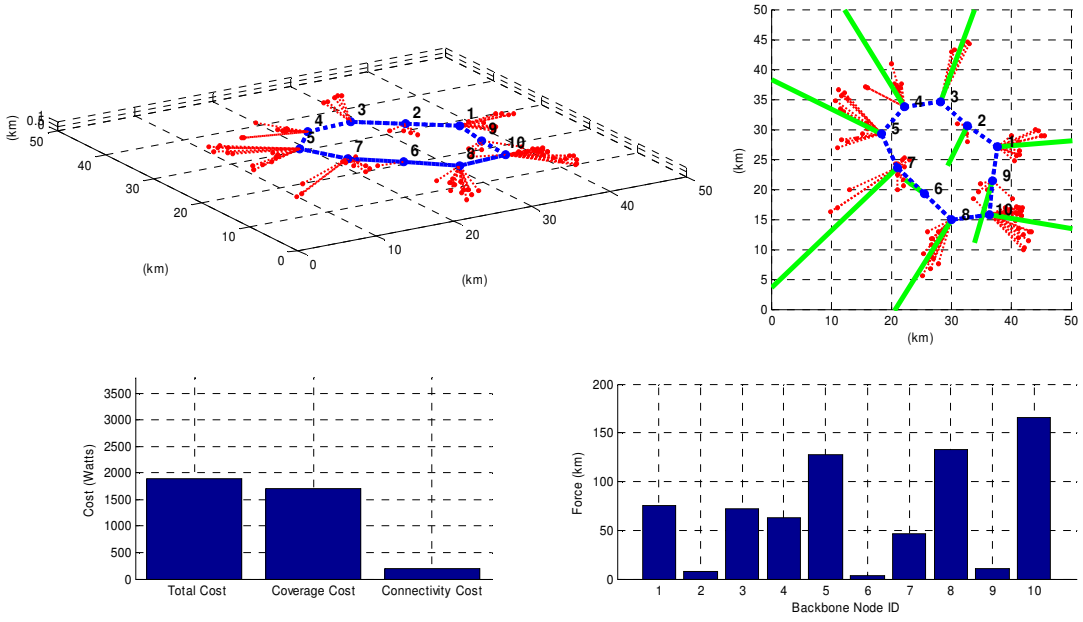

(w) Atmospheric attenuation update ($\alpha = 1.4\ km^{-1}$) (10 min):
U = 1902.1W; G = 1708.1W; F = 194.0W

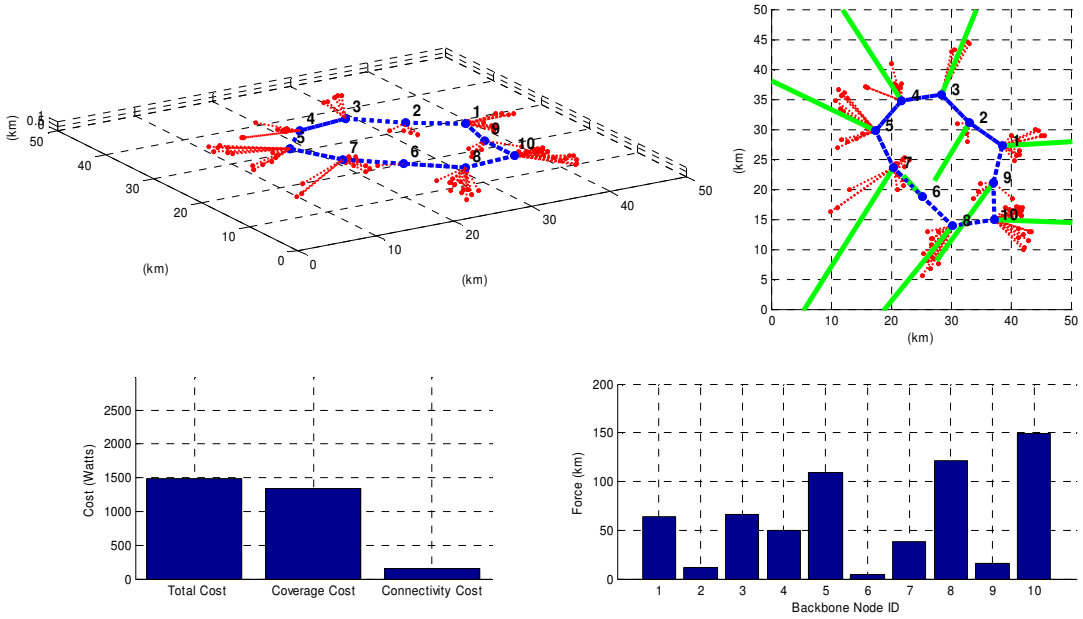

(x) Atmospheric attenuation update ($\alpha = 1.2\ km^{-1}$) (11 min):
U = 1496.0W; G = 1346.2W; F = 149.8W

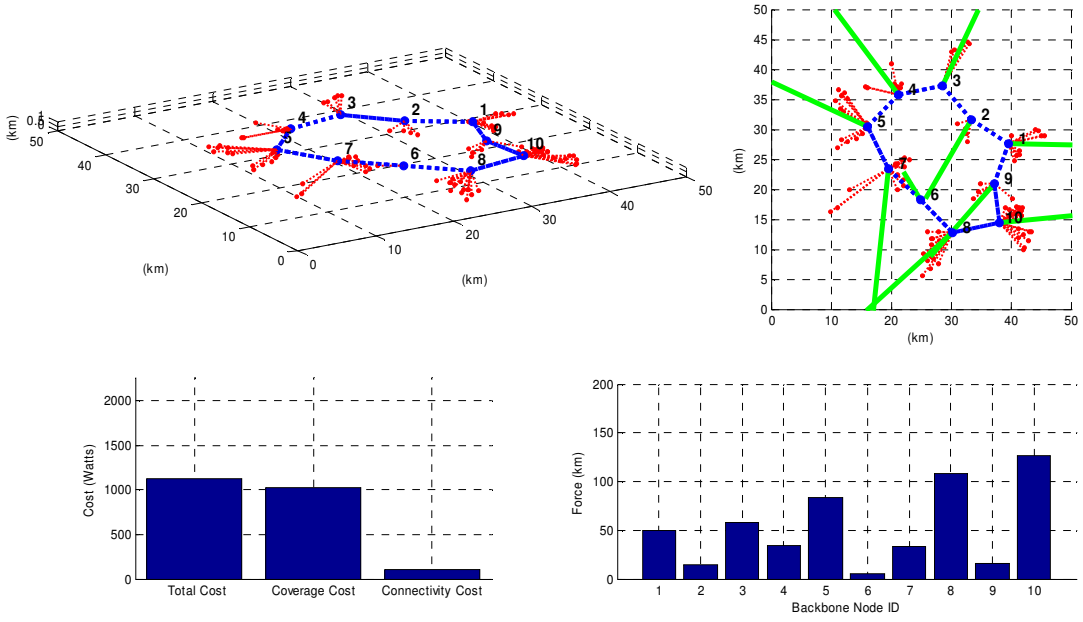

(y) Atmospheric attenuation update ($\alpha = 1.0\ km^{-1}$) (12 min):
U = 1132.8W; G = 1031.2W; F = 101.6W

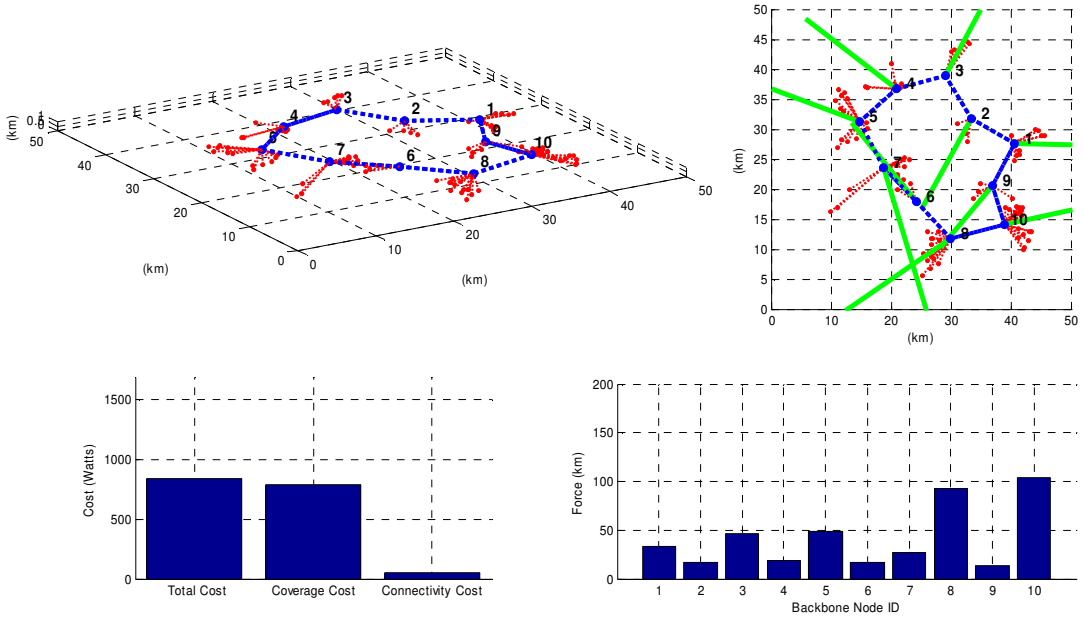

(z) Atmospheric attenuation update ($\alpha = 0.8\ km^{-1}$) (13 min):
U = 843.4W; G = 785.4W; F = 58.0W

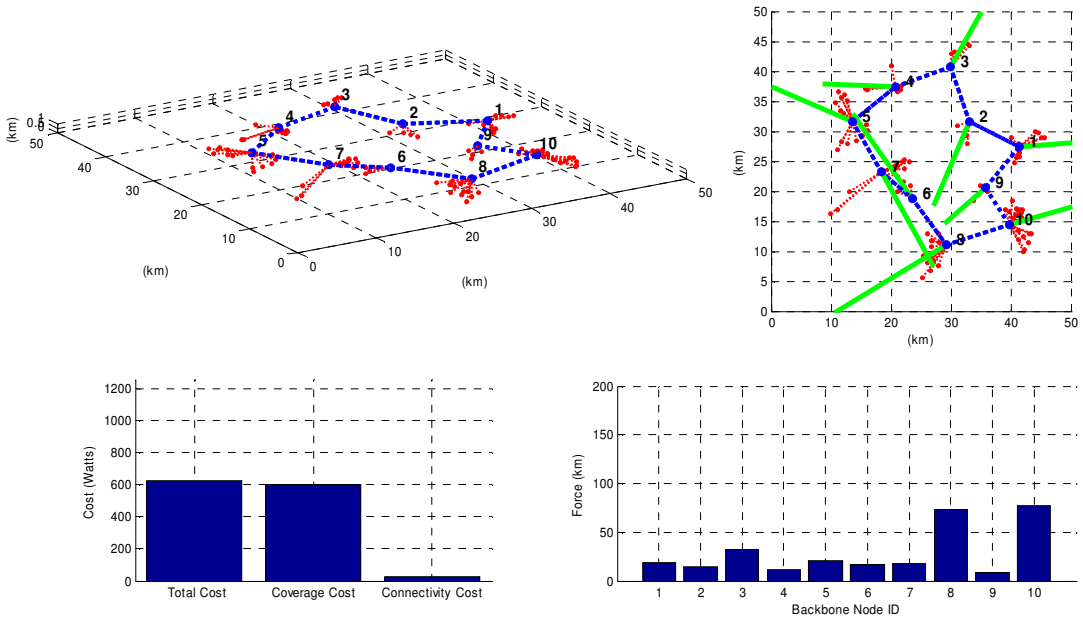

(aa) Atmospheric attenuation update ($\alpha = 0.6\ km^{-1}$) (14 min):
U = 630.3W; G = 602.2W; F = 28.1W

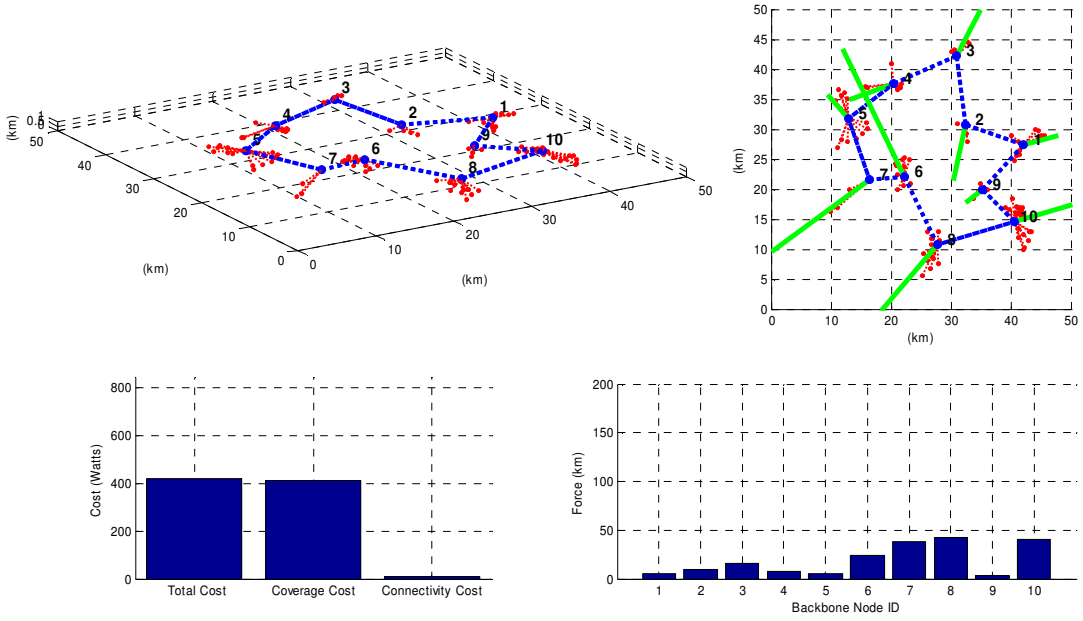

(bb) Atmospheric attenuation update ($\alpha = 0.4\ km^{-1}$) (15 min):
U = 421.5W; G = 410.1W; F = 11.4W

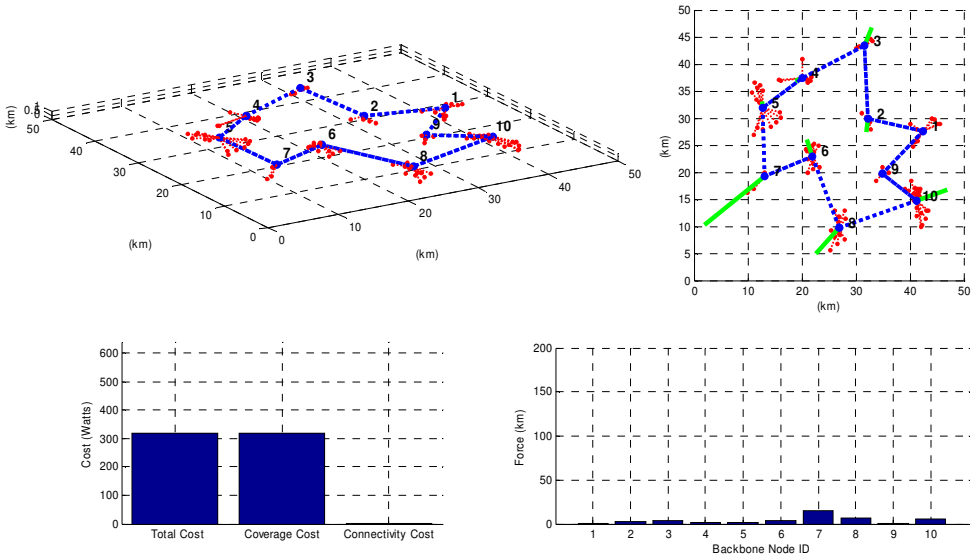

(cc) Atmospheric attenuation update ($\alpha = 0.2\ km^{-1}$) (16 min):
U = 319.9W; G = 318.0W; F = 1.9W

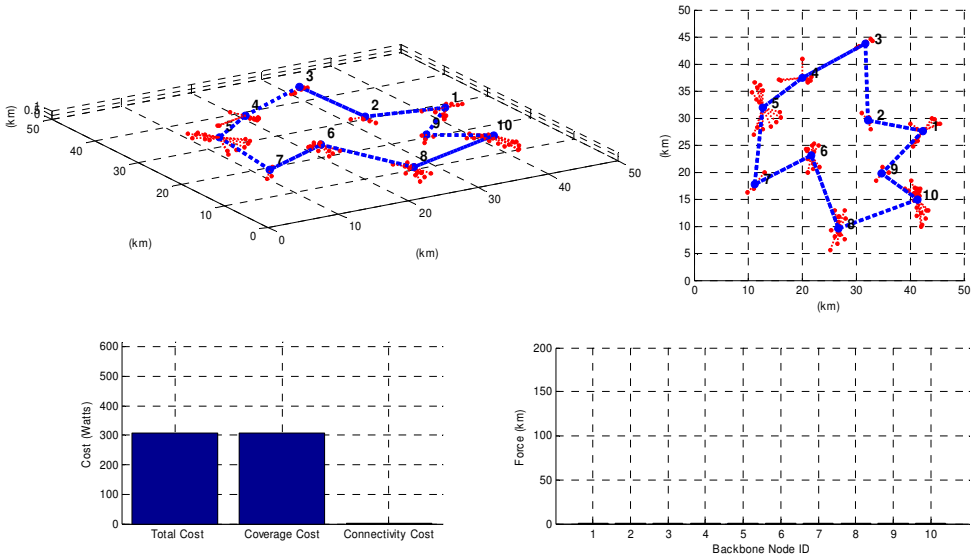

(dd) Backbone reaction (17 min):
Equilibrium: U = 308.88W; G = 308.73W; F = 0.15W

Figure 6.8: Network evolution with terminal clusters moving according to the RPGM model and backbone reacting using the FORCE algorithm.

In order to show the improved performance of our extended FORCE mobility control algorithm in the presence of atmospheric obscuration, we compared the average energy per unit time used in networks using the FORCE mobility control algorithm, with respect to SPRING algorithm. We again executed simulations for 10 and 20 backbone node networks, and for 10 different 1 hour scenario patterns (involving different terminal node placement and mobility patterns). The atmospheric attenuation pattern for this simulation used the 20 min pattern in table 6.2 repeated 3 times for the complete 1 hour simulation.

Time (minutes)	$\alpha\,(km^{-1})$
1	0.1
2	0.2
3	0.3
4	0.4
5	0.5
6	0.6
7	0.7
8	0.8
9	0.9
10	1.0
11	1.0
12	0.9
13	0.8
14	0.7
15	0.6
16	0.5
17	0.4
18	0.3
19	0.2
20	0.1

Table 6.2: Atmospheric attenuation pattern. Average attenuation coefficient (α) in km^{-1} for the backbone FSO links, for each minute of a 20 min scenario.

Table 6.3 shows the results obtained. As expected, when using the SPRING algorithm the network is able to react to the mobility of the terminal nodes, but does not react to changes in atmospheric attenuation. Thus, the energy needed to maintain the FSO links forming the backbone network is excessively high. The FORCE algorithm, on the other hand, is able to maintain lower values of backbone connectivity cost at the expense of a higher coverage cost, but minimizing the overall energy function *U*. Note from table 6.3 that the average power usage for the SPRING algorithm under atmospheric obscuration is 17 orders of magnitude greater than using the FORCE algorithm. This result indicates the tremendous effect of atmospheric attenuation on long distance FSO links. Recall that the path loss due to atmospheric attenuation is an exponential function of the link distance *L* with exponent the atmospheric attenuation coefficient α, described in Eq. 4.20 as: $\tau_{obs} = e^{\alpha L}$. Thus, the additional path loss due to atmospheric attenuation for a link of distance $L = 40$ km when $\alpha = 1\ km^{-1}$ becomes $\tau_{obs} = 2.35x10^{17}$, which explains the large energy values obtained using the SPRING algorithm. This result corroborates the importance of including the effects of atmospheric attenuation in the link cost model and validates the effectiveness of our FORCE mobility control algorithm in accurately taking into account the effects of the physical layer and drive the network topology accordingly.

In table 6.3, we also show the average power usage using the AVG algorithm. Note that the AVG algorithm outperforms the SPRING algorithm. Recall that AVG algorithm treats the network as a homogeneous network. Thus, the AVG algorithm does not allow excessive stretch of the backbone topology, which would be the optimal thing to do in clear atmosphere conditions, as high directional links need

much less energy to communicate over long distances. This effect was shown in section 6.5.3. Under atmospheric attenuation, on the other hand, long directional wireless links suffer excessive attenuation, effect that the AVG algorithm is able to attenuate by treating communications links homogeneously. In any case, the FORCE algorithm clearly outperforms both AVG and the SPRING algorithms precisely taking into account the heterogeneous nature of the network architecture.

	10 backbone nodes	**20 backbone nodes**
SPRING algorithm	744.8×10^{17} W	111.8×10^{17} W
AVG algorithm	476.7×10^{6} W	268.8×10^{4} W
FORCE algorithm	964.1 W	325.7 W
Percentage improvement (FORCE vs AVG)	99.99 %	99.98 %
Percentage improvement (FORCE vs SPRING)	100 %	100 %

Table 6.3: Average percentage improvement in total average power usage using the FORCE mobility control algorithm versus using the SPRING algorithm and versus using the AVG algorithm, for networks with 10 and 20 backbone nodes.

6.7 Power constraints

The results presented in sections 6.5 and 6.6 show the efficiency of our self-organized mobility control system in terms of jointly optimizing coverage and connectivity in dynamic scenarios. In our simulations we measure the cost of coverage and connectivity in terms of the energy metrics F and G defined in section 6.3. In practical situations, the energy available at the network nodes will be limited. In this section, we include power limitation constraints in the optimization problem.

Note that with power constraints, wireless links will not always be available. Exceeding link distances and atmospheric obscuration will cause link breaks that will terminate source-to-destination (SD) connections in the network. To take into account this effect, we introduce the following metric of interest: SD connections. We refer to SD connections as the number of SD pairs connected in the network; that is the number of SD pairs for which a path exists between them. This metric will be used as a measure of network performance under power limitation constraints.

6.7.1 Exponential constraint force

The FORCE mobility control algorithm presented in this dissertation is able to drive the network topology to energy minimizing configurations by moving backbone nodes in the direction that causes the steepest decrease of the system's potential energy function U, defined as the total power usage in the network. Power limitations impose constraints on the optimization problem as link distances that require excessive transmitted power will not be available for communications.

In this section, we include power limitation constraints as an additional exponential force that avoids nodes moving further apart from the maximum distance allowed by the maximum transmitted power available at the network nodes. We define the exponential constraint force at the location of node *i* due to its interaction with node *j* as:

$$f_{ij}^{c} = e^{m\left(\left\|R_i - R_j\right\| - \left(d_{ij}^{\max} - \delta\right)\right)} \tag{6.39}$$

where *m* is the constraint force exponent and $d_{ij}^{\max}$ is the maximum distance allowed between node *i* and node *j* in order to maintain the specified link BER when node *i* transmits with maximum transmit power $P_{Ti}^{\max}$, and δ is a positive distance value.

Note that

$$f_{ij}^{c} \begin{cases} \leq 1 & L \leq d_{ij}^{\max} - \delta \\ \geq 1 & L \geq d_{ij}^{\max} - \delta \end{cases} . \tag{6.40}$$

The values for *m* and δ are chosen to make f_{ij}^{c} negligible for values of $L \leq d_{ij}^{\max}$ and large enough to compensate other forces and avoid link breaks for values of $L \geq d_{ij}^{\max}$.

In order to define the total force acting on node *i* due to its interaction with node *j* under power limitation constraints, we now refer to the unconstrained force f_{ij} defined in Eq. 6.15 as f_{ij}^{u}:

$$\mathrm{f}_{ij}^{u} = \left(P_{R0}^{j} \frac{4\pi}{D_T^j A_{eR}^j} \right) \left(n \left\| \mathrm{R_i} - \mathrm{R_j} \right\|^{n-2} e^{\alpha_{ij} \left\| \mathrm{R_i} - \mathrm{R_j} \right\|} + \alpha_{ij} \left\| \mathrm{R_i} - \mathrm{R_j} \right\|^{n-1} e^{\alpha_{ij} \left\| \mathrm{R_i} - \mathrm{R_j} \right\|} \right) \mathrm{R_{ij}} . \tag{6.41}$$

The total force acting on backbone node *i* due to its interaction with node *j* is then defined as:

$$\mathrm{f}_{ij} = \mathrm{f}_{ij}^{u} + f_{ij}^{c}$$

$$\mathrm{f}_{ij} = \left(P_{R0}^{j} \frac{4\pi}{D_T^j A_{eR}^j} \right) \begin{pmatrix} n\left\|\mathrm{R_i} - \mathrm{R_j}\right\|^{n-2} e^{\alpha_{ij}\left\|\mathrm{R_i} - \mathrm{R_j}\right\|} \\ + \alpha_{ij}\left\|\mathrm{R_i} - \mathrm{R_j}\right\|^{n-1} e^{\alpha_{ij}\left\|\mathrm{R_i} - \mathrm{R_j}\right\|} \end{pmatrix} \mathrm{R_{ij}} + e^{m\left(\left\|\mathrm{R_i} - \mathrm{R_j}\right\| - \left(d_{ij}^{\max} - \delta\right)\right)} \tag{6.42}$$

Thus, when power limitations are imposed on network nodes, the force-driven mobility control algorithm is updated with f_{ij} computed using Eq. 6.42. The rest of the optimization algorithm follows the general methodology described in section 6.4.2.

6.7.2 Simulation results

In this section we compare the performance of the FORCE mobility control algorithm with and without the additional exponential constraint force.

For this simulation we use the same atmospheric obscuration pattern as in section 6.7.3 and a maximum transmitted power of 5, 10 and 15 Watts for all network nodes. We again use 10 different 1 hour dynamic scenarios changing the placement of the terminal nodes and the mobility patterns (always using the RPGM model). We use the FORCE mobility control algorithm to update the backbone topology and compare the average number of SD connections with and without the exponential constraint force. Table 6.4 shows the results obtained. When the maximum transmitted power is 5 W the average percentage improvement in SD connections is 30%. As expected, the

improvement is still significant but decreases with higher values of the maximum transmitted power. As the maximum transmitted power increases, the constraints are less restrictive and backbone links have larger margins to elongate before the constraint force appears to avoid exceeding distances. As seen in table 6.4, the average improvement goes down to 29% and 24% when the maximum transmitted power increases to 10 W and 15 W respectively.

	SD conns P_{Tmax} = 5 W	**SD conns P_{Tmax} = 10 W**	**SD conns P_{Tmax} = 15 W**
FORCE (unconstraint)	3112.1	4874.2	5915.3
FORCE (constraint)	4107.8	6325.0	7388.9
Average Percentage improvement	32%	29%	25%

Table 6.4: Average percentage improvement in SD connections using the additional constraint force for networks using the FORCE mobility control algorithm with maximum transmitted power of 5W, 10W and 15W.

Chapter 7: Conclusions

This dissertation provides a novel approach to the topology control problem in next generation wireless networks, which are becoming increasingly complex systems due to their heterogeneity (hierarchical architectures with diverse communication technologies) and dynamic behavior (high node mobility and changing atmospheric conditions).

In this work, heterogeneous and dynamic communication networks are modeled as physical systems where network robustness is characterized in terms of the system's potential energy. The potential energy of a physical system is defined as the energy stored within the system due to its position in space (its physical configuration). That is, the energy required to maintain its physical configuration. Analogously, the potential energy of a communications networks is defined as the communications energy stored in the wireless links forming the network. That is, the total communications energy needed to maintain its physical network topology at the required target performance, which in this dissertation is specified by the required bit-error-rate (BER).

Link physics models that account for the variation of the wireless channel due to atmospheric attenuation, turbulence-induced fading, node mobility, and different antenna patterns, have been developed. The developed link physics models are used to characterize the dynamic behavior of the potential energy stored at the

heterogeneous set of wireless links forming the network. The potential energy of the network system or total communications energy per unit time needed to maintain the specified target performance is shown to be a convex function of the link distance.

The topology control problem in next generation wireless networks is then formulated as an energy minimization problem whose solution is shown to jointly optimize coverage and connectivity in highly dynamic scenarios.

Uncontrolled network dynamics such as the mobility of end users or hosts and changing atmospheric conditions are modeled as external forces changing the energy of the network system. Topology control mechanisms are modeled as internal forces that the network system uses to react to external excitations by driving the network topology to energy minimizing configurations, based on local forces exerted on network nodes. The net force acting on a backbone node is computed as the negative gradient of the potential energy function at the node's location. Mobility control algorithms have been designed to reposition backbone nodes in the direction of the net force. The algorithms developed are completely distributed, show constant time complexity and produce optimal solutions from local interactions, thus proving the system's self-organizing capability.

Under clear atmospheric conditions, a quadratic optimization method is derived in which the energy function to be minimized is shown to be analogous to the potential energy of a spring system. Consequently, the SPRING mobility control algorithm is presented as a completely distributed algorithm which makes nodes react to Hooke-type forces to achieve energy minimizing configurations. Wireless communication links are shown to behave as springs which exert attraction forces

between neighbor nodes, with spring constants defined by the link directionality. High directional links are characterized by low spring constants which allow for higher link distances. Simulation results are presented in the context of DWB-based networks where directional wireless communications technologies are used at the backbone layer to provide end-to-end broadband connectivity to capacity-limited networks or hosts. End hosts or terminal nodes move according to the RPGM model and the SPRING algorithm is able to track the network dynamics by effectively reacting to the external excitations caused by the mobility of the terminal nodes.

In the presence of atmospheric obscuration, a more general convex optimization method is derived which results in the FORCE mobility control algorithm. FORCE takes into account the exponential attenuation of the signal power in the presence of atmospheric obscuration in order to generate exponential forces that make backbone nodes come closer to each other to maintain connectivity. Simulations results show how FORCE is able to "contract" and "stretch" the backbone topology as a function of atmospheric attenuation for joint coverage-connectivity optimization in highly dynamic environments.

In practical situations, transmitted power limitations are imposed on network nodes. This dissertation presents an extension to the force-driven mobility control algorithm that results from including power limitation constraints in the optimization problem. As a result, an additional exponential force is shown to appear between backbone nodes when the link distance approaches the maximum distance allowed by the maximum transmitted power at the network nodes. The average number of SD pairs connected is used as a measure of the effectiveness of the exponential constraint

force to maintain the backbone topology connected when power limitations constraints are imposed on network nodes. Simulations were performed in dynamic scenarios with 100 terminal nodes placed in a 50km x 50km area and 10 backbone nodes at an altitude of 500 meters. Mobility patterns for the terminal nodes were generated using the RPGM model [54]. A significant improvement in the average number of SD connections was obtained for the network scenarios generated. Specifically, a 30%, 29%, and 24% increase was obtained for networks using a maximum transmitted power of 5 W, 10 W and 15 W respectively.

Future work will investigate the performance of force-driven mobility control algorithms with respect to: 1) spatial variations of atmospheric attenuation and turbulence conditions, 2) different backbone topology structures, and 3) priority SD connections. Also, the combination of TR and MC topology control mechanisms will be studied.

Bibliography

[1] C.C. Davis, I.I. Smolyaninov, and S.D. Milner, “Flexible Optical Wireless Links and Networks”, *IEEE Comm. Mag.*, 41, 51-57, 2003.

[2] Acampora, A., “Last Mile by Laser.” *Scientific American*, vol. 287, 48-53, 2002.

[3] Milner, S., A. Desai, T. Ho, J. Llorca, S. Trisno, and C.C. Davis, “Self-Organizing Broadband Hybrid Wireless Networks." *Journal of Optical Networking* 4, 446-459, 2005.

[4] P. Gupta and P. R. Kumar, “The capacity of wireless networks,” *IEEE Trans. Inform. Theory*, vol. 46, no. 2, pp. 388–404, Mar. 2000.

[5] Davis, C., Z. Haas, and S. Milner. (2006). “On How To Circumvent The Manet Scalability Curse." *Proceedings of IEEE MILCOM*, Washington, DC.

[6] T. S. Rappaport, *Wireless Communications: Principles and Practice,* Englewood Cliffs, NJ: Prentice-Hall, 1996.

[7] W. C. Jakes, *Microwave Mobile Communications.* Piscataway, NJ: IEEE Press, 1994.

[8] Proakis, *Digital Communications,* 3rd ed. New York: McGraw-Hill, 1995.

[9] G. Keiser, *Optical Fiber Communications*, McGraw-Hill, New York, 2000.

[10] Christopher C. Davis, *Lasers and Electro-Optics,* Cambridge University Press, 1996.

[11] L.C. Andrews, R.L. Phillips, and C.Y. Hopen, *Laser Beam Scintillation with Applications*, SPIE Press, Bellingham, 2001.

[12] R. S. Lawrence and J.W. Strohbehn, “A survey of clear-air propagation effects relevant to optical communications”, Proc. SPIE Vol. 58, 1523-1545, 1970.

[13] Steven F. Clifford and John W. Strohbehn, “The Theory of Microwave Line-of-Sight Propagation Through a Turbulent Atmosphere”, IEE Trans., AP-18, pp. 264-274, 1970.

[14] A. Gurvich, M. Kallistrova, and N. Time, “Fluctuations in the parameters of a light wave from a laser during propagation in the atmosphere”, *Radiophys. Quant. Electron.*, 11, 771-776, 1968.

[15] C.C. Davis and I.I. Smolyaninov, “Effect of Atmospheric Turbulence on Bit-Error-Rate in an On-Off-Keyed Optical Wireless System”, Proc. SPIE Vol. 4489, 126-137, 2002.

[16] Christopher C. Davis, “Correlation Functions, Aperture Averaging, And Related Issues For Line-Of-Sight Optical Links Through Weak and Strong Scattering,” A Tutorial Discussion, Not Published to date.

[17] X. Zhu and J.M. Kahn, “Free-Space Optical Communication through Atmospheric Turbulence Channels”, *IEEE Trans. Comm.*, 50, 1293-1300, 2002.

[18] X. Zhu and J.M. Kahn, “Mitigation of Turbulence-Induced Scintillation Noise in Free-Space Optical Links Using Temporal-Domain Detection Techniques”, *IEEE Photon. Tech. Lett.*, 15, 623-625, 2003.

[19] H. Yuksel, L. Wasiczko, C.C. Davis, “Aperture Averaging for Optimizing Receiver Design and System Performance on Free Space Optical Communication Links”, *Journal of Optical Networking*, 2005.

[20] S. Trisno, I.I. Smolyaninov, S.D. Milner, and C.C. Davis, "Delayed diversity for fade resistance in optical wireless communications through turbulent media", Proc. SPIE, 2004.

[21] Brian R. Strickland, Michael J. Lavan, Eric Woodbridge, and Victor Chan, "Effects of fog on the bit-error-rate of a free space laser communication system", Applied Optics, Vol. 38, No. 3, January 1999.

[22] A. Parent, K.J. Snell, G. Lafrance, P. Grenier, S.Thibault, P. Galarneau, "Laser-diode array collimation for scene illumination purposes", SPIE Proceedings, vol. 3267, pp. 84-90, 2006.

[23] Achour, M. (2002). "Simulating atmospheric free-space optical propagation, part II: haze, fog, and low clouds attenuations." *SPIE Proceedings* 4873, 1-12.

[24] A. Dissanayake, J. Allnutt, and F. Haidara, "A prediction model that combine rain attenuation and other propagation impairments along earth-satellite paths", Online J. Space Comm. 2 (2002).

[25] M. Hess, P. Koepke, and I. Schult, "Optical Properties of Aerosols and Clouds: The Software Package OPAC", in *Bulletin of the American Meteorological Society*, Vol. 79, No. 5, 831-844, May 1998.

[26] N. Miles, J. Verlinde, E. Clothiaux, "Cloud Droplet Size Distributions in Low-Level Stratiform Clouds", American Meteorological Society, 2000.

[27] "Upper air digital data sets", National Climate Data Center (NCDC), NOAA.

[28] Ho T., Trisno S., Smolyaninov I., Milner S., Davis C., "Studies of Pointing Acquisition, and Tracking of Agile Optical Wireless Transceivers for Free Space

Optical Communication Networks". Optics in Atmospheric Propagation and Adaptive Systems VI, Proceedings of SPIE, 5237, 137-158, 2004.

[29] Ho T., Davis C., "Three-dimensional Optical Pointing System Encoded by Radial Trifocal Tensor". Proceedings of SPIE, San Diego, 2006.

[30] C. E. Jones, K. M. Sivalingam, P. Agrawal, and J. C. Chen, "A survey of energy efficient network protocols for wireless networks," *Wireless Networks*, vol. 7, no. 4, pp. 343–358, Aug. 2001.

[31] S. Narayanaswamy, V. Kawadia, R. S. Sreenivas, and P. R. Kumar, "Power control in ad-hoc networks: Theory, architecture, algorithm and implementation of the COMPOW protocol," in *Proc. of European Wireless 2002, Next Generation Wireless Networks: Technologies, Protocols, Services and Applications*, Florence, Italy, Feb. 2002, pp. 156–162.

[32] V. Rodoplu and T. H. Meng, "Minimum energy mobile wireless networks," *IEEE J. Select. Areas Commun.*, vol. 17, no. 8, pp. 1333–1344, Aug. 1999.

[33] R. Ramanathan and R. Rosales-Hain, "Topology control of multihop wireless networks using transmit power adjustment," in *Proc. IEEE INFOCOM 2000*, Tel Aviv, Israel, Mar. 2000, pp. 404–413.

[34] V. Kawadia and P. Kumar, "Power control and clustering in ad hoc networks," in *Proc. IEEE INFOCOM 2003*, San Francisco, California, US, Apr. 2003.

[35] S. A. Borbash and E. H. Jennings, "Distributed topology control algorithm for multihop wireless networks," in *Proc. 2002 World Congress on Computational Intelligence (WCCI 2002)*, Honolulu, Hawaii, US, May 2002.

[36] N. Li, J. C. Hou, and L. Sha, “Design and analysis of an MST-based topology control algorithm,” in *Proc. IEEE INFOCOM 2003*, San Francisco, California, US, Apr. 2003.

[37] Ning Li and Jennifer C. Hou, “Topology Control in Heterogeneous Wireless Networks: Problems and Solutions,” in *Proc. IEEE INFOCOM* 2004.

[38] Matthias Grossglauser and David N. C. Tse, “Mobility Increases the Capacity of Ad Hoc Wireless Networks,” IEEE/ACM Transactions on Networking vol. 10, no. 4, August 2002, pp.477-486.

[39] David K. Goldenberg, Jie Lin, A. Stephen Morse, Brad E. Rosen, Y. Richard Yang, “Towards Mobility as a Network Control Primitive,” *Mobihoc’04*, May 2004, Roppongi, Japan.

[40] M. R. Garey and D. S. Johnson. “Computers and Intractability: A Guide to the theory of NP-Completeness”. Freeman, San Francisco, 1979.

[41] T. Cormen, C. Leiserson, R. Rivest: “Introduction to Algorithms”, Eastern Economy Edition, First Edition (2001).

[42] Llorca, J., A. Desai, and S. Milner. (2004). "Obscuration Minimization in Dynamic Free Space Optical Networks through Topology Control." *Proc. IEEE MILCOM* 3, 1247-1253.

[43] P. C. Gurumohan and J. Hui. “Topology Design for Free Space Optical Networks”, IEEE 2003.

[44] Llorca, J., A. Desai, U. Vishkin, C. Davis and S. Milner. (2004). “Reconfigurable Optical Sensor Networks." *Proceedings of SPIE conference, Remote Sensing*, Barcelona, Spain, vol 5237, 136-146 (2004).

[45] Desai, A., and S. Milner. (2005). “Autonomous Reconfiguration in Free-Space Optical Sensor Networks." *IEEE JSAC* 23(8), 1556 – 1563.

[46] Llorca, J., A. Desai, E. Baskaran, and S. Milner. "Optimizing Performance of Hybrid FSO/RF Networks in Realistic Dynamic Scenarios." *Proc. SPIE* 5892, 52-60, 2005.

[47] A. Kashyap, S. Khuller and M. Shayman, ``Topology Control and Routing over Wireless Optical Backbone Networks," *Conference on Information Sciences and Systems,* Princeton University, March 2004.

[48] A. Kashyap, K. Lee, M. Kalantari, S. Khuller and M. Shayman, “Integrated topology control and routing in wireless optical mesh networks,” *Computer Networks Journal,* Vol. 51, October 2007, 4237-4251.

[49] A. Kashyap, S. Khuller and M. Shayman, “Relay Placement for Higher Order Connectivity in Wireless Sensor Networks,” *IEEE Infocom,* Barcelona, April 2006.

[50] A. Kashyap and M. Shayman, “Relay placement and movement control for realization of fault-tolerant ad hoc networks,” *Conference on Information Sciences and Systems,* Johns Hopkins University, March 2007.

[51] F. Liu, U. Vishkin, S. Milner, “Boostrapping Free Space Optical Networks”, Proc. 19th International Parallel and Distributed Processing Symp., April 2005.

[52] J. Llorca, A. Anibha, S. Milner, “Design and implementation of a bootstrapping model for free-space optical backbone networks”, Free-Space Laser Communications VI, Proceedings of the SPIE, Volume 6304, pp. 63041D (2006).

[53] Stephen T. Thornton, Jerry B. Marion, *Classical Dynamics of Particles and Systems*, Brooks Cole, 2003.

[54] Xiaoyan Hong, Mario Gerla, Guangyu Pei and Ching-Chuan Chiang, "A Group Mobility Model for Ad Hoc Wireless Networks", In Proceedings of the 2nd ACM international workshop on Modeling, analysis and simulation of wireless and mobile systems, pages 53-60, 1999.

[55] J. Llorca, S. D. Milner, C. C. Davis, "Mobility Control for Joint Coverage-Connectivity Optimization in Directional Wireless Backbone Networks", *IEEE MILCOM,* November 2007.

[56] J. Llorca, M. Kalantari, S. D. Milner, C. C. Davis, "A Quadratic Optimization Method for Connectivity and Coverage Control in Backbone-Based Wireless Networks", *Autonomous Configurability and Control in Dynamic Wireless Networks Symposium, ISSNP,* December 2007.